IOWA STATE UNIVERSITY
Digital Repository

2016

The Central Iowa Expo site pavement foundation stabilization and paving project: an investigation into the influence of pavement foundation stiffness on pavement design, construction, and performance

Peter Jacob Becker
Iowa State University

**The Central Iowa Expo site pavement foundation stabilization and paving project:
An investigation into the influence of pavement foundation stiffness on pavement
design, construction, and performance**

by

Peter Jacob Becker

A dissertation submitted to the graduate faculty

in partial fulfillment of the requirements for the degree of

DOCTOR OF PHILOSOPHY

Major: Civil Engineering (Geotechnical Engineering)

Program of Study Committee:
David White, Co-Major Professor
Douglas Gransberg, Co-Major Professor
Pavana Vennapusa
Halil Ceylan
Huaiqing Wu

Iowa State University

Ames, Iowa

2016

This work is dedicated to
my wife, Rita, and
my children, Montgomery and Evelyn

TABLE OF CONTENTS

LIST OF TABLES

LIST OF FIGURES

CHAPTER 1. INTRODUCTION

1.1 Dissertation Overview

1.1.1 Background

Great strides have been made in recent years to improve pavement design and construction in practice. Highway agencies have begun implementing the mechanistic-empirical pavement design guide (MEPDG) for pavement design (Baus & Stires, 2010; Darter, Titus-Glover, Von Quintus, Bhattacharya, & Mallela, 2014; Pierce & McGovern, 2014; Wisconsin Department of Transportation (WisDOT), 2013) and performance-related specifications for pavement construction (Epps et al., 2002). Despite the progress made toward designing and constructing durable and long lasting pavements, not nearly enough attention has been made to the role of pavement foundations in pavement design, construction, and performance.

In terms of resistance to load-induced pavement distresses, pavement foundation (i.e., subbase and subgrade layers) condition is arguably the most important aspect of pavement performance. Prevalence of fatigue cracking, rutting (i.e., permanent deformations), and thermal cracking govern flexible pavement (e.g., hot mix asphalt) performance; and prevalence of joint faulting and transverse cracking governs rigid pavement (i.e., Portland cement concrete) performance. Flexible pavement fatigue cracking and rutting are the products of excessive in situ stresses and strains, which depend the elastic moduli of all pavement layers (asphalt, subbase, and subgrade) per the Burmister (1945) stress distribution solution. Rigid pavement fatigue cracking depends on PCC slab response to applied loading, which depends on foundation stiffness and is

predicted using the Winkler foundation model; and rigid pavement joint faulting depends on the quality of the support layers (e.g., drainage characteristics).

Although pavement foundation modulus or stiffness is closely associated with pavement performance, stiffness-related quality control (QC) and quality assurance (QA) methods are seldom used for pavement foundation construction. Ever since Proctor (1933) discovered the moisture-density relationship of soils, density has been the accepted QC/QA criterion for pavement foundation construction. QC/QA methods that use density are still in existence because of the presumption that soil strength and stiffness increase within increasing density (Selig, 1982), even though density is only one of the many factors that affect soil strength and stiffness. However, there has been growing interest in implementing strength- and stiffness-based QC/QA methods as highway agencies move toward adopting performance-related specifications. Newcomb and Birgisson (1999) and Puppala (2008) summarized many in situ test methods that have been developed over the past five decades for characterizing stiffness or strength based properties of pavement foundation layers. Recently, there has been increasing interest in incorporating roller-integrated compaction monitoring (RICM) technologies (i.e., intelligent compaction) in earthwork construction and relating their measurements to pavement design parameters (Mooney et al., 2010; White, Vennapusa, Zhang, Gieselman, & Morris, 2009).

Strength- and stiffness-based QC/QA methods are highly applicable to the implementation of soil stabilization techniques (e.g., chemical stabilization) in pavement foundation construction. Soil stabilization presents a unique opportunity for pavement design engineers because it potentially allows for engineers to specify pavement

foundation stiffness regardless of natural subgrade or local aggregate conditions. In practice, soil stabilization is commonly used to construct working platforms (i.e., staging areas for contractors) and improve the support conditions for pavement systems. However, Winterkorn and Pamukcu (1991) state that soil stabilization techniques improve mechanical properties and environmental resistances of soils, so stabilization of pavement foundations can be used to counteract the effects of freeze-thaw weakening. Several studies (Bin-Shafique, Rahman, Yaykiran, & Azfar, 2010; Johnson, 2012; Parsons & Milburn, 2003; Solanki, Khoury, & Zaman, 2009; Solanki, Zaman, & Deabn, 2010; Walker & Karabulut, 1965) have demonstrated that stabilized soils are more resistant to freeze-thaw weakening, although many of these studies were limited to only laboratory testing. The lack of long-term field data has resulted in frequent omissions of soil stabilization techniques from pavement foundation design altogether despite its potential for enhancing pavement performance.

Although pavement foundation stabilization can enhance overall pavement performance, it has the unintended consequence of impeding implementation of RICM technologies for asphalt pavement construction in practice. In a review of several RICM studies, White and Vennapusa (2010) reported that RICM technologies typically have measurement influence depths of over 1 m, so pavement foundation condition likely influences RICM measurements taken during asphalt pavement construction. White and Vennapusa (2008) reported a case study in which subbase layer RICM measurements strongly correlated with asphalt pavement layer RICM measurements. Although there is a new guide specification (Federal Highway Administration (FHWA), 2014) to incorporate

RICM into asphalt pavement construction applications, the guide specification does not take into account influence of the pavement foundation other than to detect weak spots.

Transportation agencies must not only design and construct quality pavements with regards to performance, but also with regards to sustainability. Current sustainable pavement rehabilitation methods allow for the use of recycled materials instead of virgin materials. Several cases have demonstrated successful use of on-site pavement recycling rehabilitation techniques by transportation agencies (Bemanian, Polish, & Maurer, 2006; Diefenderfer, Apeagyei, Gallo, Dougald, & Weaver, 2012; Lewis, Jared, Torres, & Mathews, 2006; Mallick et al., 2002; Maurer, Bemanian, & Polish, 2007; Miller et al., 2011; Romanoschi, Hossain, Gisi, & Heitzman, 2004; Wen, Tharaniyil, Ramme, & Krebs, 2004). On-site recycling of pavement materials has proven to be successful for pavement structure rehabilitation, but questions remain on whether or not on-site recycled pavement materials can increase pavement foundation quality.

1.1.2 The Central Iowa Expo site pavement foundation stabilization and pavement placement project

The Central Iowa Expo (CIE) site in Boone, Iowa comprises a 0.5-km^2 area meant for outdoor festivals and events. Nearly 10 km of roadways are arranged in a grid over the course of the CIE site. In 2012, the CIE site roadways needed to be reconstructed with stable pavement foundations and bound pavement layers. The reconstruction project created a unique opportunity to conduct research on soil stabilization techniques, strength- and stiffness-based QC/QA test methods, RICM technologies, and long-term pavement performance. Roadways at the CIE site do not support regular traffic, so a lack of traffic loading is a limitation of any research conducted at the CIE site.

Pavement reconstruction took place in two phases. The Phase I contractor, who submitted the lowest of six bids, constructed the pavement foundations in summer 2012. Phase II involved placement of either flexible or rigid pavements in summer 2013.

1.3 Research Objectives and Anticipated Benefits

The primary objectives of this research are:

- to assess the applicability of strength- and stiffness-based spot testing and RICM continuous compaction control (CCC) for pavement foundation construction;
- to study in situ the effects of freeze-thaw weakening on stabilized pavement foundation mechanical properties (i.e., stiffness);
- to study the influence of pavement foundation condition on RICM measurements taken during asphalt pavement construction; and
- to compare the in situ performance and relative costs of pavement foundation test sections constructed with on-site recycled materials.

This study will provide improved knowledge in the state-of-the-practice for secondary and primary roadways, pavement foundations, emerging compaction technologies, and granular surface stabilization. The project will result in improved transportation infrastructure decision-making and investment.

1.4 Dissertation Organization

This dissertation comprises four scholarly journal articles that have been submitted for publication as well as an overview of the handling of pavement foundation design and construction in current pavement design guides. The four papers and the pavement foundation design overview appear as standalone chapters that include references to pertinent literature, analysis and discussion of significant findings, and conclusions and

recommendations. The final chapter of the dissertation summarizes the key findings in the study and proposes recommendations for future research.

Chapter 2 provides an overview of pavement foundation design and construction procedures in the AASHTO 1993 pavement design guide and in the MEPDG. Discussion is made on the impact of pavement foundation condition on both flexible pavement and rigid pavement performance. Although the MEPDG has allowed for the design of better performing pavements, there needs to be improved handling of the pavement foundation in pavement design and construction.

The first paper (Chapter 3) reports an assessment of strength- and stiffness-based QC/QA methods for the construction of pavement foundations. Measurements from falling weight deflectometer (FWD), light weight deflectometer (LWD), dynamic cone penetrometer (DCP), and RICM systems were used to assess soil stiffness. Results of soil stiffness were compared with two independent groups of nuclear moisture-density measurements to demonstrate some of the shortcomings of traditional nuclear gauge testing for quality assessment. The findings from this paper show the value in using soil stiffness measurements to characterize ground variations.

The second paper (Chapter 4) reports an assessment of stabilized pavement foundation performance during both never-frozen and thaw-weakened conditions. FWD and DCP tests were performed during the never-frozen condition in October 2012 and during the thaw-weakened condition in April/May 2013. FWD and DCP test results indicated that sections with cement stabilization provided the highest values in April 2013. Multivariable statistical analyses and first-order, variance-based sensitivity analyses of FWD and DCP measurements showed that overall pavement foundation

stiffness is entirely governed by subgrade stiffness during the thaw-weakened condition. Analysis is made on the load-spreading effectiveness of subbase layers during both never-frozen and thaw-weakened conditions. Results from this study demonstrate the significance and value in stabilizing a foundation layer to achieve better freeze-thaw performance.

The third paper (Chapter 5) reports a study on the influence of pavement foundation condition on RICM measurements taken during asphalt pavement construction. Asphalt pavements overlying pavement foundations of variable stiffnesses were compacted using a Hamm HD+ 120 VV dual smooth-drum vibratory roller. The roller was equipped with an RICM system that yielded Hamm measurement value (HMV) and temperature measurements in real time. To compare influence of the pavement foundation, HMV measurements were taken on the subbase layer prior to paving then correlated to HMV measurements taken during paving. Comparisons were made between RICM measurements and QC/QA test methods such as relative compaction, FWD modulus, and asphalt surface temperature. Recommendations are provided for improving asphalt pavement construction specifications that use RICM technologies.

The fourth paper (Chapter 6) describes results from a study comparing the performance of side-by-side test sections of pavement foundation layers constructed with on-site recycled materials and surfaced with hot mix asphalt. Test sections included recycled materials blended with subgrade to create a mechanically stabilized subgrade layer and recycled materials placed in an over excavated subgrade layer. FWD and DCP in situ tests and laboratory freeze-thaw tests were used to assess the performance of the test sections, in comparison with a control section where recycled materials were not

used. Findings indicate that test sections with on-site recycled materials provided improved support conditions for the pavements during both before and after freeze-thaw conditions, when compared to the control section.

1.5 References

Baus, R.L., & Stires, N.R. (2010). *Mechanistic-empirical pavement design guide implementation* (FHWA-SC-10-01). Washington, DC: Federal Highway Administration.

Bemanian, S., Polish, P., & Maurer, G. (2006). Cold in-place recycling and full-depth reclamation projects by Nevada Department of Transportation: State of the practice. *Transportation Research Record, 1949*(1), 54-71. doi:10.3141/1949-06

Bin-Shafique, Sazzad, Rahman, K., Yaykiran, Mustafa, & Azfar, Ireen. (2010). The long-term performance of two fly ash stabilized fine-grained soil subbases. *Resources, Conservation & Recycling, 54*(10), 666-672. doi: 10.1016/j.resconrec.2009.11.007

Burmister, D. M. (1945). The general theory of stresses and displacements in layered systems: I. *Journal of Applied Physics, 16*(89), 89-94. doi: 10.1063/1.1707558

Darter, M. I., Titus-Glover, L., Von Quintus, H., Bhattacharya, B. B., Mallela, J. (2014). *Calibration and implementation of the AASHTO mechanistic-empirical pavement design guide in Arizona* (FHWA-AZ-14-606). Phoenix: Arizona Department of Transportation.

Diefenderfer, B., Apeagyei, A., Gallo, A., Dougald, L., & Weaver, C. (2012). In-place pavement recycling on I-81 in Virginia. *Transportation Research Record: Journal of the Transportation Research Board, 2306*(1), 21-27. doi: 10.3141/2306-03

Epps, J.A., Hand, A., Seeds, S., Schulz, T., Alavi, S., Ashmore, C., Monismith, C.L., Deacon, J.A., Harvey, J.T., & Leahy, R. (2002). *Recommended performance-related specification for hot-mix asphalt construction: Results of the WesTrack project* (NCHRP 455). Washington, DC: National Cooperative Highway Research Program.

Federal Highway Administration. (2014*). Intelligent compaction technology for asphalt applications: Generic IC specifications for asphalt materials.* Washington, DC: Federal Highway Administration

Johnson, A. E. (2012). *Freeze-thaw performance of pavement foundation materials* (Master's thesis). Available from ProQuest Dissertations and Theses database. (UMI No. 1531431)

Lewis, D., Jared, D., Torres, H., & Mathews, M. (2006). Georgia's use of cement-stabilized reclaimed base in full-depth reclamation.*Transportation Research Record, 1952*(1), 125-133. doi: 10.3141/1952-14

Mallick, R., Bonner, D., Bradbury, R., Andrews, J., Kandhal, P., & Kearney, E. (2002). Evaluation of performance of full-depth reclamation mixes. *Transportation Research Record, 1809*(1), 199-208. doi: 10.3141/1809-22

Maurer, G., Bemanian, S., & Polish, P. (2007). Alternative strategies for rehabilitation of low-volume roads in Nevada. *Transportation Research Record, 1989*(1), 309-320. doi: 10.3141/1989-78

Miller, H., Kestler, M., Amatrudo, M., Eaton, R., & Hall, A. (2011). Comparison of test sections of low-volume roadways reconstructed with conventional techniques and full-depth reclamation. *Transportation Research Record: Journal of the Transportation Research Board, 2204*(1), 206-214. doi: 10.3141/2204-26

Mooney, M., Rinehart, R., White, D.J., Vennapusa, P., Facas, N., & Musimbi, O. (2010). *Intelligent soil compaction systems* (NCHRP Report 676). Washington, DC: National Cooperative Highway Research Program.

Newcomb, D.E., & Birgisson, B. (1999). *Measuring in situ mechanical properties of pavement subgrade soils* (NCHRP Synthesis 278). Washington, DC: National Cooperative Highway Research Program.

Parsons, R., & Milburn, J. (2003). Engineering behavior of stabilized soils. *Transportation Research Record, 1837*(1), 20-29. doi: 10.3141/1837-03

Pierce, L.M., & McGovern, G. (2014). *Implementation of the AASHTO mechanistic-empirical pavement design guide and software* (NCHRP Synthesis 457). Washington, DC: National Cooperative Highway Research Program.

Proctor, R.R. (1933). Fundamental principles of soil compaction. *Engineering News Record, 111*(9), 245–248.

Puppala, A. (2008). *Estimating stiffness of subgrade and unbound materials for pavement design* (NCHRP Synthesis 382). Washington, DC: National Cooperative Highway Research Program.

Romanoschi, S., Hossain, M., Gisi, A., & Heitzman, M. (2004). Accelerated pavement testing evaluation of the structural contribution of full-depth reclamation material stabilized with foamed asphalt. *Transportation Research Record, 1896*(1), 199-207. doi: 10.3141/1896-20

Selig, E.T. (1982). Compaction procedures, specifications, and control considerations. *Transportation Research Record, 897*, 1–8.

Solanki, Pranshoo, Khoury, Naji, & Zaman, M.M. (2009). Engineering properties and moisture susceptibility of silty clay stabilized with lime, class c fly ash, and cement kiln dust. *Journal of Materials in Civil Engineering, 21*(12), 749-757.

Solanki, P., Zaman, M., & Dean, J. (2010). Resilient modulus of clay subgrades stabilized with lime, class c fly ash, and cement kiln dust for pavement design. *Transportation Research Record: Journal of the Transportation Research Board, 2186*(1), 101-110. doi: 10.3141/2186-11

Walker R.D, & Karabulut, C. (1965) Effect of freezing and thawing on unconfined compressive strength of lime-stabilized soils. *Highway Research Record, 92,* 1–11.

Wen, H., Tharaniyil, M., Ramme, B., & Krebs, S. (2004). Field performance evaluation of class c fly ash in full-depth reclamation: Case history study. *Transportation Research Record,1869*(1), 41-46. doi: 10.3141/1869-05

Winterkorn, H.F., & Pamukcu S. (1991). Soil stabilization. In H. Fang (Ed.). *Foundation engineering handbook* (pp. 317–378). New York: Van Nostrand Reinhold.

Wisconsin Department of Transportation. (2013). *WisDOT MEPDG implementation peer exchange* (0092-13-17). Madison: Wisconsin Department of Transportation.

White, D.J., & Vennapusa, P. (2008). *Accelerated implementation of intelligent compaction monitoring technology for embankment subgrade soils, aggregate base, and asphalt pavement materials* (TPF-5(128)). Washington, DC: Federal Highway Administration.

White, D.J., & Vennapusa, K.R. (2010). *A review of roller-integrated compaction monitoring technologies for earthworks* (ER10-04). Ames: Earthworks Engineering Research Center.

White, D. J., Vennapusa, P., Zhang, J., Gieselman, H., & Morris, M. (2009). *Implementation of intelligent compaction performance based specifications* (MN/RC 2009-14). St. Paul: Minnesota Department of Transportation.

CHAPTER 2. OVERVIEW OF PAVEMENT FOUNDATION DESIGN AND CONSTRUCTION IN CURRENT PAVEMENT DESIGN GUIDES

Pavement foundation quality is critical to the pavement design process because load-related distresses that govern pavement performance are significantly associated with pavement foundation condition. In flexible pavements [e.g., hot mix asphalt (HMA)], the prevalence of fatigue cracking and rutting (i.e., permanent deformations) governs performance (Epps et al., 2002), and the prevalence of joint faulting and transverse cracking governs rigid pavement [i.e., Portland cement concrete (PCC)] performance (National Cooperative Highway Research Program (NCHRP), 2004). Flexible pavement fatigue cracking and rutting are the products of excessive in situ stresses and strains, which depend the elastic moduli of all pavement layers (asphalt, subbase, and subgrade) per the Burmister (1945) stress distribution solution. Rigid pavement fatigue cracking depends on PCC slab response to applied loading, which depends on foundation stiffness and is predicted using the Winkler foundation model; and rigid pavement joint faulting depends on the quality of the support layers (e.g., drainage characteristics). The following sections in this chapter will discuss the handling of pavement foundation design, characterization, and verification by the American Association of State Highway and Transportation Officials (AASHTO) (1993) pavement design guide and the Mechanistic-Empirical Pavement Design Guide (MEPDG) (NCHRP, 2004).

2.1 Pavement Foundation Design in the AASHTO 1993 Pavement Design Guide

For both flexible and rigid pavements, the AASHTO (1993) pavement design guide uses empirical equations to predict the number of 18 kip equivalent single-axle load (ESAL) applications that a pavement can resist during its service life. Flexible pavement design is based on the calculation of minimum structural numbers (SN) from layer thicknesses, structural coefficients (a), and drainage coefficients (m) to *protect* each underlying pavement layer from applied ESAL applications. Rigid pavement design is based on the selection of a minimum slab thickness to resist design ESAL applications using effective modulus of subgrade reaction (k), concrete modulus of rupture (S_c), load transfer coefficient (J), drainage coefficient (C_d). The following sections examine pavement foundation design in both flexible and rigid pavement design procedures using the AASHTO (1993) pavement design guide.

2.1.1 Subgrade design per AASHTO (1993)

Pavement subgrades are layers of soil underlying all bound and unbound pavement layers and comprise either natural soil deposits or compacted embankments. The requisite subgrade engineering properties for pavement design pertain to stiffness (e.g., elastic modulus) and sensitivity to seasonal reductions in stiffness.

The AASHTO (1993) pavement design guide does not provide a subgrade design procedure per se, but rather an approach for the determination of subgrade engineering properties. This is a severe limitation of the AASHTO (1993) pavement design guide because pavement design engineers must simply cope with given subgrade conditions, instead of having the ability to specify a design subgrade condition.

The AASHTO (1993) pavement design guide uses resilient modulus (M_R) to characterize subgrade engineering behavior. M_R is a measure of soil elasticity that is, in general, calculated from equation 2.1

$$M_R = \frac{\sigma_d}{\varepsilon_r} \qquad (2.1)$$

where M_R = resilient modulus, σ_d = deviator stress, and ε_r = recoverable strain for applied deviator stress. Soil is non-linear elastic and experiences both permanent (plastic) strain and recoverable (elastic) strain when subjected to axial loading. However, as the number of load repetitions increases, the plastic strain due to each load repetition decreases while the recoverable strain stays the same. After 100 to 200 load repetitions (Huang, 2004) the amount of plastic strain becomes negligible, so all strains are purely elastic. Because pavements can be subjected to more than several millions of load repetitions within their service lives, M_R is an appropriate engineering property in pavement design. The AASHTO 1993 pavement design guide recommends that engineers determine subgrade resilient modulus [$M_{R(SG)}$] using laboratory testing (AASHTO T 274). In addition, there are several correlations that relate California bearing ratio (CBR), R-value, or soil classification to $M_{R(SG)}$.

$M_{R(SG)}$ is an input for flexible pavement design, but not for rigid pavement design. Because rigid pavement analysis is based on the Winkler foundation model, $M_{R(SG)}$ must be converted to a spring constant or, rather, modulus of subgrade reaction (k) using equation 2.2

$$k = \frac{M_R}{19.4} \qquad (2.2)$$

where k = modulus of subgrade reaction, and M_R = resilient modulus. Authors of the

AASHTO (1993) pavement design guide derived equation 2.2 by combining the

definition of modulus of subgrade reaction (applied stress per vertical deflection) with the

Boussinesq solution for a uniformly-loaded, flexible circular-area equation 2.3

$$\delta_o = \frac{2\sigma_o(1 - \mu^2)r}{M_R} \tag{2.3}$$

where δ_o = vertical deflection, σ_o = applied stress, μ = Poisson's ratio, r = radius of

loaded area, and M_R = resilient modulus. However, vertical deflection per the Boussinesq

solution takes into account the radius of the loaded area, while vertical deflection per the

Winkler foundation model (i.e., modulus of subgrade reaction) does not. Therefore,

equation 2.4 better describes the relationship between k and M_R

$$k = \frac{2M_R}{\pi(1 - \mu^2)r} \tag{2.4}$$

where k = modulus of subgrade reaction, μ = Poisson's ratio, r = radius of loaded area,

and M_R = resilient modulus.

When soil becomes saturated internal pore water pressures increase and effective

stresses decrease, so soil strengths and stiffnesses worsen. In general, subgrade degree of

saturation varies during the course of a year because groundwater table elevation

fluctuates with climatic season. During the summer months, a subgrade may be

unsaturated, but the subgrade may then saturate during the spring months as a result of

freezing and thawing. To account for seasonal effects on $M_{R(SG)}$, the AASHTO (1993)

pavement design guide recommends determining an effective subgrade resilient modulus

$[M_{R(SG)-eff}]$. $M_{R(SG)-eff}$ is based on an average of the predicted relative damage ($\bar{u}_f$) to

a pavement over the course of a year. If $M_{R(SG)}$ is known for each season, then

$M_{R(SG)-eff}$ can be calculated from equations 2.5 and 2.6

$$\bar{u}_f = \frac{1}{n}\sum_{i=1}^{n}\left[1.729 \times 10^8 M_{R(SG)_i}^{-2.32}\right] \tag{2.5}$$

$$M_{R(SG)-eff} = 3005 \times \bar{u}_f^{-0.431} \tag{2.6}$$

where $\bar{u}_f$ = average predicted relative damage over course of year, n = number of seasons

in year, $M_{R(SG)_i}$ = i^{th} season subgrade resilient modulus [in psi (1 psi = 6.89 kPa)], and

$M_{R(SG)-eff}$ = effective subgrade resilient modulus [in psi (1 psi = 6.89 kPa)].

Determination of effective modulus of subgrade reaction (k_{eff}) follows a similar

procedure to that of $M_{R(SG)-eff}$ (i.e., based on $\bar{u}_f$); however, $\bar{u}_f$ in rigid pavements

depends on concrete slab thickness (D_{PCC}) in addition to k. So, if k is known for each

season, then k_{eff} can be iteratively calculated from equations 2.7 and 2.8

$$\bar{u}_f = \frac{1}{n}\sum_{i=1}^{n}\left[D_{PCC}^{0.75} - 0.39 \times k_i^{0.25}\right]^{3.42} \tag{2.7}$$

$$\bar{u}_f = \left[D_{PCC}^{0.75} - 0.39 \times k_{eff}^{0.25}\right]^{3.42} \tag{2.8}$$

where $\bar{u}_f$ = average predicted relative damage over course of year, n = number of seasons

in year, D_{PCC} = concrete slab thickness [in in. (1 in. = 25.4 mm)], k_i = i^{th} season modulus

of subgrade reaction [in psi/in. (1 psi/in. = 0.271 kPa/mm)], and k_{eff} = effective modulus

of subgrade reaction [in psi/in. (1 psi/in. = 0.271 kPa/mm)].

2.1.2 Subbase design per AASHTO (1993)

Flexible pavement subbase design per AASHTO 1993 involves determining a

minimum subbase thickness (D_{SB}) using asphalt surface course, asphalt base course and

subbase stiffness and drainage properties, such that the subbase layer *protects* the underlying subgrade. D_{SB} is calculated from equation 2.9

$$D_{SB} \geq \frac{SN_{SG} - a_{SC}D_{SC} - a_{BC}m_{BC}}{a_{SB}m_{SB}} \tag{2.9}$$

where D_{SB} = subbase thickness, SN_{SG} = structural number required to *protect* the subgrade, a_{SC} = asphalt surface course structural coefficient, m_{SC} = asphalt surface course drainage coefficient, a_{BC} = asphalt base course structural coefficient, m_{BC} = asphalt base course drainage coefficient, a_{SB} = subbase structural coefficient, and m_{SB} = subbase drainage coefficient. Using statistical and traffic loading inputs, SN_{SG} is empirically calculated from equation 2.10

$$\log W_{18} = Z_R S_o + 9.36 \log(SN_{SG} + 1) - 0.20 +$$
$$\left[\frac{\log(\Delta PSI) - \log(4.2 - 1.5)}{0.4 + 1094(SN_{SG} + 1)^{-5.19}}\right] + \tag{2.10}$$
$$2.32 \log M_{R(SG)} - 8.07$$

where W_{18} = number of 18 kip single-axle load applications over pavement design life, Z_R = normal deviate for a given reliability, S_o = standard deviation, SN_{SG} = structural number required to protect the subgrade, ΔPSI = serviceability loss over pavement design life, and $M_{R(SG)}$ = subgrade resilient modulus [in psi (1 psi = 6.89 kPa)].

Rigid pavement design is limited to the determination of a minimum concrete slab thickness (D_{PCC}) to resist a design ESAL input (i.e., W_{18}). D_{PCC} is determined from equation 2.11

$$\log(W_{18}) = Z_R S_o + 7.35 \log(D_{PCC} + 1) - 0.06 +$$

$$\left[\frac{\log(\Delta PSI) - \log(4.2 - 1.5)}{1 + 1.624 \times 10^7 (D_{PCC} + 1)^{-8.46}} \right] +$$

$$(4.22 - 0.32 p_t) \log \left\{ \frac{S_c C_d \left(D_{PCC}^{0.75} - 1.132 \right)}{215.63 J \left[D_{PCC}^{0.75} - 18.42 \left(\frac{E_c}{k_c} \right)^{0.25} \right]} \right\}$$

(2.11)

where W_{18} = number of 18 kip single-axle load applications over pavement design life,

Z_R = normal deviate for a given reliability, S_o = standard deviation, D_{PCC} = concrete slab

thickness [in in. (1 in. = 25.4 mm)], ΔPSI = serviceability loss over pavement design life,

p_t = terminal serviceability, S_c = concrete modulus of rupture [in psi (1 psi = 6.89 kPa)],

C_d = drainage coefficient, J = load transfer coefficient, E_c = concrete modulus of

elasticity [in psi (1 psi = 6.89 kPa)], and k_c = composite modulus of subgrade reaction [in

psi/in. (1 psi/in. = 0.271 kPa/mm)]. Although neither subbase stiffness nor subbase

thickness appears in equation 2.11, both parameters contribute to composite modulus of

subgrade reaction (k_c) and, therefore, design concrete slab thickness. The following

section describes the procedure for determining k_c from subbase stiffness properties and

subbase thickness.

2.1.2.1 Subbase stiffness characteristics

Equation 2.12 provides a correlation between a_{SB} and $M_{R(SB)}$ developed by Van Til,

McCullough, Vallerga, and Hicks (1972):

$$a_{SB} = 0.227 \log M_{R(SB)} - 0.839$$

(2.12)

where a_{SB} = subbase structural coefficient, $M_{R(SB)}$ = subbase resilient modulus [in psi

(1 psi = 6.89 kPa)]. Because $M_{R(SB)}$ depends on subbase stress state, the

AASHTO (1993) pavement design guide recommends a nonlinear regression model

(equation 2.13) to calculate $M_{R(SB)}$ from in situ bulk stress (equation 2.14)

$$M_{R(SB)} = k_1 \theta^{k_2} \tag{2.13}$$

$$\theta = \sigma_z + \sigma_r + \sigma_\theta \tag{2.14}$$

where $M_{R(SB)}$= subbase elastic modulus [in psi (1 psi = 6.89 kPa)], k_1, k_2 = regression

constants, θ = bulk stress [in psi (1 psi = 6.89 kPa)], σ_z = in situ vertical stress [in psi (1

psi = 6.89 kPa)], σ_r = in situ radial stress [in psi (1 psi = 6.89 kPa)], and σ_θ = in situ

tangential stress [in psi (1 psi = 6.89 kPa)]. Table 2.1 provides typical values for k_1 and

k_2, and Table 2.2 provides typical values for θ.

Subbase layer stiffness is accounted for in AASHTO (1993) rigid pavement design

using composite modulus of subgrade reaction (k_c), which is based off of the

Burmister (1945) stress distribution solution and calculated from equation 2.15.

$$\ln(k_c) = -2.807 + 0.1253[\ln(D_{SB})]^2 + 1.062\ln[M_{R(SG)}] +$$
$$0.1282[\ln(D_{SB})]\{\ln[M_{R(SB)}]\} - 0.4114\ln(D_{SB}) - \tag{2.15}$$
$$0.0581\ln[M_{R(SB)}] - 0.1317[\ln(D_{SB})]\ln[M_{R(SG)}]$$

where k_c = composite modulus of subgrade reaction [in psi/in. (1 psi/in. =

0.271 kPa/mm)], D_{SB} = subbase layer thickness [in in. (1 in. = 25.4 mm)], $M_{R(SB)}$ =

subbase elastic modulus [in psi (1 psi = 6.89 kPa)], and $M_{R(SG)}$ = subgrade elastic

modulus [in psi (1 psi = 6.89 kPa)]. Equation 2.15 is a regression model relating 125

combinations of $M_{R(SB)}$, $M_{R(SG)}$, and D_{SB} to predicted deflection for a two-layer elastic

system per the Burmister (1945) stress distribution solution [American Association of

State Highway and Transportation Officials (AASHTO), 1986]. AASHTO (1986) only

reports an r^2 value equal to 0.961 for this correlation, so the confidence in predicting k_c from equation 2.15 is unknown. Effective composite modulus of subgrade reaction (k_{c-eff}) due to seasonal variations can then be determined using the same procedure for determining k_{c-eff}.

<u>2.1.2.2 Subbase drainage characteristics</u>

The drainage coefficient, m_{SB}, characterizes subbase drainage quality in flexible pavement design, and the drainage coefficient, C_d, characterizes subbase drainage quality in rigid pavement design. Both drainage coefficients depend on subbase hydraulic conductivity and the percentage of time during which the pavement is exposed to moisture levels approaching saturation. Table 2.3 provides recommended m_{SB} values, and Table 2.4 provides recommended C_d values.

2.2 Pavement Foundation Design in the Mechanistic-Empirical Pavement Design Guide (MEPDG)

Unlike the AASHTO (1993) pavement design Guide, there is no difference in pavement foundation design inputs between rigid and flexible pavement design guides for the mechanistic-empirical pavement design guide (MEPDG). In addition, the MEPDG handles subgrade design inputs in the same manner as subbase design inputs. Both pavement subbase and subgrade materials are considered as simply unbounded materials.

The MEPDG uses a tiered hierarchy of leveled design inputs for predicting pavement performance. Level 1 inputs provide the most accurate predictions of pavement performance, level 2 inputs provide less accurate predictions of pavement performance, and level 3 inputs provide the least accurate predictions of pavement performance. MEPDG software uses the designs input with empirical relationships, mechanistic

equations, and climatic models to predict pavement distress prevalence and, therefore,

pavement performance. Pavement foundation design inputs that are taken into account by

the MEPDG include stiffness, drainage, and seasonal effects on stiffness.

2.2.1 Pavement foundation stiffness in the MEPDG

Similar to the AASHTO (1993) pavement design guide, the MEPDG uses resilient

modulus to characterize the stiffness of unbound pavement materials. For level 1

pavement performance predictions, the MEPDG software uses a generalized nonlinear

model to calculate resilient modulus for given stress conditions. The generalized model

used by the MEPDG for calculating resilient modulus comprises equations 2.16, 2.17,

and 2.18

$$M_R = k_1 P_a \left(\frac{\theta}{P_a}\right)^{k_2} \left(\frac{\tau_{oct}}{P_a} + 1\right)^{k_3} \qquad (2.16)$$

$$\theta = \sigma_z + \sigma_r + \sigma_\theta \qquad (2.17)$$

$$\tau_{oct} = \frac{1}{3}\sqrt{(\sigma_z - \sigma_r)^2 + (\sigma_z - \sigma_\theta)^2 + (\sigma_r - \sigma_\theta)^2} \qquad (2.18)$$

where M_R = resilient modulus; k_1, k_2, k_3 = regression constants; P_a = atmospheric

pressure; θ = bulk stress; τ_{oct} = in situ octahedral shear stress; σ_z = in situ vertical stress;

σ_r = in situ radial stress; and σ_θ = in situ tangential stress. The regression constants k_1,

k_2, and k_3 are material specific properties, so pavement design engineers must determine

the regression constants from laboratory resilient modulus testing.

Level 2 and level 3 pavement foundation stiffness design inputs are based on linear

elastic resilient modulus values. The level 2 resilient modulus input can be determined

from either laboratory resilient modulus testing or correlations with related properties

such as CBR. The level 3 resilient modulus input is determined from material soil classifications.

2.2.2 Pavement foundation enhanced integrated climatic model (EICM) inputs

The MEPDG combines pavement foundation drainage properties and seasonal effects on pavement foundation stiffness into a single input category relating to the MEPDG's enhanced integrated climatic model (EICM). For the level 1 design input, the pavement design engineering inputs material index properties (e.g., plasticity index) and gradation properties (e.g., effective size). In the level 2 design input, the pavement design engineer inputs different resilient moduli for the different seasons. The level 3 design input simply requires a single value for effective resilient modulus (equations 2.5 and 2.6).

2.3 Verification of Pavement Foundation Design Parameters During Construction

With regards to verification of design parameters during construction, the AASHTO (1993) Design Guide and the MEPDG are identical. Both design guides do not take into account quality control (QC) and quality assurance (QA) procedures for attaining pavement foundation design values during construction. The lack of QC and QA procedures is a severe limitation in both design guides.

Christopher, Schwartz, & Boudreau (2006) provide recommendations for QC and QA testing for pavement foundation design inputs. Traditional methods include proof rolling and nuclear density gauge testing, however these test methods do not provide performance-related parameters. Emerging technologies that can be used for QC and QA testing for performance-related parameters include the dynamic cone penetrometer, plate load test, falling weight deflectometer, light weight deflectometer, field CBR test, and the GeoGauge. Each of these methods accounts for stiffness and can be correlated to design

inputs (i.e., resilient modulus). Commentary on the verification of pavement foundation verification testing should be incorporated into the design guides because pavement designs can be updated based on the results of testing.

2.4 References

American Association of State Highway and Transportation Officials (AASHTO). (1986). *AASHTO Guide for Design of Pavement Structures.* Washington, DC: American Association of State Highway and Transportation Officials.

American Association of State Highway and Transportation Officials (AASHTO). (1993). *AASHTO guide for design of pavement structures.* Washington, DC: American Association of State Highway and Transportation Officials.

Burmister, D. M. (1945). The general theory of stresses and displacements in layered systems: I. *Journal of Applied Physics, 16*(89), 89-94. doi: 10.1063/1.1707558

Christopher, B. R., Schwartz, C., & Boudreau, R. (2006). *Geotechnical aspects of pavements. Federal Highway Administration* (NHI-05-037). Washington, DC: Federal Highway Administration.

Epps, J.A., Hand, A., Seeds, S., Schulz, T., Alavi, S., Ashmore, C., Monismith, C.L., Deacon, J.A., Harvey, J.T., & Leahy, R. (2002). *Recommended performance-related specification for hot-mix asphalt construction: Results of the WesTrack project* (NCHRP 455). Washington, DC: National Cooperative Highway Research Program.

Huang, Y.H. (2004). *Pavement analysis and design*. Upper Saddle River: Pearson Prentice Hall.

National Cooperative Highway Research Program (NCHRP). (2004). *Guide for mechanistic-empirical design of new and rehabilitated pavement structures* (NCHRP 1-37A). Washington, DC: National Cooperative Highway Research Program.

Van Til, C.J., McCullough, B.F., Vallerga, B.A., & Hicks, R.G. (1972). *Evaluation of AASHO interim guides for design of pavement structures* (NCHRP 128). Washington, DC: National Cooperative Highway Research Program.

Table 2.1. Typical values for k_1 and k_2 for determining subbase elastic modulus [after AASHTO (1993)]

Moisture condition	k_1	k_2
Dry	6,000 – 8,000	0.4 – 0.6
Wet	4,000 – 6,000	0.4 – 0.6
Damp	1,500 – 4,000	0.4 – 0.6

Note: For θ and $M_{R(SB)}$ in psi (1 psi = 6.89 kPa)

Table 2.2. Typical in situ bulk stress values for determining subbase resilient modulus [after AASHTO (1993)]

Asphalt concrete thickness (mm)	In situ bulk stress (kPa)
< 51	68.9
51 – 102	51.7
> 102	34.4

Table 2.3. Recommended subbase drainage coefficients (m_{SB}) for flexible pavement design [after AASHTO (1993)]

Quality of Drainage		Percentage of time pavement structure is exposed to moisture levels approaching saturation			
Rating	Water removed within	< 1%	1 – 5%	5 – 25%	> 25%
Excellent	2 hours	1.40 – 1.35	1.35 – 1.30	1.30 – 1.20	1.20
Good	1 day	1.35 – 1.25	1.25 – 1.15	1.15 – 1.00	1.00
Fair	1 week	1.25 – 1.15	1.15 – 1.05	1.00 – 0.80	0.80
Poor	1 month	1.15 – 1.05	1.05 – 0.80	0.80 – 0.60	0.60
Very Poor	Never drain	1.05 – 0.95	0.95 – 0.75	0.75 – 0.40	0.40

Table 2.3. Recommended subbase drainage coefficients (C_d) for rigid pavement design [after AASHTO (1993)]

Quality of Drainage		Percentage of time pavement structure is exposed to moisture levels approaching saturation			
Rating	Water removed within	< 1%	1 – 5%	5 – 25%	> 25%
Excellent	2 hours	1.25 – 1.20	1.20 – 1.15	1.15 – 1.10	1.10
Good	1 day	1.20 – 1.15	1.15 – 1.10	1.10 – 1.00	1.00
Fair	1 week	1.15 – 1.10	1.10 – 1.00	1.00 – 0.90	0.90
Poor	1 month	1.10 – 1.00	1.00 – 0.90	0.90 – 0.80	0.80
Very Poor	Never drain	1.00 – 0.90	0.90 – 0.80	0.80 – 0.70	0.70

CHAPTER 3. ASSESSING SOIL STIFFNESS OF STABILIZED PAVEMENT FOUNDATIONS

David J. White, Peter Becker, Pavana K.R. Vennapusa, Mark Dunn, and Christianna White

3.1 Abstract

The quality of constructed pavement foundation layers was studied with rapid and near-continuous soil stiffness measurements as alternatives to traditional nuclear gauge moisture-density measurements. Sixteen sections of stabilized pavement foundations covering 7.7 km, with ground conditions ranging from soft to very stiff, were studied. Measurements from falling weight deflectometer, light weight deflectometer, dynamic cone penetrometer, and roller-integrated compaction monitoring systems were used to assess soil stiffness. Statistical analyses of the results were reported in the form of coefficient of variation and empirical correlations between measurements. Results of soil stiffness were compared with two independent groups of nuclear moisture-density measurements to demonstrate some of the shortcomings of traditional nuclear gauge testing for quality assessment. The findings from this paper show the value in using soil stiffness measurements to characterize ground variations. Cost data are also reported for the stabilized sections.

3.2 Introduction

Use of stiffness/strength based quality control (QC) and quality assurance (QA) procedures in pavement foundation layer construction is gaining significant interest among the state and federal agencies in the U.S. Newcomb and Birgisson (1999) and Puppala (2008) summarized many in situ test methods that have been developed over the past five decades for characterizing stiffness or strength based properties of pavement foundation layers. Non-destructive testing methods, such as falling weight deflectometer (FWD) and light weight deflectometer (LWD), and intrusive test methods, such as dynamic cone penetrometer (DCP) tests, are the most common among the various stiffness- or strength-based QC/QA test methods. These tests provide rapid measurements of elastic modulus or shear strength of compacted material in situ, which are useful to verify design assumptions.

Recently, there has been increasing interest in incorporating roller-integrated compaction monitoring (RICM) technologies (i.e., intelligent compaction) in earthwork construction and relating their measurements to pavement design parameters (Mooney et al., 2010; White, Vennapusa, Zhang, Gieselman, & Morris, 2009). RICM technologies involve sensors and control systems that are integrated in the machine to provide a record of machine-ground interaction in real time to roller operators through computer displays. Using RICM values for QC/QA can be a paradigm shift from traditional earthwork construction practices. However, challenges exist with interpreting measurements and linking RICM values to traditional in situ measurements. Significant efforts have been made over the past three decades in developing and understanding empirical relationships between different RICM technologies and soil mechanistic properties (Brandl & Adam,

1997; Floss, Bräu, Gahbauer, Gruber, & Obermayer, 1991; Forssblad, 1980; Kröber, Floss, & Wallrath, 2001; Mooney et al., 2010; Preisig, Caprez, & Ammann, 2003; Samaras, Lamm, & Treiterer, 1991; Thompson & White, 2008a; Thompson & White, 2008b; Thurner & Sandström, 1980; Vennapusa, White, & Morris, 2010; White, Thompson, & Vennapusa, 2007a; White, Thompson, & Vennapusa, 2007b; White, Thompson, Vennapusa, & Siekmeier, 2008; White, Vennapusa, & Gieselman, 2012; White, Vennapusa, Gieselman, Johanson, & Siekmeier, 2009). Many researchers have documented that RICM values are better correlated with strength/stiffness based measurements (e.g., FWD, DCP) than with density measurements (Floss et al., 1991; Forssblad, 1980; Mooney et al., 2010; White et al., 2012; White et al., 2009).

Although traditional density-based QC/QA test methods are not normally used to assess performance characteristics of stabilized layers, stiffness-based QC/QA tests and RICM technologies are particularly well suited for stabilized pavement foundations. The QC/QA methods and RICM technologies discussed in this paper provide performance-related parameters that transportation agencies can use to develop specifications for constructing stabilized pavement foundations.

The project described in this paper was designed by the Iowa Department of Transportation (DOT) to assess soil stiffness based measurements in comparison to traditional nuclear density gauge testing. The 7.7 km test area incorporated several 200 m long sections of stabilization with the goals of (1) developing local experience with new stiffness measurement technologies to assist with near-term implementation; (2) increasing the range of stabilization technologies to be considered for future pavement foundation design to optimize the pavement system, and (3) constructing a test area that

will allow long-term performance monitoring. Geosynthetics, chemical stabilizers, and recycling of existing materials were developed into a matrix of sixteen different test sections. This paper reports the findings of in situ measurements during and shortly after construction, material and placement unit costs, and comparisons between the soil stiffness measurements. Agencies interested in soil stiffness measurements as an alternative to nuclear density testing and optimization of the pavement system through foundation stabilization will find this paper of interest.

3.3 Project Conditions

The project was constructed in Boone, Iowa in May–July 2012. In brief, the test site subgrade conditions primarily consisted of soils classified as CL or A-6(5). The ground water table was about 0.9 to 1.5 m below grade. In general, construction required the removal of 152 to 305 mm of subgrade from each test section. Select test sections were backfilled with 305 mm of recycled subbase classified as SM or A-1-a (14% fines content). All sections were topped with a nominal 305 mm of crushed limestone subbase classified as GP-GM or A-1-a (7% fines content). One exception was the 305 mm geocell section that required 178 mm of crushed limestone. Over the length of the 7.7 km of roadway, 16 different sections were constructed: woven and non-woven (NW) geosynthetic materials placed at the subgrade/crushed limestone subbase interface; triaxial and biaxial geogrids placed at the subgrade/crushed limestone subbase interface; 102 mm and 152 mm geocell sections filled with crushed limestone subbase; cement (PC) and fly ash stabilization of the subgrade layer; cement stabilization of the recycled subbase layer; fiber stabilization of the subbase layer with polypropylene (PP) fibers and monofilament-polypropylene (MF-PP) fibers; and mechanical stabilization by mixing the

subgrade with the recycled subbase. The test sections are noted by street name and north or south orientation (e.g., 1st N) in Figures 3.3, 3.4, 3.6, and 8 and in Table 3.1. Detailed information about the various mixtures and products and detailed cross-sections is beyond the scope of the paper, but can be obtained from the authors.

Figure 3.1 summarizes the combined material and installation costs for the test sections used on this project. The cost data was compiled from all six contractor bidders' unit prices as requested in the plans and specifications. Geosynthetics are at the low end of the cost range, chemical stabilization is at the intermediate range, and special products (fibers and geocell) are at the high end of the range. The quantities used on this project ranged from about 140 m^2 to 420 m^2.

3.4 In Situ Testing Methods

A brief overview of the FWD, LWD, and DCP test measurement procedures and the two RICM technologies—compaction meter value (CMV) and machine drive power (MDP)—used in this paper are described in the following sections.

3.4.1 Light weight deflectometer (LWD)

Light weight deflectometer (LWD) tests were conducted using a Zorn LWD setup with 300 mm diameter plate and 0.71 m drop height. The tests were conducted following manufacturer recommendations (Zorn, 2003). Elastic modulus values were determined using equation 3.1, where E = elastic modulus (MPa), D_o = measured deflection under the plate (mm), v = Poisson's ratio (assumed as 0.4), σ_o = applied stress (MPa), r = radius of the plate (mm), f = shape factor depending on stress distribution (assumed as 8/3) (Vennapusa & White, 2009). The modulus values determined from LWD test are reported herein as E_{SB-LWD}.

$$E = \frac{\sigma_o r(1 - v^2)f}{D_o} \qquad (3.1)$$

3.4.2 Falling weight deflectometer (FWD)

Falling weight deflectometer (FWD) tests were conducted using a Kuab FWD setup with 300 mm diameter loading plate by applying one seating drop and four loading drops. The applied loads varied from about 22 kN to 67 kN in the four loading drops. The actual applied forces were recorded using a load cell and deflections were recorded using seismometers mounted on the device. Elastic modulus values from the FWD tests (E_{SB-FWD}) were determined using equation 3.1.

The loading plate used in this study consisted of a segmented plate leading to uniform stress distribution; therefore, the shape factor F was assumed as 2 in equation 3.1. To compare E_{SB-FWD} from different test locations at same applied contact stress, the deflection values at each test location were normalized to a 62 kN load. As discussed later in this paper, the plate contact stress at 62 kN load corresponds to in ground stress under roller in vibratory compaction mode.

3.4.3 Dynamic cone penetrometer (DCP)

Dynamic cone penetrometer (DCP) tests were conducted in accordance with ASTM D6951. The test involves dropping an 8 kg hammer from a height of 0.575 m and measuring the resulting penetration. California bearing ratio (CBR) values were determined using equation 3.2, where CBR = California bearing ratio, PI = penetration index (mm/blow).

$$CBR = \frac{292}{PI^{1.12}} \qquad (3.2)$$

3.4.4 Roller integrated compaction monitoring system (RICM)

A Caterpillar CS683 vibratory smooth drum roller weighing 13,200 kg equipped with roller integrated compaction monitoring system (RICM) was used on this project. The machine's RICM system consisted of recording and displaying compaction meter value (CMV), resonant meter value (RMV), machine drive power (MDP), and machine operating conditions (i.e., roller speed, vibration amplitude, vibration frequency) integrated with real time kinematic (RTK) GPS measurements (i.e., northing, easting, and elevation) in real time.

3.4.4.1 Compaction meter value (CMV) and resonant meter value (RMV)

CMV is a dimensionless compaction parameter developed by Geodynamik that depends on roller dimensions, (i.e., drum diameter and weight) and roller operation parameters (e.g., frequency, amplitude, speed), and is determined using the dynamic roller response (Sandström, 1994). CMV is calculated using equation 3.3, where C is a constant (300), $A_{2\Omega}$ = the acceleration of the first harmonic component of the vibration, A_{Ω} = the acceleration of the fundamental component of the vibration (Sandström & Petterson, 2004). Correlation studies relating CMV to soil dry unit weight, strength, and stiffness are documented in the literature (Brandl & Adam, 1997; Floss, Gruber, & Obermayer, 1983; Samaras et al., 1991; Sandström & Petterson, 2004; Thompson & White, 2007; Vennapusa, White, & Gieselman, 2009; White, Jaselskis, Schaefer, & Cackler, 2005; White et al., 2012).

$$CMV = C \times \frac{A_{2\Omega}}{A_{\Omega}} \tag{3.3}$$

RMV provides an indication of the drum behavior (e.g. continuous contact, partial uplift, double jump, rocking motion, and chaotic motion) and is calculated using equation 3.4, where $A_{0.5\Omega}$ = sub-harmonic acceleration amplitude caused by jumping (the drum skips every other cycle). It is important to note that the drum behavior affects the CMV measurements (Brandl & Adam, 1997) and therefore must be interpreted in conjunction with the *RMV* measurements (Vennapusa et al., 2010; White et al., 2008).

$$RMV = C \times \frac{A_{0.5\Omega}}{A_\Omega} \tag{3.4}$$

3.4.2 Machine drive power (MDP) value

Caterpillar's MDP technology relates mechanical performance of the roller during compaction to the properties of the compacted soil. Detailed background information on the MDP system is provided by White et al. (2005). Controlled field studies documented by White and Thompson (2007); Thompson and White (2008); and Vennapusa, White, and Giesleman (2009) verified that MDP values are empirically related to soil compaction characteristics (e.g., density, stiffness, and strength). MDP is calculated using equation 3.5:

$$MDP = P_g - W_v \left(\sin \alpha + \frac{\acute{A}}{g} \right) - (mv + b) \tag{3.5}$$

where MDP = machine drive power [lb-ft/s (1 lb-ft/s = 1.36 watts)], P_g = gross power needed to move the machine [lb-ft/s (1 lb-ft/s = 1.36 watts)], W = roller weight [lb (1 lb = 0.45 kg)], $\acute{A}$ = machine acceleration [ft/sec² (1 ft/sec² = 0.31 m/s²)], g = acceleration of gravity [ft/sec² (1 ft/sec² = 0.31 m/s²)], α = slope angle (roller pitch from a sensor), v = roller velocity [ft/sec (1 ft/sec = 0.31 m/s)], and m [lb-ft/ft (1 lb-ft/ft = 0.45 kg-m/m)] and b [lb-ft/s (1 lb-ft/s = 1.36 watts)] = machine internal loss coefficients specific to a

particular machine (White et al., 2005). MDP is a relative value referencing the material

properties of the calibration surface, which is generally a hard compacted surface [MDP

= 0 lb-ft/s (1 lb-ft/s = 1.36 watts)]. Positive MDP values therefore indicate material that is

less compact than the calibration surface, while negative MDP values indicate material

that is more compacted than the calibration surface (i.e., less roller drum sinkage). The

MDP values obtained from the machine were recalculated to range between 1 and 150,

and these re-scaled values are referred to as $MDP*$. While the original MDP values

decrease in increasing compaction, the $MDP*$ values increase with increasing

compaction.

A recent study documented by White et al. (2012) on a Caterpillar's CS74 vibratory

smooth drum roller indicated that the $MDP*$ values are influenced by the direction of

travel. This is because the $MDP*$ measurements represent the mechanical performance

of the whole roller, which are affected by the roller-soil interaction at the front drum and

the rear tires, but the results are only reported at the center of the drum. The offset

distance for $MDP*$ measurements was observed to be about 2.60 m behind the drum

center. Therefore, the $MDP*$ values at 2.60 m offset distance was used for correlation

analysis presented in this paper.

3.5 Analysis of Field Test Results

To assess the as-constructed conditions for the 16 different pavement foundation

sections, a test plan was devised to determine soil stiffness using FWD and LWD point

measurements. About 10 tests were performed in each of the test sections. Results were

used to correlate with the RICM measurements (CMV and MDP). DCP tests were

performed approximately 3 months after construction. An array of 102 mm diameter

piezoelectric earth pressure cells were carefully installed under one of the test sections to measure the dynamic vertical stress at depths from about 0.3 m to 1.5 m below the top of the crushed limestone subbase. The stress cell measurements results were used to assess the measurement influence depth for each of the in situ test devices. RICM maps were generated to show the spatial variability of stiffness throughout the site and between sections. Comparisons are made with the QC/QA nuclear density gauge testing throughout the site.

3.5.1 Measurement influence depth for stiffness measurements

To implement soil stiffness measurements, the assessment of measurement influence depth (MID) is needed so that the measurement value is assigned to a volume of soil beneath the test device. It has been demonstrated that RICM values are influenced by ground conditions to depths of about 0.3 m to more than 0.9 m (Floss et al., 1983; Mooney et al., 2010; Thompson & White, 2007; Vennapusa, White, Siekmeier, & Embacher, 2012; White et al., 2009;). An influence zone can be defined as analogous to a strip footing where the depth of influence is proportional to the footing width and length. Complicating factors for determining influence depth include layered soft to stiff materials and setting a value for stress increase. In this paper, the authors assigned MID based on a total vertical stress increase equal to 10 psi (1 psi = 6.89 kPa) as the defining value. This simple approach eliminates more complicated analyses that require assumptions for unknown parameters. The MID values are shown in Figure 3.2. Establishing MID values is important as part of understanding analyses of correlations between test devices and in determining remedial actions for areas of non-compliance—is it a shallow problem or an unstable deeper layer?

3.5.2 Comparison of soil stiffness measurements

Figure 3.3 shows the summary results of the FWD and LWD measurements for each test section. The sections with fly ash and cement stabilized subgrade produced the highest stiffness values. Figure 3.4 establishes the correlations between FWD and LWD results. The correlation analysis indicates that LWD MID values are lower than FWD MID values, and that FWD MID values better reflect stiff underlying layers better than LWD measurements. Note that the FWD and LWD results from 11th St. show increased differences in moduli due to differences in the MID. 11st St. included a subgrade stabilized layer 305 mm below the surface.

Figure 3.5 shows the summary results of the CBR measurements for each layer within the test sections. Generally, CBR values within the test sections are consistent with the FWD and LWD results. The exception however is the polymer grid test sections, which produced CBR values higher than most of the other test sections. The sections underlain by stiff layers (e.g., cement stabilized subgrade) produced the highest CBR values within the crushed limestone subbase layer.

Figure 3.6 summarizes RICM measurement results. RICM correlations analyses with FWD and LWD are presented in Figure 3.7. Results show that the CMV measurements are better correlated to FWD than LWD for the range of materials and conditions tested at this site. The FWD produced vertical stress conditions more similar to the roller in comparison with the LWD vertical stress profile (see Figure 3.2). Geospatially referenced maps of the CMV and $MDP*$ values for low amplitude vibratory operations are presented in Figure 3.8. Follow-up RICM mapping is planned after the 2013 spring thaw in Iowa to give a measure of the durability of the treated sections. Note that the installation of the

geosynthetic sections was to aid in control of rutting/permanent deformation and to provide a durable layer during spring thaw, because drawing conclusions of "effectiveness" solely based on as-constructed stiffness measurements would not necessarily be a complete assessment of the benefits of the products.

Table 3.1 summarizes the average values for the various measurements for each test section. The coefficients of variation (COV) values are also reported for each section. It is worth noting that the COV for CMV is in line with stiffness based values whereas the $MDP*$ is very low. Low COV values for $MDP*$ are attributed to a higher scaled value; lower sensitivity to variations in stiffness of underlying layers (i.e., lower MID) compared to the CMV measurements; and lower sensitivity to variations in stiffness for very stiff materials.

3.5.3 Shortcomings of nuclear density gauge testing

Traditional nuclear gauge moisture-density testing has played an important role in earthwork quality assessment specifications in the U.S. for decades. This form of QC/QA can be effective, but has shortcomings due to regulations, test reproducibility, limited test frequency, and only serving as a surrogate to strength and stiffness design requirements. Figure 3.9 shows the QC agent and QA agent test results for the project described herein. Results show that the QC agent results all meet the minimum 95% criteria and ±2% moisture control criteria. In contrast, the QA agent results are much more variable on both accounts. At this point, one could only speculate about these differences. It is clear though that the nuclear density testing does not indicate the wide stiffness variations resulting from treatments and materials.

The distinct advantage of FWD and LWD soil stiffness measurements on this project is the identification of variations in support values between different stabilization sections that will provide inputs to the pavement thickness design phase of the project (to be completed in 2013). The advantage of RICM measurements is that they are reported electronically on a near-continuous basis and are available to the contractor in real-time such that the construction process can be controlled around identifying "soft spots" that need remediation and achieving design target values.

The primary weakness with soil stiffness assessment is that moisture control remains the critical factor in the construction process. Although moisture-strength and moisture-stiffness relationships developed in situ or from laboratory tests address this aspect, describing these processes is beyond the scope of this paper.

3.6 Summary and Key Conclusions

This paper compares soil stiffness measurements with two roller-integrated compaction monitoring results. Sixteen different pavement foundation stabilization materials that covered 7.7 km were compared. Cost data that includes installation was provided for the stabilization materials. The key findings presented in this paper are as follows:

- Cost, average stiffness values, and COV were reported for all of the pavement foundation sections. Analysis of this data is useful to optimize pavement foundation design.

- Measurement influence depth can be assessed from piezoelectric earth pressure cells and selection of a target vertical stress increase [+10 psi (1 psi = 6.89 kPa)]used in this paper].

- Regression analysis demonstrated that the LWD is correlated to the FWD, but does not reflect stiff underlying layers as measured from the FWD. The measurement influence depth is greater for the FWD compared to the LWD. Ground stresses were higher for the FWD.

- The roller-integrated compaction values (CMV and $MDP*$) provided near-continuous electronic records of ground stiffness and showed variations between the test sections and locations of lower stiffness materials within sections.

- The CMV values correlated better to the LWD and FWD values than $MDP*$ values. CMV values correlated better to FWD values than LWD values.

- The QC/QA nuclear density testing showed that this approach to quality assessment can lead to shortcomings (including lack of reproducibility and infrequent testing) and does not capture the wide range in stiffness values measured from the other devices.

3.7. References

Brandl, H., & Adam, D. (1997). Sophisticated continuous compaction control of soils and granular materials. *Proceedings of the 14th International Conference on Soil Mechanics and Foundation Engineering*. (pp. 1–6).

Floss, R., Bräu, G., Gahbauer, M. Gruber, N., & Obermayer, J. (1991) Dynamische verdichtungsprüfung bei erd-und straßenbauten. *Prüfamt fur Grundbau, Boden-und Felsmechanik Technische Universität München, Heft 612.*

Floss, R., Gruber, N., & Obermayer, J. (1983). A dynamical test method for continuous compaction control. In Rathmayer, H.G. & Saari, K. H. O. (Eds.), *Improvement of*

ground: Proceedings of the 8th European Conference on Soil Mechanics and Foundation Engineering (pp. 25–30). Exton: A. A. Balkema Publishers.

Forssblad, L. (1980). Compaction meter on vibrating rollers for improved compaction control. *Proceedings of the International Conference on Compaction: Vol. 2.* (pp. 541–546).

Kröber, W., Floss, E., & Wallrath, W. (2001). Dynamic soil stiffness as quality criterion for soil compaction. In A. Gomes Correia & H. Brandl (Eds.), *Geotechnics for roads, rail tracks and earth structures* (pp. 189-199). Exton: A. A. Balkema Publishers.

Mooney, M., Rinehart, R., White, D.J., Vennapusa, P., Facas, N., & Musimbi, O. (2010). *Intelligent soil compaction systems* (NCHRP Report 676). Washington, DC: National Cooperative Highway Research Program.

Newomb, D.E., & Birgisson, B. (1999). *Measuring in situ mechanical properties of pavement subgrade soils.* Washington, DC: National Academy Press.

Preisig, M., Caprez, M., & Ammann, P. (2003). Validation of continuous compaction control (CCC) methods. *Workshop on Soil Compaction*, Hamburg.

Puppala, A. (2008). *NCHRP synthesis 382: Estimating stiffness of subgrade and unbound materials for pavement design*. Washington, DC: Transportation Research Board of the National Academies.

Samaras, A.A., Lamm, R., & Treiterer, J. (1991). Application of continuous dynamic compaction control for earthworks in railroad construction. *Transportation Research Record,* 1309, 42–46.

Sandström, Å. (1994). *Numerical simulation of a vibratory roller on cohesionless soil.* Retrieved from Geodynamik website: http://www.geodynamik.com/languages/pdf/Simvib2.pdf

Sandström Å., & Pettersson, C.B. (2004). Intelligent systems for QA/QC in soil compaction [CD]. *Proceedings of the 83rd Annual Meeting of the Transportation Research Board*, Washington, D.C.

Thompson, M., & White, D.J. (2007). Field calibration and spatial analysis of compaction monitoring technology measurements. *Transportation Research Record*, 2004, 69–79.

Thompson, M. J., & White, D. (2008a). Relationships between in situ and roller-integrated compaction measurements for granular soils. *Journal of Geotechnical and Geoenvironmental Engineering, 134*(2), 1763–1770. doi: 10.1061/(ASCE)1090-0241(2008)134:12(1763)

Thompson, M. J., & White, D. (2008b). Estimating compaction of cohesive soils from machine drive power. *Journal of Geotechnical and Geoenvironmental Engineering, 134*(12), 1771–1777. doi: 10.1061/(ASCE)1090-0241(2008)134:12(1771)

Thurner, H., & Sandström, Å. (1980). A new device for instant compaction control. *Proceedings of the International Conference on Compaction: Vol. 2.* (pp. 611–614).

Vennapusa, P., & White, D.J. (2009). Comparison of light weight deflectometer measurements for pavement foundation materials. *Geotechnical Testing Journal, 32*(3), 239–251. doi: 10.1520/GTJ101704

Vennapusa, P., White, D.J., & Gieselman, H. (2009). Influence of support conditions on roller-integrated machine drive power measurements for Granular Base. In Iskander, M., Laefer, D. F., & Hussein, M. H. (Eds.), *Contemporary Topics in Ground Modification, Problem Soils, and Geo-Support* (pp. 425–432). Reston, VA: American Society of Civil Engineers.

Vennapusa, P., White, D.J., & Morris, M. Geostatistical analysis for spatially referenced roller-integrated compaction measurements. *Journal of Geotechnical and Geoenvironmental Engineering, (136)*6, 813–*822.* doi*:* 10.1061/(ASCE)GT.1943-5606.0000285

Vennapusa, P., White, D.J., Siekmeier, J., & Embacher, R. (2012). In Situ Mechanistic Characterizations of Granular Pavement Foundation Layers. *International Journal of Pavement Engineering*, 13(1). 52–67. *doi*: 10.1080/10298436.2011.564281

White, D.J., Jaselskis, E., Schaefer, V. & Cackler, T. (2005). Real-time Compaction Monitoring in Cohesive Soils from Machine Response. *Transportation Research Record,* 1936, 173–180.

White, D.J., & Thompson, M.J. (2008). Relationships between in situ and roller-integrated compaction measurements for granular soils. *Journal of Geotechnical and Geoenvironmental Engineering, 134*(12), 1763–1768. doi:10.1061/(ASCE)1090-0241(2008)134:12(1763)

White, D.J.,Thompson, M., & Vennapusa, P. (2007a). *Field validation of intelligent compaction monitoring technology for unbound materials* (MN/RC-2007-10). St. Paul: Minnesota Department of Transportation.

White, D.J., Thompson, M., & Vennapusa, P. (2007b). Field study of compaction monitoring systems: Self-propelled non-vibratory 825G and vibratory smooth drum CS-533 E rollers. Ames: Center of Transportation Research and Education.

White, D.J., Thompson, M., Vennapusa, P., & Siekmeier, J. (2008). Implementing intelligent compaction specification on Minnesota TH-64: Synopsis of measurement values, data management, and geostatistical analysis. *Transportation Research Record,* (2045), 1–9.

White, D.J., Vennapusa, P., Zhang, J., Gieselman, H., & Morris, M. (2009). *Implementation of intelligent compaction performance based specifications* (MN/RC 2009-14). St. Paul: Minnesota Department of Transportation.

White, D., Vennapusa, P., & Gieselman, H. (2011). Field assessment and specification review for roller-integrated compaction monitoring technologies. *Advances in Civil Engineering, 2011*, 15. doi: 10.1155/2011/783836

White, D.J., Vennapusa, P., Gieselman, H., Johanson, L., & Siekmeier, J. (2009). Alternatives to heavy test rolling for cohesive subgrade assessment. In Tutumluer, E. & Al-Qadi, I. L. (Eds.), *Bearing capacity of roads, railways and airfields: Proceedings of the 8th International Conference on the Bearing Capacity of Roads, Railways and Airfields* (pp.45–56). Illinois: CRC Press.

White, D.J., Vennapusa, P., Han, J., Christopher, B., Gieselman, H., Wang, S., Riko, W., Becker, P., Horhota, D., Pokharel, S., & Thakur, J. (2012). *Geotechnical Solutions for Soil Improvement, Rapid Embankment Construction, and Stabilization of the Pavement Working Platform: Compaction "Roadeo" Field Demonstration: Roller-*

Integrated Compaction Monitoring and Subgrade Geosynthetic Reinforcement.

Ames, IA: Center for Earthworks Engineering Research.

Zorn, G. (2003). Operating manual: Light drop-weight tester ZFG2000, Germany: Zorn

Instruments.

Table 3.1. Summary Statistics of In Situ Test Measurements on Each Road Segment

Street Name[fg]	Foundation Layer Description	$E_{SB\text{-}FWD}$[a] (MPa) [COV[b]%]	$E_{SB\text{-}LWD}$[a] (MPa) [COV[b]%]	CBR[c] in Crushed Limestone Subbase (%) [COV[b]%]	CBR[c] in Subgrade (%) [COV[b]%]	MDP*[d] [COV[b]%]	CMV[e] [COV[b]%]
1st S	Control	45 [24]	58 [25]	121 [25]	18 [21]	132 [3]	6 [48]
1st N	Control	57 [15]	77 [12]	134 [74]	10 [53]	121 [5]	6 [43]
2nd S	Mechanical Stabilization	65 [15]	81 [10]	90 [20]	20 [47]	120 [3]	6 [44]
2nd N	Mechanical Stabilization	51 [46]	64 [42]	107 [44]	19 [18]	121 [3]	7 [25]
3rd S	6 in. Geocell + NW Geotextile	25 [65]	22 [34]	83 [55]	13 [54]	124 [3]	3 [40]
3rd N	4 in. Geocell + NW Geotextile	28 [29]	23 [25]	48 [16]	18 [27]	124 [2]	4 [31]
4th S	Woven Geotextile	34 [19]	52 [30]	89 [65]	26 [52]	132 [4]	4 [43]
4th N	NW Geotextile	38 [39]	44 [42]	121 [23]	17 [36]	133 [4]	5 [42]
5th S	Biaxial Polymer Geogrid Geogrid	33 [28]	56 [28]	148 [34]	17 [42]	132 [4]	5 [42]
5th N	Triaxial Polymer	21 [39]	31 [44]	234 [38]	16 [42]	129 [6]	6 [39]
6th S	5% PC Subbase + MF-PP Fibers	73 [30]	84 [27]	252 [23]	9 15]	123 [3]	7 [43]
6th N	5% PC Subbase + PP Fibers	82 [32]	97 [18]	230 [24]	14 [91]	129 [6]	7 [33]

Notes: [e]CMV = compaction meter value
[f]S = south
[g]N = north
[a]E = elastic modulus
[b]COV = coefficient of variation
[c]CBR = California bearing ratio
[d]MDP* = machine drive power
[h]Data not available

Table 3.1. Summary statistics of in situ test measurements on each road segment (continued)

Street Name[fg]	Foundation Layer Description	$E_{SB\text{-}FWD}$[a] (MPa) [COV[b] %]	$E_{SB\text{-}LWD}$[a] (MPa) [COV[b] %]	CBR[c] in Crushed Limestone Subbase (%) [COV[b]%]	CBR[c] in Subgrade (%) [COV[b]%]	MDP*[d] [COV[b] %]	CMV[e] [COV[b] %]
7th S	5% PC Subbase	60 [16]	93 [12]	163 [39]	10 [20]	122 [2]	10 [35]
7th N	5% PC Subbase	95 [16]	106 [23]	232 [28]	15 [44]	123 [2]	6 [44]
8th S	Control	16 [5]	35 [22]	69 [24]	21 [23]	120 [6]	4 [53]
8th N	Control	20 [32]	55 [40]	91 [34]	32 [4]	124 [5]	6 [56]
9th S	Recycled Existing Base	62 [18]	104 [24]	399 [20]	[h]	136 [1]	8 [41]
9th N	Recycled Existing Base	57 [39]	79 [35]	178 [15]	17 [38]	133 [3]	14 [35]
10th S	Control	18 [21]	30 [32]	117 [27]	19 [18]	118 [3]	5 [43]
10th N	Control	35 [39]	62 [41]	112 [22]	14 [25]	127 [5]	5 [40]
11th S	20% Fly Ash Subgrade	147 [37]	119 [23]	117 [27]	19 [18]	137 [2]	52 [21]
11th N	10% PC Subgrade	304 [16]	148 [14]	644 [32]	131 [7]	145 [2]	28 [39]
12th S	10% Fly Ash Subgrade	98 [52]	124 [25]	186 [24]	33 [57]	137 [3]	21 [31]
12th N	15% Fly Ash Subgrade	138 [19]	137 [14]	204 [11]	56 [38]	137 [3]	18 [66]

Notes: [e]CMV = compaction meter value
[f]S = south
[g]N = north
[a]E = elastic modulus
[b]COV = coefficient of variation
[c]CBR = California bearing ratio
[d]MDP* = machine drive power
[h]Data not available
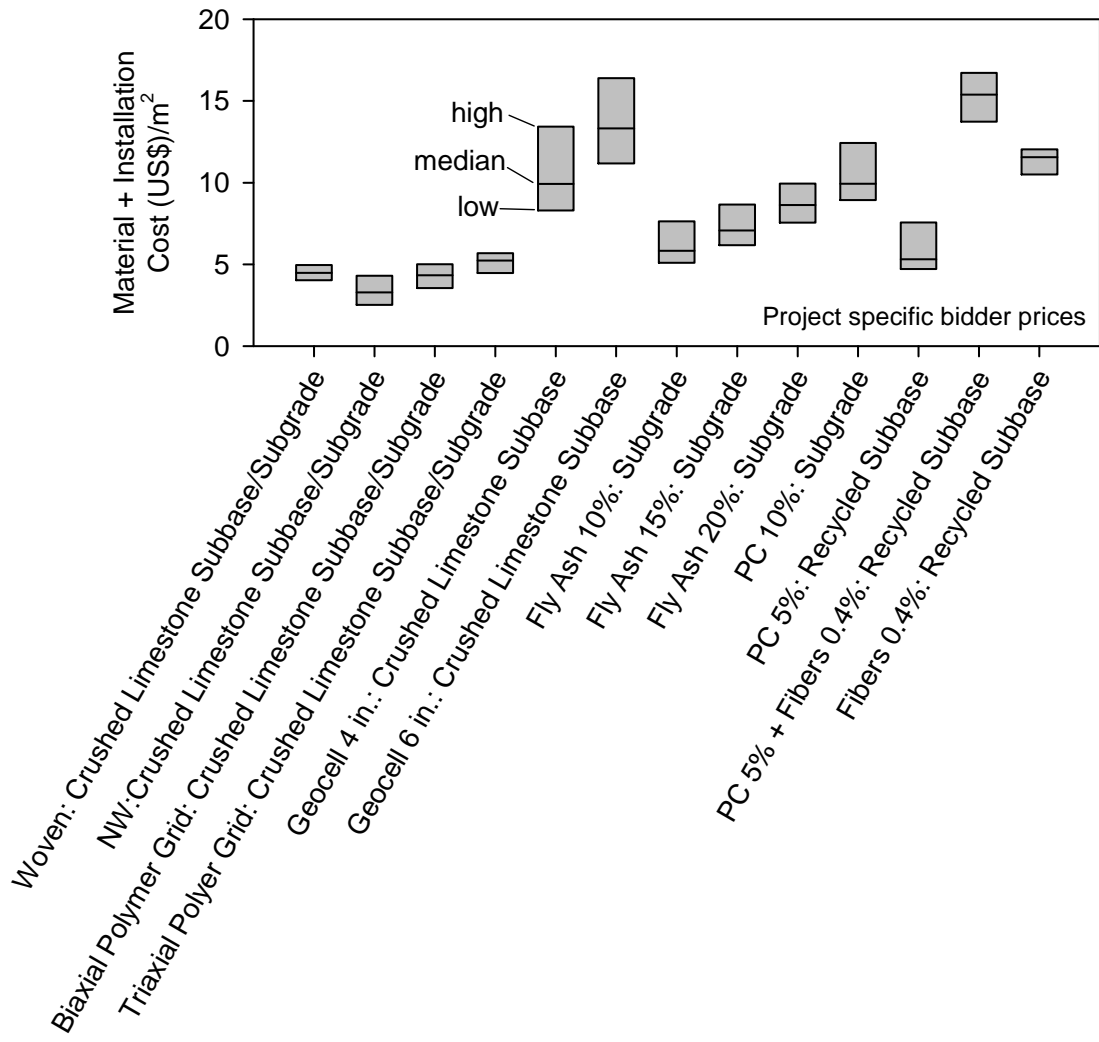
Figure 3.1. Bid prices for stabilization material + placement based on six bidders
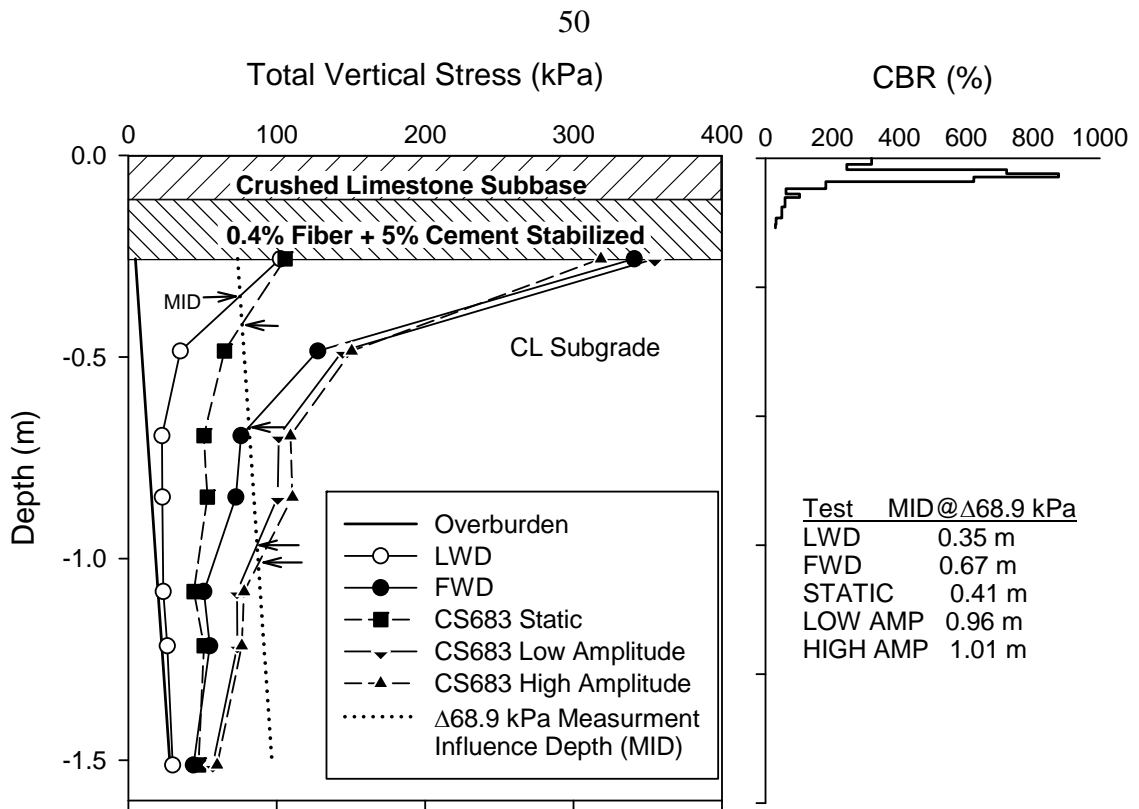
Figure 3.2. Measurement influence depth (MID) for LWD, FWD, and smooth drum roller using +10 psi criteria from piezoelectric earth pressure cells.
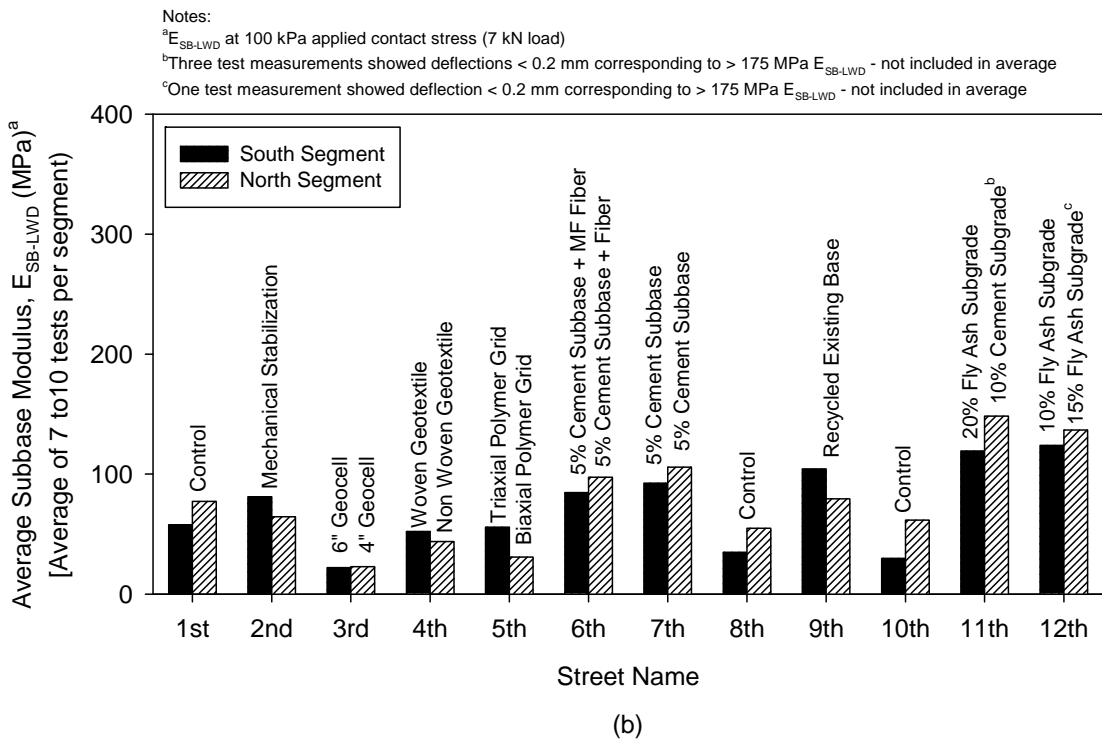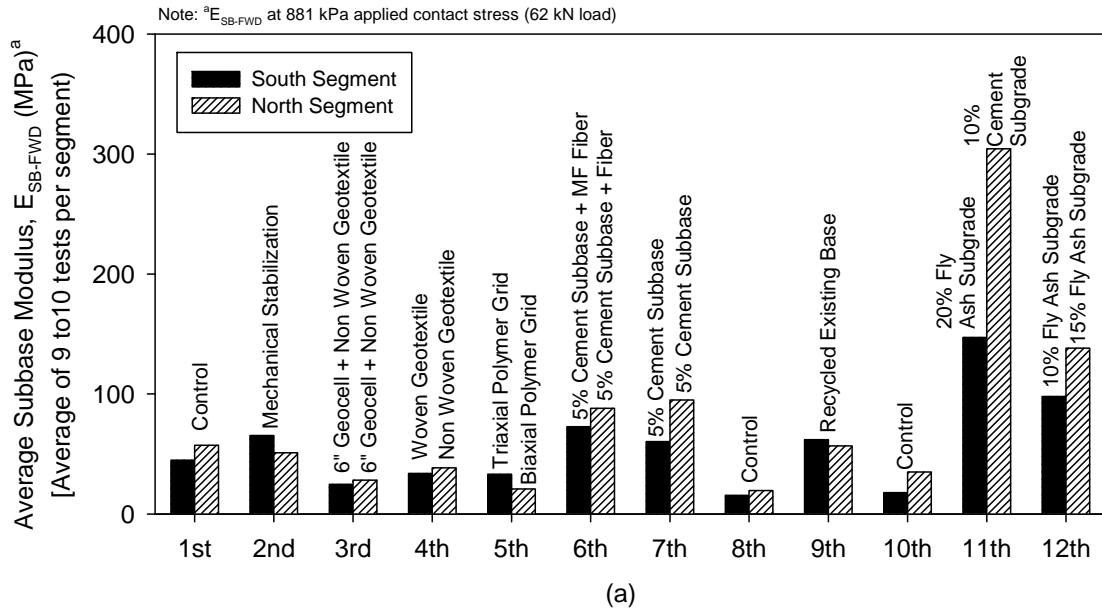
Figure 3.3. Average subbase elastic modulus measurements from (a) FWD tests and

(b) LWD tests on each segment.

(a)

(b)
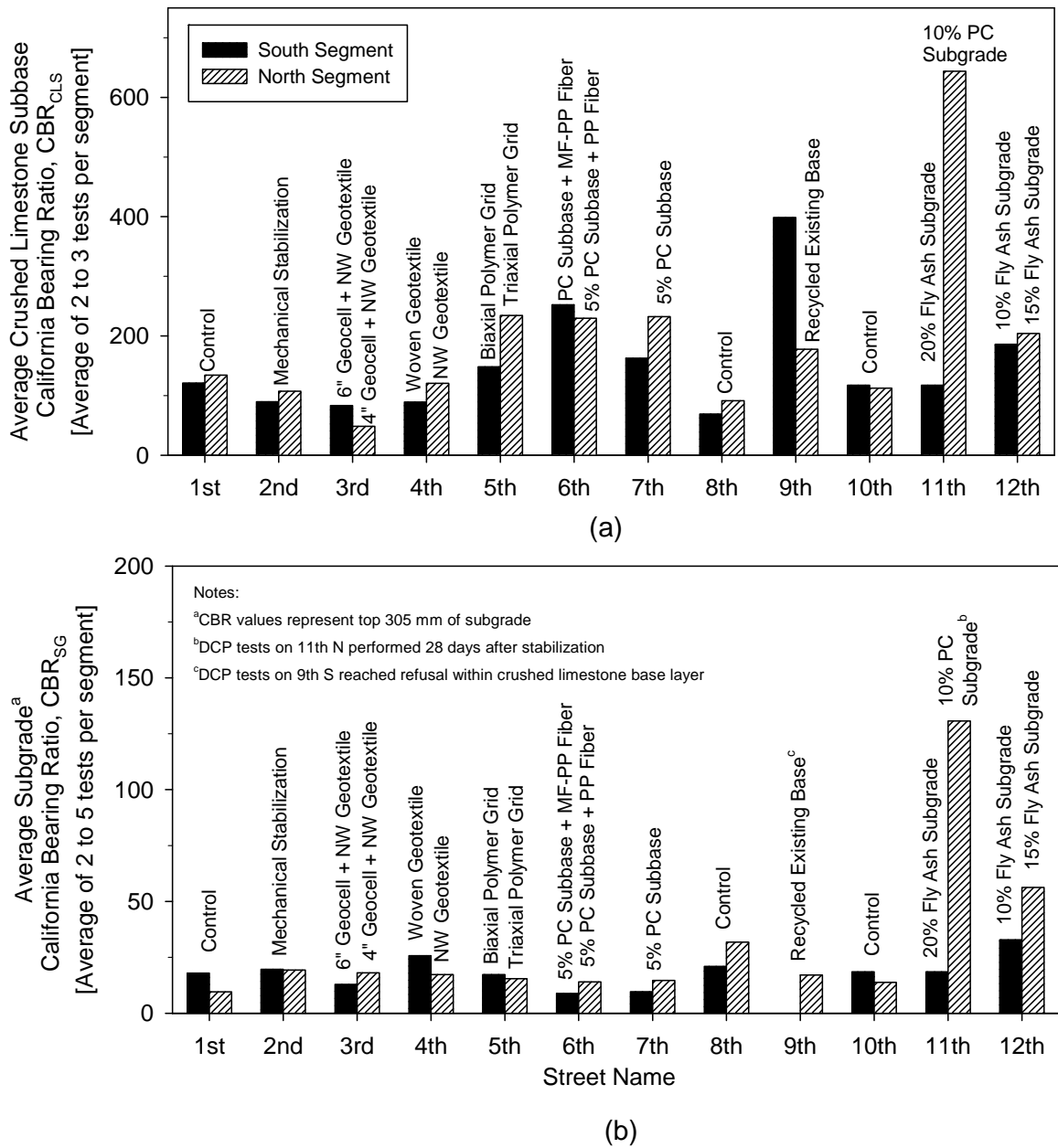
Figure 3.4. Average California bearing ratio from DCP tests within (a) crushed limestone subbase and (b) subgrade.
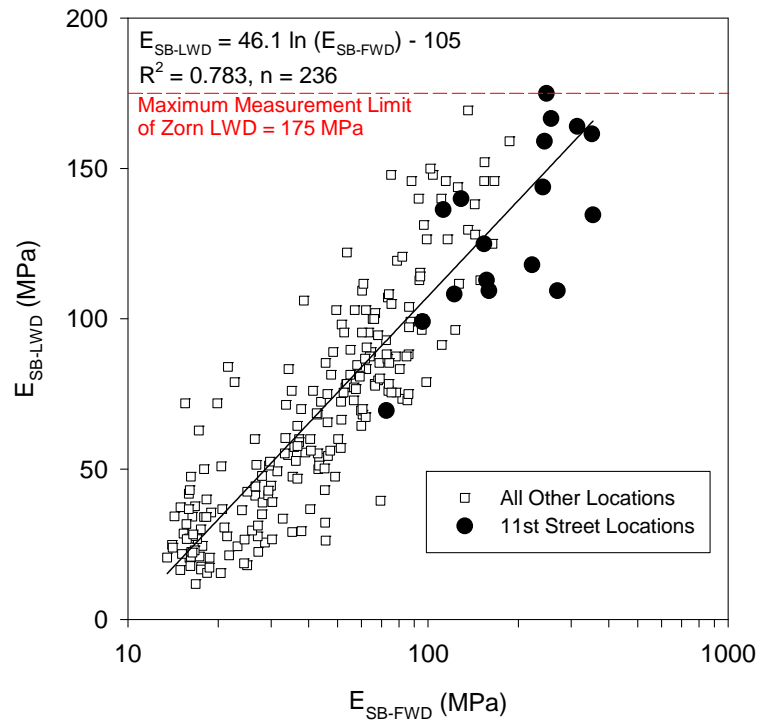
Figure 3.5. Correlations between subbase elastic modulus measurements from LWD and FWD tests (note log scale for FWD) that compare 11ᵗʰ St. with all other locations.

54
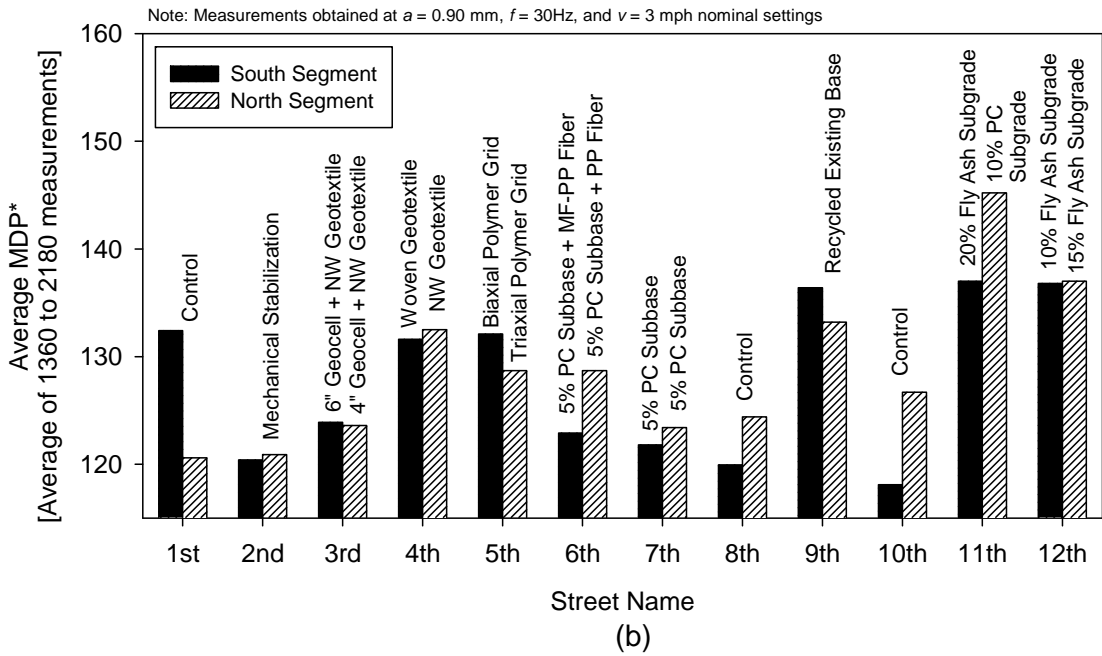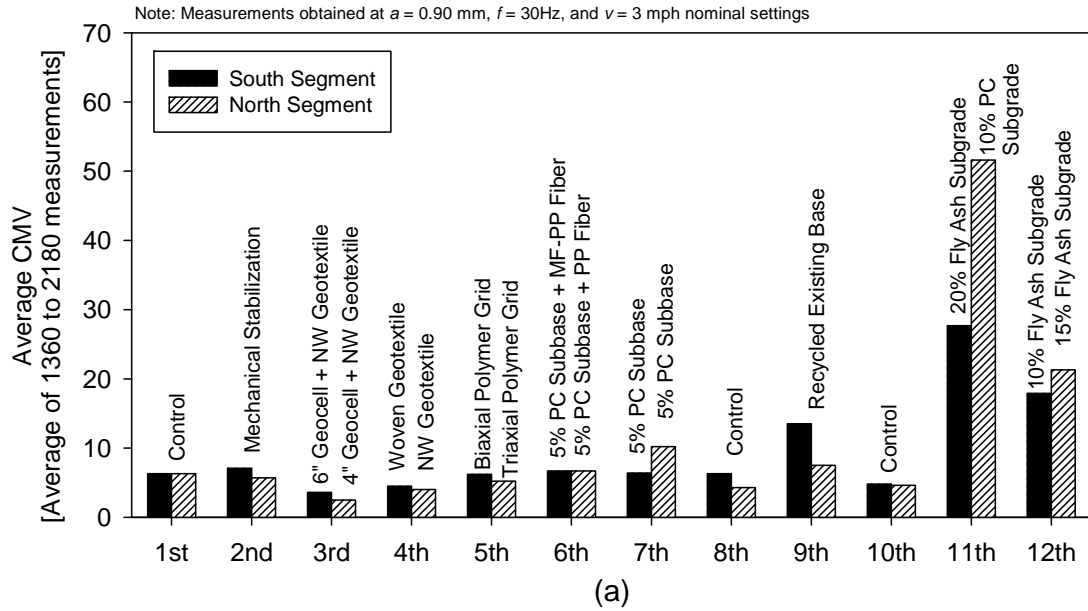
Figure 3.6. RICM results of each test segment: (a) average CMV and (b) average MDP*.
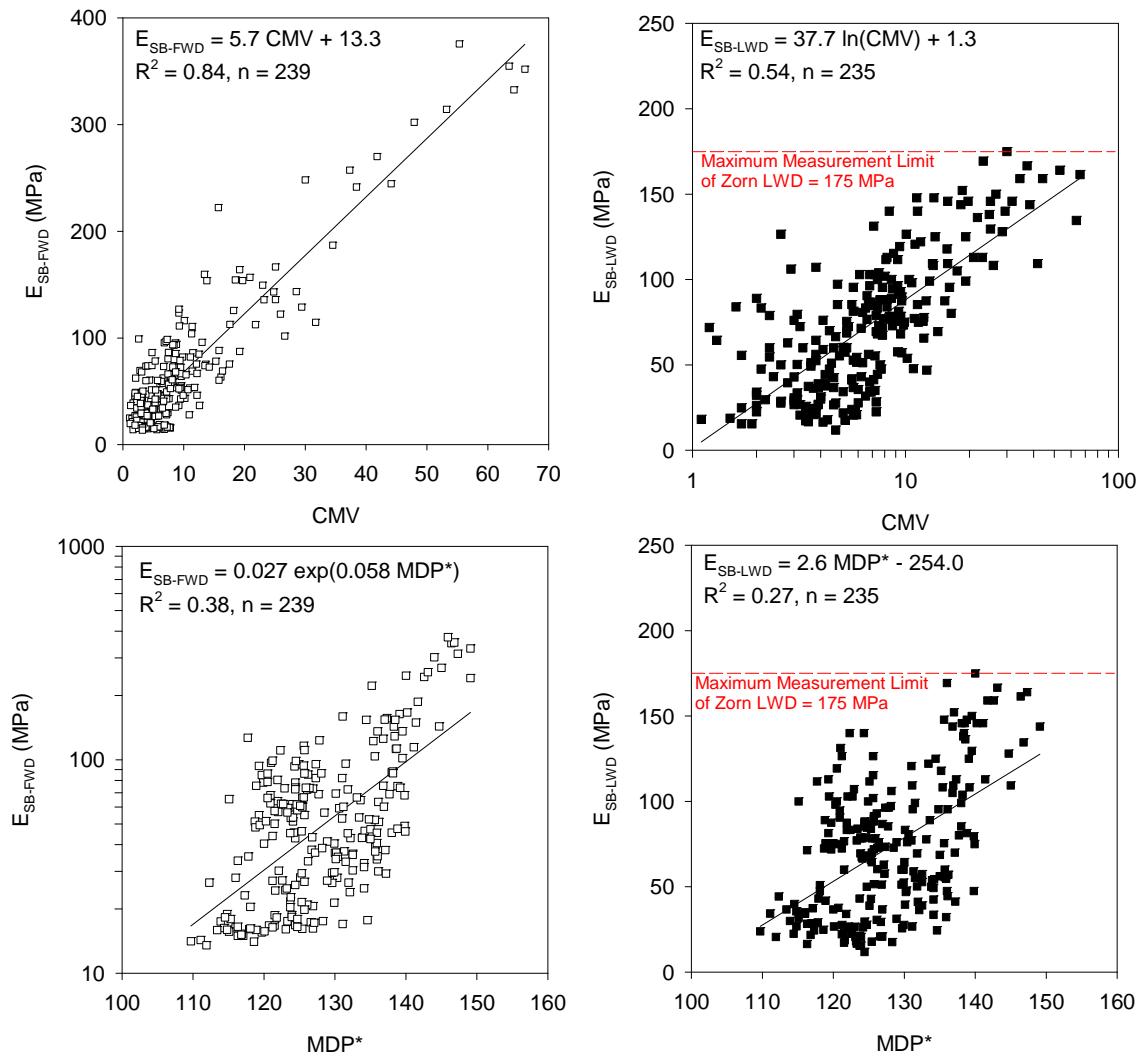
Figure 3.7. Correlations between (a) CMV and E_{SB-FWD}, (b) CMV and E_{SB-LWD}, (c) MDP* and E_{SB-FWD}, and (d) MDP* and E_{SB-LWD}.
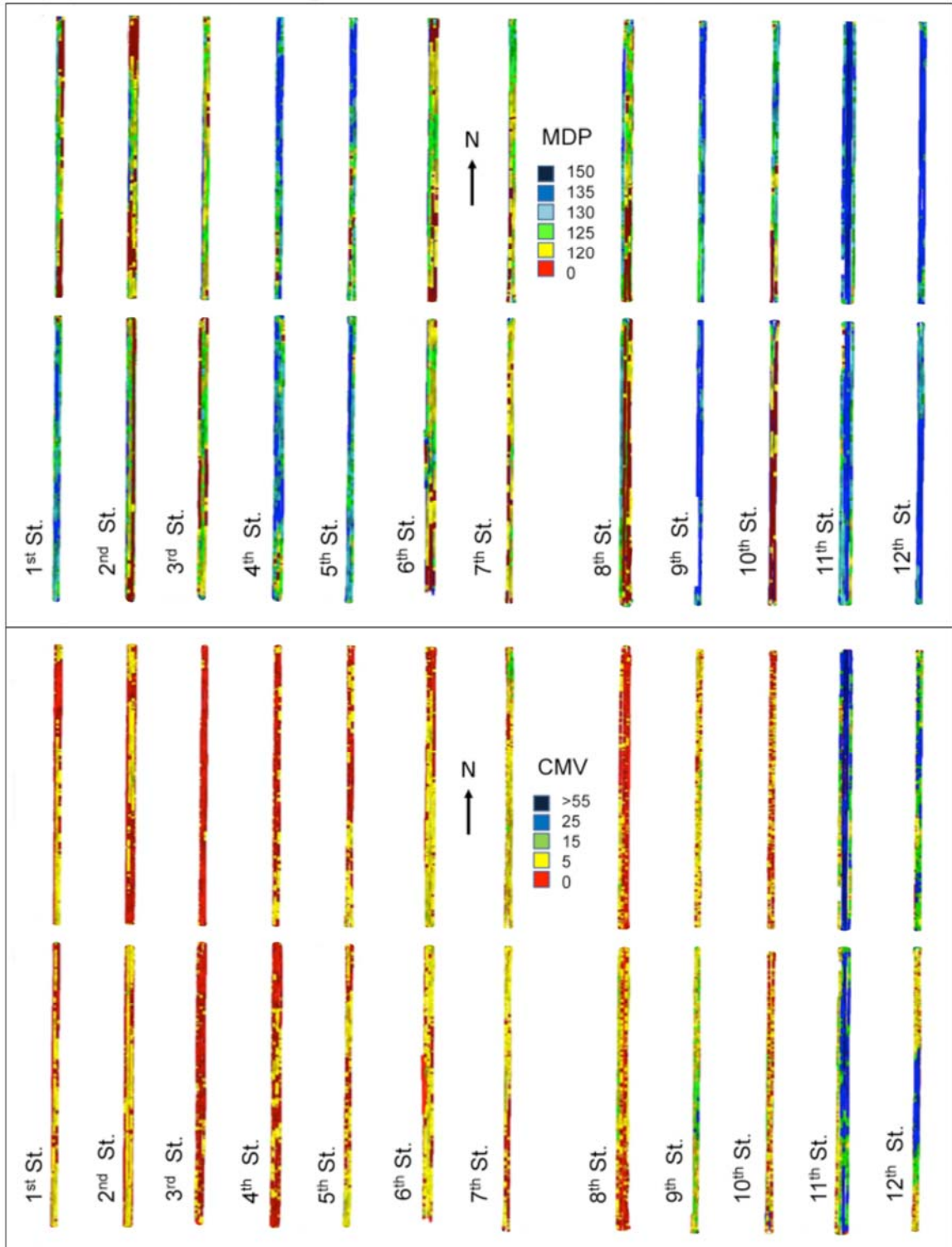
Figure 3.8. RICM spatial color-coded maps for MDP* (top) and CMV (bottom).
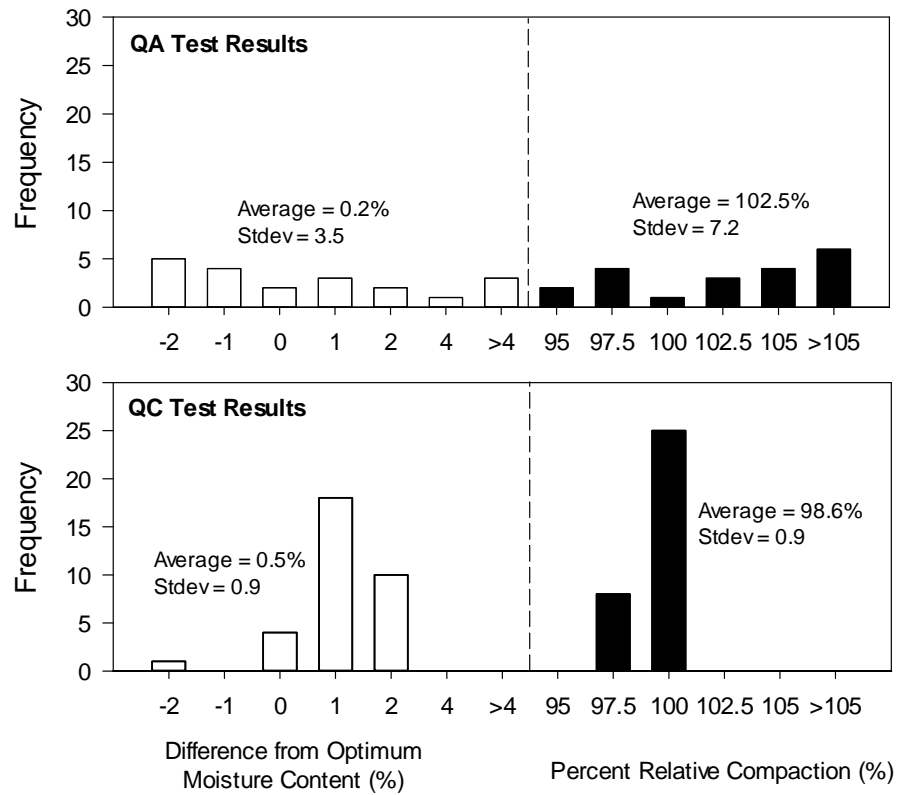
Figure 3.9. Comparison of nuclear density/moisture measurements for the QC and QA agents.

CHAPTER 4. IN SITU STIFFNESS ASSESSMENT OF THAW-WEAKENED STABILIZED PAVEMENT FOUNDATIONS

Peter J. Becker, David J. White, and Pavana K.R. Vennapusa

4.1 Abstract

This paper presents results of an in situ experimental investigation assessing the freeze-thaw performance of pavement foundation subbase and subgrade layer test sections constructed in Boone, Iowa with fifteen different stabilization techniques including geosynthetics, chemical stabilizers, and use of recycled materials. Falling weight deflectometer (FWD) and dynamic cone penetrometer (DCP) tests were performed during the never-frozen condition in October 2012 and during the thaw-weakened condition in April/May 2013. FWD and DCP test results indicated that sections with cement stabilization provided the highest values in April 2013. Multivariable statistical analyses and first-order, variance-based sensitivity analyses of FWD and DCP measurements showed that overall pavement foundation stiffness is entirely governed by subgrade stiffness during the thaw-weakened condition. Analysis is made on the load-spreading effectiveness of subbase layers during both never-frozen and thaw-weakened conditions. Results from this study demonstrate the significance and value in stabilizing a foundation layer to achieve better freeze-thaw performance.

4.2 Introduction

Pavement structures that exist within temperate and subarctic climates experience freezing during winter followed by thawing during subsequent springs (i.e., freeze-thaw).

During freeze-thaw conditions, the mechanical properties (e.g., resilient modulus) of pavement foundations (i.e., subbase and subgrade) weaken due to the saturation of these unbound layers. Doré and Zubeck (2009) identified two freeze-thaw weakening critical periods in pavements: (1) during partial winter thaw events and in early spring affecting granular subbase material, and (2) at the end of spring when the ice rich subgrade is thawing.

Pavements with foundations that comprise inadequate materials will accumulate significant amounts of distresses and will therefore experience decreased pavement performance (Christopher, Schwartz, & Boudreau, 2006; Kim, Ceylan, & Golpalakrishan, 2007; Saad, 2014). Simonsen and Isacsson (1999) summarized several examples of pavement distresses that are the result of freeze-thaw weakening of the pavement foundation.

According to Winterkorn and Pamukcu (1991), soil stabilization techniques improve mechanical properties and environmental resistances of soils, so stabilization of pavement foundations can be used to counteract the effects of freeze-thaw weakening. Several studies (Bin-Shafique, Rahman, Yaykiran, & Azfar, 2010; Johnson, 2012; Parsons & Milburn, 2003; Solanki, Khoury, & Zaman; 2009; Walker & Karabulut, 1965) have demonstrated that stabilized soils are more resistant to freeze-thaw weakening, although many of these studies were limited to only laboratory testing. There is a limited availability of detailed field studies that assess in situ freeze-thaw performance of stabilized pavement foundation materials.

The purpose of this paper is: (1) to provide a detailed field study on the effect of freeze-thaw weakening on stabilized pavement foundation mechanical properties (i.e.,

stiffness) and (2) to determine which stabilization approach, subgrade stabilization or subbase stabilization, will expect to yield better pavement foundation performance. The field test comprised twenty-four test sections that used stabilization techniques including geosynthetics, chemical stabilizers, and mechanical stabilization, as well as controls (i.e., no treatment). Falling weight deflectometer (FWD) and dynamic cone penetrometer (DCP) tests were used to assess in situ stiffness during never-frozen and freeze-thaw conditions. Preliminary findings shortly after construction were reported in White, Becker, Vennapusa, Dunn, and White (2013).

4.3 Project Conditions

The project test site is located in Boone, Iowa, where monthly average temperatures range from -13 °C to 28 °C (Weather Channel, 2016). Sieve analyses and Atterberg limits testing established that subgrade soil classified as CL or A-6(5), and cone penetration tests indicated that the groundwater table was located about 0.9 to 1.5 m below grade.

The project site comprised 24-200 m long, 6 m wide roadways that had been constructed in 2007. Each roadway consisted of a 152 mm thick gravel base layer that was topped with an asphalt chip seal coat layer. The roadways required reconstructing because of excessive deterioration that was partly due to annual freeze-thaw cycles and thaw-weakening.

Roadway reconstruction took place in two phases. Phase 1 construction, which occurred during the summer of 2012, involved removal of the existing gravel base and asphalt chip seal layers followed by preparation of new pavement foundations (i.e., subbase and subgrade). Each test section subbase layer consisted of modified crushed limestone (Iowa Department of Transportation (DOT), 2016) that classified as GP-GM.

Subbase layers in select test sections consisted of reclaimed gravel from the preexisting roadways that classified as SM or A-1-a in addition to modified crushed limestone. The 24-test sections were all constructed using different soil stabilization techniques: woven and nonwoven geotextiles, biaxial and triaxial polymer geogrids, geocell reinforced subbase, mechanical stabilization of subgrade (i.e., mixing natural subgrade with reclaimed gravel), Portland cement (PC) stabilized subbase and subgrade, fly ash stabilized subgrade, and polypropylene fiber and monofilament-polypropylene fiber reinforced subbase. The test sections are noted by street name and north or south orientation (e.g., 1st South), and Table 1 provides pavement foundation profile descriptions for the test sections. Phase 2 construction entailed the placement of asphalt pavement over the test section pavement foundations, which is beyond the scope of this paper.

4.4. In Situ Testing and Statistical Methods

4.4.1 Falling weight deflectometer

A Kuab falling weight deflectometer (FWD) setup with a 300 mm diameter loading plate evaluated pavement foundation stiffnesses for the test sections. At each testing location, the FWD setup applied one seating drop followed by four loading drops that ranged from approximately 22 kN to 67 kN. A load cell within the FWD setup measured the actual applied loads, and seismometers that were mounted on the FWD setup measured the resulting vertical deflections at horizontal distances of 0 m, 0.3 m, 0.5 m, 0.6 m, 0.9 m, 1.2 m, and 1.5 m relative to the center of the loading plate. Composite elastic moduli (E_c) for pavement foundations (i.e., combined subbase and subgrade layers) were determined using Equation 4.1, where σ_o = applied vertical stress, a =

loading plate radius, v_c = composite Poisson's ratio (assumed as 0.4), D_o = measured

vertical deflection under center of loading plate, f = stress distribution shape factor

(assumed as 2 for uniform stress distribution).

$$E_c = \frac{\sigma_o a(1 - v_c{}^2)f}{D_o}$$ (4.1)

Subgrade elastic moduli (E_{SG}) were determined using equations 4.2, 4.3, and 4.4

where σ_o = applied vertical stress, r = horizontal distance from center of loading plate,

D_r = measured vertical deflection at a distance r from the center of the loading plate, a =

loading plate radius, v_{SG} = subgrade Poisson's ratio (assumed as 0.45), $\acute{E}$ = complete

elliptic integral of the second kind, $\acute{K}$ = complete elliptic integral of the first kind.

$$E_{SG} = \frac{4\sigma_o r(1 - v_{SG}{}^2)}{\pi D_r}\left[\acute{E} - \left(1 - \frac{a^2}{r^2}\right)\acute{F}\right]$$ (4.2)

$$\acute{E} = \int_0^{\frac{\pi}{2}} \sqrt{1 - \left(\frac{a}{r}\right)^2 \sin^2\theta}\, d\theta$$ (4.3)

$$\acute{K} = \int_0^{\frac{\pi}{2}} \frac{d\theta}{\sqrt{1 - \left(\frac{a}{r}\right)^2 \sin^2\theta}}$$ (4.4)

Equation 4.2 assumes that vertical deflections measured at the surface equate to

vertical deflections in the subgrade layer, so only subgrade properties affect D_r values.

For the assumption to be valid, surface vertical deflections must be measured at

sufficiently large horizontal distances from the applied loadings. American Association

of State Highway and Transportation Officials (AASHTO) (1993) recommends using

equation 4.5 to determine the minimum horizontal distance between the loading plate

center and the vertical deflection measurement position, where r = horizontal distance

from center of loading plate, R_{SG} = stress bulb radius at top of subgrade.

$$r \geq 0.7R_{SG} \tag{4.5}$$

Stress distribution in layered systems does not theoretically adhere to Boussinesq's

solution (Burmister, 1945); however, if the equivalent thickness theory (Odemark, 1949)

is used to convert two-layered systems to one-layered systems, then Boussinesq's

solution can approximate stresses and displacements within two-layered systems.

Combination of the equivalent thickness theory with Boussinesq's solution yields

equation 4.6, which was used to determine R_{SG}, where R_{SG} = stress bulb radius at top of

subgrade, a = loading plate radius, h_e = subgrade equivalent thickness.

$$R_{SG} = \sqrt{a^2 + h_e{}^2} \tag{4.6}$$

The parameter h_e is the thickness of a layer with the material properties of the

subgrade, but with a flexural rigidity equal to that of the subbase layer. If $E_{SB} > E_{SG}$, then

h_e was determined from equation 4.7, where h_e = equivalent thickness, n = empirical

coefficient (equal to 0.9), h = subbase thickness, E_{SB} = subbase elastic modulus, ν_{SB} =

subbase Poisson's ratio (assumed as 0.35), E_{SG} = subgrade elastic modulus, ν_{SG} =

subgrade Poisson's ratio (assumed as 0.45).

$$h_e = nh \sqrt[3]{\frac{E_{SB}}{E_{SG}} \frac{(1 - \nu_{SG}{}^2)}{(1 - \nu_{SB}{}^2)}} \tag{4.7}$$

As recommended by Hirai (2008), if $E_{SB} < E_{SG}$, then h_e was determined from

equation 4.8, which is an interpolation of equation 4.7 and Terzaghi's approximate

formula for stress on the rigid base of an elastic layer (Terzaghi, 1943), where h_e =

equivalent thickness, n = empirical coefficient (equal to 0.9), h = subbase thickness, E_{SB} = subbase elastic modulus, v_{SB} = subbase Poisson's ratio (assumed as 0.35), E_{SG} = subgrade elastic modulus, v_{SG}, subgrade Poisson's ratio (assumed as 0.45).

$$h_e = nh \left[0.75 + 0.25 \sqrt[3]{\frac{E_{SB}}{E_{SG}} \frac{(1 - v_{SG}{}^2)}{(1 - v_{SB}{}^2)}} \right] \tag{4.8}$$

Subbase elastic moduli (E_{SB}) were determined from equation 4.9, where D_o = measured vertical deflection under center of loading plate, σ_o = applied vertical stress, a = loading plate radius, E_{SB} = subbase elastic modulus, v_{SB} = subbase Poisson's ratio (assumed as 0.35), E_{SG} = subgrade elastic modulus, v_{SG} = subgrade Poisson's ratio (assumed as 0.45), h = subgrade thickness, n = empirical coefficient (equal to 0.9), h_e = equivalent subgrade thickness.

$$D_o = 2\sigma_o a \left\{ \left[\frac{(1 - v_{SB}{}^2)}{E_{SB}} \right] \left[1 - \frac{1}{\sqrt{1 + \left(\frac{nh}{a}\right)^2}} \right] + \frac{(1 - v_{SG}{}^2)}{E_{SG}\sqrt{1 + \left(\frac{h_e}{a}\right)^2}} \right\} \tag{4.9}$$

In this study, composite elastic moduli and layer elastic moduli (e.g., subgrade elastic modulus) were determined from vertical deflections that had been normalized to applied loads equal to 40 kN [i.e., one-half equivalent single axle load (ESAL)].

Figure 4.1 provides a graphical representation of the Burmister (1945) solution for the amount of vertical stress that is distributed to the top of the subgrade layer (σ_{SG}), and was used to determine the magnitudes of vertical stress that were transferred to the subgrade layer during FWD testing

4.4.2 Dynamic cone penetrometer

DCP tests were conducted according to ASTM D6951 to determine layer penetration index (mm per blow) values. Tests were terminated at either refusal per ASTM D6951 (i.e., advancement of 2 mm or less after 5 blows) or upon reaching the maximum penetration depth that was about 0.9 m. California bearing ratio (CBR) values for subbase and mechanically stabilized subgrade materials were determined using equation 4.10, where CBR = California bearing ratio and PI = penetration index.

$$CBR = \frac{292}{PI^{1.12}} \tag{4.10}$$

Because subgrade classified as CL, CBR values for subgrade soils were determined from equation 4.11, where CBR = California bearing ratio and PI = penetration index.

$$CBR = \begin{cases} \dfrac{1}{(0.017019PI)^2}, & CBR < 10 \\ \dfrac{292}{PI^{1.12}}, & CBR > 10 \end{cases} \tag{4.11}$$

4.4.3. Statistical analysis methods

The authors of this paper developed multivariable models to empirically predict composite elastic modulus (i.e., overall pavement foundation stiffness) from average subbase and subgrade penetration indices (i.e., individual layer stiffnesses) during never-frozen and freeze-thaw conditions. Statistical significance for multivariable model parameters was based on an alpha value of 0.05 (i.e., 95% confidence). First-order, variance-based sensitivity analyses of the multivariable models assessed the sensitivity of predicted composite elastic moduli to changes in average penetration indices for the subbase and subgrade layers. Per Sobol' (1990), the influences of average subbase and subgrade penetration indices on composite elastic modulus were quantified using

sensitivity indices (S) that are calculated from equations 4.12 and 4.13, where S_i = sensitivity index of ith dependent variable, V_i = partial variance of ith dependent variable, V_Y = total unconditional variance, N = number of dependent variables.

$$S_i = \frac{V_i}{V_Y} \qquad (4.12)$$

$$V_Y = \sum_{i=1}^{N} V_i \qquad (4.13)$$

The summation of all sensitivity indices for a given model must equal unity (Sobol', 1990); therefore the authors interpreted sensitivity index for each average layer penetration index as the percent influence of each individual layer stiffness on the overall pavement foundation stiffness.

4.5 Results and Analysis

FWD and DCP testing evaluated test section pavement foundation stiffness in situ. Between 9 and 10 FWD tests at 15 m intervals were performed on each test section, and between 2 and 3 DCP tests at 46 m intervals were performed on each test section. Tests that were conducted during October 2012 represent never-frozen pavement foundation stiffness, and tests that were conducted during April 2013 and May 2013 represent freeze-thaw pavement foundation stiffness. FWD and DCP testing that evaluated never-frozen pavement foundation stiffness was conducted on October 2–3, 2012 when local temperatures ranged from a minimum of 8 °C to a maximum of 27 °C (Weather Channel, 2016). FWD testing that evaluated freeze-thaw pavement foundation stiffness was conducted on April 3, 2013 when local temperatures ranged from a minimum of –4 °C to a maximum of 8 °C (Weather Channel, 2016). DCP testing that evaluated freeze-thaw

pavement foundation stiffness was conducted on April 24–25, 2013 when local

temperatures ranged from a minimum of –3 °C to a maximum 16 °C and on May 23–24,

2013 when local temperatures ranged from a minimum of 6 °C to a maximum of 22 °C

(Weather Channel, 2016). Results and analysis from this testing are reported in the

following sections.

4.5.1 Comparison of never-frozen and freeze-thaw stiffnesses

4.5.1.1 FWD testing results

Figure 4.2 shows comparisons of average test section E_c values during October 2012

testing and April 2013 testing, and Table 4.2 reports average test section E_c values with

respective coefficients of variation during October 2012 testing and April 2013 testing.

October 2012 FWD testing yielded E_c values that ranged from about 37 MPa to 507 MPa

(Figure 4.2a). Test sections with PC stabilized subgrade (i.e., 11th North), fly ash

stabilized subgrade (i.e., 11th South, 12th South, 12th North), or PC stabilized reclaimed

gravel subbase (i.e., 6th South, 6th North, 7th South, and 7th North) produced the highest

E_c values during October 2012 testing. Other test sections that produced comparatively

higher E_c values during October 2012 testing included test sections with mechanically

stabilized subgrade (i.e., 2nd South and 2nd North), compacted subgrade (i.e., 1st South,

1st North, and 10th North), or untreated reclaimed gravel subbase (i.e., 9th South and 9th

North).

As shown in Figure 4.2c, all test sections experienced reductions in E_c (by about 2 to

9 times on average) during the spring thaw in April 2013 to where E_c values ranged from

about 11 MPa to 159 Mpa (Figure 4.2b). Test sections with PC stabilized subgrade (i.e.,

11th North) or PC stabilized reclaimed gravel subbase (i.e., 6th South, 6th North, 7th

South, and 7th North) produced the highest E_c values during April 2013 testing. Other test sections that produced comparatively higher E_c values during April 2013 testing included test sections with fly ash stabilized subgrade (i.e., 11th South, 12th South, 12th North) or untreated reclaimed gravel subbase (i.e., 9th South and 9th North).

Figure 4.3 shows correlations between E_c in April 2013 $[E_{c(Apr)}]$ and E_c in October 2012 $[E_{c(Oct)}]$. Because test sections with PC stabilization yielded both the highest $E_{c(Oct)}$ values and the highest $E_{c(Apr)}$ values, FWD test points on these test sections were plotted separately from test points on all other test sections. A power equation best fits the relationship between $E_{c(Apr)}$ and $E_{c(Oct)}$ for FWD test points with PC stabilization, and an exponential growth equation best fits the relationship between $E_{c(Apr)}$ and $E_{c(Oct)}$ for FWD test points without PC stabilization. $E_{c(Apr)}$ correlates well with $E_{c(Oct)}$ for both FWD test points with PC stabilization and FWD test points without PC stabilization. As evidenced by the 95% confidence intervals for the two correlations in Figure 4.3, $E_{c(Apr)}$ for FWD test points with PC stabilization will be predictably greater (with statistical significance) than $E_{c(Apr)}$ for FWD test points without PC stabilization. These results suggest that PC stabilized pavement foundations are less susceptible to thaw-weakening than untreated pavement foundations or fly ash stabilized pavement foundations.

4.5.1.2 DCP testing results

Figure 4.4a shows comparisons of average test section subbase CBR values during October 2012 DCP testing. With the exception of test sections on which all DCP tests reached refusal before penetrating the subbase layer, October 2012 DCP testing yielded average test section subbase CBR values that ranged from about 32% to 179%. In general, October 2012 DCP results show that test sections with stiff layers (e.g., PC

stabilized subgrade) that underlay subbase layers tend to produce comparatively higher subbase CBR values. Figure 4.5a shows comparisons of average test section subgrade CBR values during October 2012 DCP testing. For test points at which DCP tests had penetrated the subbase layer, average test section subgrade CBR values ranged from about 2.6% to 44% during October 2012 DCP testing. Test sections with fly ash stabilized subgrade (i.e., 11th South, 12th South, and 12th North) produced the highest subgrade CBR values during October 2012 DCP testing. The 6th North test section produced a relatively high average subgrade CBR value equal to approximately 33%; however, this average is the result of a single data point unlike all other test sections. Therefore the high subgrade CBR value on 6th North during October 2012 is likely an outlier in the data set.

Figure 4.4b shows comparisons of average test section subbase CBR values during April 2013 DCP testing. April 2013 DCP testing yielded average test section subbase CBR values that ranged from about 12% to 96%. Not including test sections in which DCP tests reached refusal during October 2012 testing, the average subbase CBR value decreased for all test sections during April 2013 DCP testing (by about 1.2 to 12 times on average), except for the 1st North test section, which increased by a factor of about 1.3. Figure 4.5b shows comparisons of average test section subgrade CBR values during April 2013 DCP testing. April 2013 DCP testing yielded average test section subgrade CBR values that ranged from about 1.2% to 63%. Similar to subbase CBR results, subgrade CBR on test sections on which DCP tests penetrated the subbase layer decreased during April 2013 testing (by about 1.0 to 7 on average), except for the 1st South, 1st North, 2nd South, 2nd North, and 5th South test sections, which all experienced increases in

subgrade CBR. There is no evident reason as to why subgrade CBR increased for multiple test sections during April 2013 testing; however, the authors hypothesize that these test sections were still partially frozen at the time of testing. Of the test sections that experienced decreased subgrade CBR values during April 2013 testing, test sections with PC stabilized subgrade (i.e., 11th North) and test sections with fly ash stabilized subgrade (i.e., 11th South, 12th South, and 12th North) produced the highest subgrade CBR values.

Because of the possibility that multiple test sections were still partially frozen during April 2013 DCP testing, additional DCP testing was performed in May 2013 to reassess the thaw-weakened CBR values for the test sections. Figure 4.4c shows comparisons of average test section subbase CBR during May 2013 DCP testing. May 2013 DCP testing yielded average test section subbase CBR values that ranged from about 21% to 268%. Not including test sections in which DCP tests reached refusal during October 2012 testing, average subbase CBR decreased (by about 1.1 to 8 on average), except for the 4th South, 6th North, 10th South, and 10th North test sections, which all experienced increases in subbase CBR. Most test sections produced increased subbase CBR values during May 2013 testing as compared with April 2013 testing, except for the 1st South, 1st North, 2nd South, 2nd North, and 12th South test sections, which all produced lower subbase CBR values. Test sections with PC stabilized subbase (i.e., 6th South, 6th North, 7th South, and 7th North) and the test section with woven geotextile (i.e., 4th South) produced the highest subbase CBR values during May 2013 testing. Because only these test sections have such markedly higher subbase CBR values during May 2013 testing than during April 2013 testing, these stabilization techniques (i.e., PC stabilized subbase and woven geotextiles) may hasten the rate for recovery from thaw-weakening for

subbase materials. Figure 4.5c shows comparisons of average test section subgrade CBR during May 2013 DCP testing. May 2013 DCP testing yielded average test section subgrade CBR values that ranged from about 2.7% to 57%. Not including test sections in which DCP tests reached refusal during October 2012 testing, average subgrade CBR decreased (by about 1.0 to 3 on average), except for the 1st South, 3rd South, 8th South, 10th South, 11th South, and 12th South test sections, which all experienced increases in subgrade CBR. Similar to test section subbase layers, most test sections produced increased subgrade CBR values during May 2013 testing than during April 2013 testing, except for the 1st South, 1st North, 2nd South, 2nd North, 3rd North, 5th South, and 11th North test sections, which all produced lower subgrade CBR values. Test sections with either PC stabilized subgrade (i.e., 11th North) or fly ash stabilized subgrade (i.e., 11th South, 12th South, and 12th North) yielded the highest subgrade CBR values during May 2013 DCP testing. The average subgrade CBR value for the PC stabilized subgrade test section remained relatively unchanged between April 2013 testing and May 2013 testing; however, average subgrade CBR for the fly ash stabilized subgrade test sections increased by about 1.4 to 3 times on average between April 2013 testing and May 2013 testing. Because the subgrade CBR values for fly ash stabilized subgrade are markedly higher during May 2013 testing than during April 2013 testing, fly ash stabilization may hasten the rate for recovery from thaw-weakening for cohesive subgrades.

Because multiple April 2013 DCP testing points seemed to have still been partially frozen at the time of testing and because multiple May 2013 DCP testing points seemed to have already began recovering from their initial thaw-weakened states at the time of testing, the authors combined the two data sets to best represent thaw-weakened CBR and

PI values on the test sections. Therefore, for both subbase and subgrade layers at a particular data point, thaw-weakened layer CBR equals the minimum of April 2013 layer CBR and May 2013 layer CBR, and thaw-weakened layer PI equals the maximum of April 2013 layer PI and may 2013 layer PI. Figure 4.6a correlates the minimum of April 2013 and May 2013 subbase CBR values to October 2012 subbase CBR values. As evidenced by the position of the data points relative to the line of equality, test point subbase layers all experience reductions in CBR within the thaw-weakened state. However, the correlation between thaw-weakened subbase CBR and never-frozen (i.e., October 2012 DCP testing) subbase CBR is poor ($r^2 = 0.0662$) and lacks statistical significance so thaw-weakened subbase CBR is likely independent of never-frozen subbase CBR. Figure 4.6b correlates the minimum of April 2013 and May 2013 subgrade CBR values to October 2012 subgrade CBR values. Similar to test section subbase layers, the majority of test point subgrades layers experienced reductions in CBR within the thaw-weakened state as shown by data point position relative to the line of equality. Unlike test section subbase layers, however, thaw-weakened subgrade CBR has a respectable correlation ($r^2 = 0.3799$) with statistical significance to never-frozen subgrade CBR, so never-frozen subgrade CBR is likely an indicator of thaw-weakened subgrade CBR. Only one DCP test penetrated through a PC stabilized layer during October 2012 DCP test, so no conclusions on possible decreased susceptibility of PC stabilized pavements to thaw-weakening can made.

4.5.2 Layer influence on overall pavement foundation stiffness

In this paper, the authors attempted to determined which layer, subgrade or subbase, has greater influence on the overall pavement foundation stiffness during never-frozen

and freeze-thaw conditions. E_c values from FWD testing represent overall pavement foundation stiffness, and subbase *PI* values and subgrade *PI* values represent subbase and subgrade layer stiffnesses, respectively. Figure 4.7a shows correlations between October 2012 E_c values and October 2012 subbase and subgrade *PI* values. During October 2012 testing (i.e., never frozen condition), both subbase *PI* values and subgrade *PI* values correlate well ($r^2 = 0.4059$ and $r^2 = 0.6882$, respectively) and with statistical significance to E_c values. Figure 4.7b shows correlations between April 2013 E_c values and the maximum of April 2013 and May 2013 *PI* values for subbase and subgrade layers. During April 2013 and May 2013 testing (i.e., freeze-thaw condition), subgrade *PI* values correlate well ($r^2 = 0.4844$) and with statistical significance to E_c values; however, subbase *PI* values do not correlate ($r^2 = 0.0513$) and without statistical significance to E_c values.

Table 4.4 reports the results of multivariable analyses that incorporate both subbase and subgrade layer *PI* values into models for predicting E_c for both October 2012 testing and April 2013 and May 2013 testing. 6th South and North, 7th South and North, and 9th South and North test sections were not included in the multivariable analysis because subbase layers on these test sections were nominally twice as thick as subbase layers on all other test sections, and influence of subbase thickness is beyond the scope of the multivariable analyses.

The October 2012 multivariable model for predicting E_c fits well (r^2 Adj. = 0.6978), and both subbase *PI* and subgrade *PI* model coefficients are statistically significant (p < 0.0001 and p < 0.0001, respectively). Sensitivity index for subbase *PI* equals 0.835, and sensitivity index for subgrade *PI* equals 0.165. In essence, during the never-frozen

condition, subbase layer stiffness accounts for 83.5% of the overall pavement foundation stiffness and subgrade layer stiffness accounts for 16.5% of the overall pavement foundation stiffness.

Similar to the October 2012 multivariable model, the April 2013 and May 2013 multivariable model for predicting E_c fits well (r^2 Adj. = 0.6615). However, unlike the October 2012 multivariable model, the subgrade PI model coefficient is statistically significant (p < 0.0001) while the subbase PI model coefficient is not statistically significant (p = 0.4799). Because the subbase PI model coefficient is not statistically significant for the April 2013 and May 2013 multivariable model, overall pavement foundation stiffness is independent of subbase layer stiffness (i.e., subbase PI sensitivity index equals 0) and only subgrade layer stiffness accounts for the overall pavement foundation stiffness (i.e., subgrade PI sensitivity index equals 1).

Layered stress distribution in accordance with Burmister (1945) may explain why subbase stiffness has no effect on overall pavement foundation stiffness during the thaw-weakened condition. When a stiff layer overlies a soft layer (e.g., subbase over subgrade), the stiff layer acts as a reinforcing layer with a load-spreading effect. Load-spreading effectiveness depends on the ratio of the stiff layer elastic modulus to the soft layer elastic modulus. Because DCP testing showed that thaw-weakening causes reductions in not only test section subgrade stiffness but also test section subbase stiffness, the insensitivity of overall pavement foundation stiffness to subbase stiffness during thaw-weakening may therefore be the result of reduced load-spreading effectiveness.

Using equations 4.2 to 4.9, subbase elastic moduli (E_{SB}) and subgrade layer elastic moduli (E_{SG}) were backcalculated for October 2012 and April 2013 FWD testing.

Figure 4.8a shows boxplot comparisons of E_{SB} to E_{SG} ratios for October 2012 and April 2013 FWD testing. The average E_{SB} to E_{SG} ratio during October 2012 FWD testing equals about 7.6, and the average E_{SB} to E_{SG} ratio during April 2013 FWD testing equals about 1.6. A Welch's t test analysis (i.e., assumed unequal variances) showed with statistical significance ($p < 0.001$) that the average E_{SB} to E_{SG} ratio during October 2012 FWD testing does not equal the average E_{SB} to E_{SG} ratio during April FWD testing. Because the ratio of E_{SB} to E_{SG} decreases by about 4.6 times on average from the never-frozen condition to the thaw-weakened condition, the load-spreading effectiveness of test section subbase layers also decreases from the never-frozen condition to the thaw-weakened condition.

Ratios of σ_{SG} to σ_o for October 2012 and April 2013 testing were determined using the Burmister solution for stress distribution (Figure 4.1) and values for E_{SB} and E_{SG} from FWD testing. Figure 4.8b shows boxplot comparisons of σ_{SG} to σ_o for October 2012 and April 2013 testing. The average σ_{SG} to σ_o ratio during October 2012 FWD testing equals about 0.406, and the average σ_{SG} to σ_o ratio during April 2013 FWD testing increased as compared with October 2012 testing (by about 1.5 times on average) to about 0.593. A Welch's t test analysis showed with statistical significance ($p < 0.001$) that the average σ_{SG} to σ_o ratio during October 2012 FWD testing does not equal the average σ_{SG} to σ_o ratio during April FWD testing. If the subbase load-spreading effect is ignored (i.e., applying the Boussinesq solution), then the ratio of σ_{SG} to σ_o equals about 0.638.

To quantitatively describe load-spreading effectiveness, the authors introduced the load-spreading effectiveness index (*LEI*) that is shown in in equation 4.14:

$$LEI = \frac{\sigma_{SG(Bouss.)} - \sigma_{SG(Bur.)}}{\sigma_{SG(Bouss.)}}, \qquad \sigma_{SG(Bouss.)} \geq \sigma_{SG(Bur.)} > 0 \qquad (4.14)$$

where LEI = load-spreading effectiveness index; $\sigma_{SG(Bouss.)}$ = distributed stress on

subgrade using the Boussinesq solution; $\sigma_{SG(Bur.)}$ = distributed stress on subgrade using

the Burmister solution. The lower limit for LEI is 0 (i.e., no load-spreading effect), and

the upper limit for LEI is 1 (i.e., complete load-spreading effectiveness). Average test

section subbase LEI equaled about 0.364 for October 2012 FWD testing, and average test

section subbase LEI equaled about 0.070 for April 2013 FWD testing. As environmental

test section condition transitioned from never-frozen to thaw-weakened, LEI decreased

by about 5 times on average to the point where the load-spreading effect was nearly

negligible. With decreased subbase load-spreading effectiveness, subgrade layers must

endure higher levels of stress and therefore must experience greater amounts of

deformation. Increased deformation from reduced subbase load-spreading effectiveness

during thaw-weakening therefore results in the apparent softening of pavement

foundations. So reduction of overall pavement foundation stiffness during thaw-

weakening is likely the result of reduced load-spreading effectiveness, in addition to the

saturation of unbound layers from freeze-thaw processes.

4.6 Summary and Key Conclusions

This paper compares stiffnesses of never-frozen and thaw-weakened stabilized

pavement foundations. FWD and DCP tests were conducted in situ on twenty-four test

sections to assess pavement foundation stiffness during never-frozen (October 2012) and

thaw-weakened (April 2013, May 2013) conditions. Statistical analyses of in situ test

measurements describe the relative importance of subbase and subgrade layers to the

overall pavement foundation stiffness during never-frozen and thaw-weakened conditions. The following key findings can be determined from this study:

- Average test section composite elastic moduli (E_c) during October 2012 (i.e., never-frozen) FWD testing ranged from 37 MPa to 507 MPa. Test sections with Portland cement (PC) stabilized subgrade, fly ash stabilized subgrade, or PC stabilized reclaimed gravel subbase produced the highest E_c values. Test sections with mechanically stabilized subgrade, compacted subgrade, or untreated reclaimed gravel subbase produced comparatively high E_c values. Subbase and subgrade layer CBR values from DCP testing in October 2012 revealed test section stiffnesses that were consistent with FWD testing.

- Average test section composite elastic moduli (E_c) during April 2013 (i.e., thaw-weakened) FWD testing ranged from 11 MPa to 159 MPa. All test sections experience reductions in E_c values as conditions transitioned from never-frozen to thaw-weakened (by about 2 to 9 times on average). Test sections with PC stabilized subgrade or PC stabilized reclaimed gravel subbase produced the highest E_c values. Test sections with fly ash stabilized subgrade or untreated reclaimed gravel subbase produced relatively high E_c values as well. Similar to testing during the never-frozen condition, subbase and subgrade layer CBR values from DCP testing in April 2013 and May 2013 reflect FWD testing during April 2013.

- Correlations between thaw-weakened and never-frozen E_c values suggest that PC stabilized pavement foundations are less susceptible to thaw-weakening than untreated pavement foundations or fly ash stabilized pavement foundations.

Because of a lack of data, DCP results could neither support nor oppose this
claim. The authors recommend future research to investigate the claim further.

- There is no correlation between thaw-weakened and never-frozen subbase CBR
  values, so thaw-weakened subbase CBR is likely independent of never-frozen
  subbase CBR. However, there is a statistically significant correlation between
  thaw-weakened and never-frozen subgrade CBR values, so so never-frozen
  subgrade CBR is likely an indicator of thaw-weakened subgrade CBR.

- Never-frozen E_c correlated to both never-frozen subbase penetration index (PI)
  and never-frozen subgrade PI, while thaw-weakened E_c only correlated with
  thaw-weakened subgrade PI. Multivariable analyses that related E_c to subbase
  and subgrade layer PI showed with statistical significance that both subgrade and
  subbase layer stiffnesses account for overall pavement foundation stiffness during
  the never-frozen condition (83.5% and 16.5%, respectively), while only subgrade
  layer stiffness account for overall pavement foundation stiffness during the thaw-
  weakened condition.

- Loss in subbase layer load-spreading effectiveness during thaw-weakening may
  explain why subbase layer stiffness does not contribute to overall pavement
  foundation stiffness during thaw-weakening. Application of Burmister stress
  distribution with backcalculated layer elastic moduli showed that the average
  distributed stress on the subgrade layer increased by about 1.5 times on average as
  conditions transitioned from never-frozen to thaw-weakened.

- The authors introduced the load-spreading effectiveness index (LEI), which
  ranges from 0 (no load-spreading effectiveness) to 1 (complete load-spreading

effectiveness), to quantify the effectiveness of the subbase layer to distribute applied loading to the underlying subgrade layer. As conditions transitioned from never-frozen to thaw-weakened, subbase layer *LEI* decreased by about a factor of 5 from 0.364 to 0.070, so reduction of overall pavement foundation stiffness during thaw-weakening is likely the result of reduced load-spreading effectiveness.

4.7 Acknowledgments

4.8 References

American Association of State Highway and Transportation Officials (AASHTO). (1993). *AASHTO guide for design of pavement structures*. Washington, D.C.: American Association of State Highway and Transportation Officials.

Bin-Shafique, S., Rahman, K., Yaykiran, M., & Azfar, I. (2010). The long-term performance of two fly ash stabilized fine-grained soil subbases. *Resources, Conservation and Recycling*, 54(10), 666–672. doi: 10.1016/j.resconrec.2009.11.007

Burmister, D.M. (1945). The general theory of sresses and displacements in layered systems: I. *Journal of Applied Physics*, 16(89), 89–94. doi: 10.1063/1.1707562

Christopher, B.R., Schwartz, C., & Boudreau, R. (2006). *Geotechnical aspects of pavement*s (FHWA NHI-05-037). Washington, D.C.: National Highway Institute.

Doré, G., & Zubeck, H.K. (2009). *Cold regions pavement engineering*. Reston, VA: ASCE Press.

Hirai, H. (2004). Settlements and stresses of multi-layered grounds and improved grounds by equivalent elastic method. *International Journal for Numerical and Analytical Methods in Geomechanics*, 32(5), 523–557. doi: 10.1002/nag.636

Huang, Y.H. (2004). *Pavement analysis and design* (2nd ed.) Upper Saddle River, NJ; Pearson Prentice Hall.

Iowa Department of Transportation (DOT). (2016). *Standard specifications with GS-15002: Section 2115. Modified subbase*. Ames, Iowa: Iowa Department of Transportation.

Johnson, A. (2012). *Freeze-thaw performance of pavement foundation materials* (Master's thesis). Available from ProQuest Dissertations and Theses database. (UMI No. 1531431)

Kim, S., Ceylan, H., Golpalakrishan, K. (2007). Effect of M-E design guide input parameters on flexible pavement performance predictions. *Road Materials and Pavement Design*, 8(3), 375–397. doi: 10.1080/14680629.2007.9690080

Odemark, N. (1949). *Undersökning av elasticitetsegenskaperna hos olika jordarter samt teori för beräkning av beläggningar enligt elasticitetsteorin* (Meddelande 77). Stockholm: Statens Väginstitut.

Newcomb, D.E., & Birgisson, B. (1999). *Measuring in situ mechanical properties of pavement subgrade soils*. Washington, D.C.: National Cooperative Highway Research Program.

National Cooperative Highway Research Program (NCHRP). (2004). *Guide for mechanistic-empirical design of new and rehabilitated pavement structures* (NCHRP 1-37A). Washington, D.C.: National Cooperative Highway Research Program.

Parsons, R., & Milburn, J. (2003). Engineering Behavior of Stabilized Soils. *Transportation Research Record*, 1837, 20–29.

Saad, B. (2014). Analysis of excess water impact on the structural performance of flexible pavements. *International Journal of Pavement Engineering*, 15(5), 409–426. doi: 10.1080/10298436.2013.790546

Simonsen, E., & Isacsson, U. (1999). Thaw weakening of pavement structures in cold regions. *Cold Regions Science and Technology*, 29(2), 135–151. doi:10.1016/S0165-232X(99)00020-8

Sobol', I.M. (1990). On sensitivity estimation for nonlinear mathematical models. *Matematicheskoe modelirovanie*, 2(1), 112–118.

Solanki, P., Khoury, N., Zaman, M. (2009). Engineering properties and moisture susceptibility of silty clay stabilized with lime, class C fly ash, and cement kiln dust. *Journal of Materials in Civil Engineering*, 21(12), 749–757. doi: 10.1061/(ASCE)0899-1561(2009)21:12(749)

Solanki, P., Zaman, M.M., & Dean, J. (2010). Resilient modulus of clay subgrades stabilized with lime, class C fly ash, and cement kiln dust for pavement design. *Transportation Research Record*, 2186, 101–110.

Terzaghi, K. (1943). *Theoretical Soil Mechanics*. New York: J Wiley and Sons, Inc.

Vennapusa, P., White, D.J. (2009). Comparison of light weight deflectometer measurements for pavement foundation materials. *Geotechnical Testing Journal*,

32(3), 239–251.

doi: 10.1520/GTJ101704

Walker, R.D., & Karabulut, C. (1965). Effect of freezing and thawing on unconfined

compressive strength of lime-stabilized soils. *Highway Research Record*, 92, 1–11.

Weather Channel, The (2016). [Average monthly temperatures for Boone, Iowa] *Weather*

History for KBNW. Retrieved from

http://www.wunderground.com/history/airport/KBNW/2016/01/25/DailyHistory.html

?req_city=Boone&req_state=IA&reqdb.zip=50036&reqdb.magic=1&reqdb.wmo=99

999.

White, D.J., Becker, P., Vennapusa, P.K.R., Dunn, M.J., & White, C.I. (2013). Assessing

soil stiffness of stabilized pavement foundations. *Transportation Research Record*,

2235, 99–109.

Winterkorn, H.F., & Pamukcu S. (1991). Soil stabilization. In H. Fang (Ed.). *Foundation*

engineering handbook (pp. 317–378). New York: Van Nostrand Reinhold.

Zapata, C.E., Andrei, D., Witczak, M.W., & Houston, W.N. (2007). Incorporation of

environmental effects in pavement design. *Road Materials and Pavement Design*,

8(4), 667–693. doi: 10.1080/14680629.2007.9690094

Table 4.1. Test section pavement foundation descriptions

Test Section		Pavement Foundation Description
1st	South	**Subbase:** 152 mm modified SB[a] **Subgrade:** 305 mm compacted SG[b]; natural SG[b]
	North	**Subbase:** 152 mm modified SB[a] **Subgrade:** 305 mm compacted SG[b]; natural SG[b]
2nd	South	**Subbase:** 152 mm modified SB[a] **Subgrade:** 305 mm mechanically stabilized SG[b]; natural SG[b]
	North	**Subbase:** 152 mm modified SB[a] **Subgrade:** 305 mm mechanically stabilized SG[b]; natural SG[b]
3rd	South	**Subbase:** 25 mm modified SB[a]; 152 mm geocell reinforced modified SB[a]; nonwoven geotextile **Subgrade:** natural SG[b]
	North	**Subbase:** 51 mm modified SB[a]; 102 mm geocell reinforced modified SB[a]; nonwoven geotextile **Subgrade:** natural SG[b]
4th	South	**Subbase:** 152 modified SB[a]; woven geotextile **Subgrade:** natural SG[b]
	North	**Subbase:** 152 modified SB[a]; nonwoven geotextile **Subgrade:** natural SG[b]
5th	South	**Subbase:** 152 modified SB[a]; biaxial polymer geogrid **Subgrade:** natural SG[b]
	North	**Subbase:** 152 modified SB[a]; triaxial polymer geogrid **Subgrade:** natural SG[b]
6th	South	**Subbase:** 152 mm modified SB[a]; 152 mm 5% Portland cement & 0.4% monofilament-polypropylene fiber stabilized reclaimed SB[a] **Subgrade:** Natural SG[b]
	North	**Subbase:** 152 mm modified SB[a]; 152 mm 5% Portland cement & 0.4% polypropylene fiber stabilized reclaimed SB[a] **Subgrade:** Natural SG[b]
7th	South	**Subbase:** 152 mm modified SB[a]; 152 mm 5% Portland cement stabilized reclaimed SB[a] **Subgrade:** Natural SG[b]
	North	**Subbase:** 152 mm modified SB[a]; 152 mm 5% Portland cement stabilized reclaimed SB[a] **Subgrade:** Natural SG[b]
8th	South	**Subbase:** 152 mm modified SB[a] **Subgrade:** natural SG[b]
	North	**Subbase:** 152 mm modified SB[a] **Subgrade:** natural SG[b]
9th	South	**Subbase:** 152 mm modified SB[a]; 152 mm reclaimed SB[a] **Subgrade:** Natural SG[b]
	North	**Subbase:** 152 mm modified SB[a]; 152 mm reclaimed SB[a] **Subgrade** Natural SG[b]
10th	South	**Subbase:** 152 mm modified SB[a] **Subgrade:** natural SG[b]
	North	**Subbase:** 152 mm modified SB[a] **Subgrade:** 305 mm compacted SG[b]; natural SG[b]
11th	South	**Subbase:** 152 mm modified SB[a] **Subgrade:** 305 mm 20% fly ash stabilized SG[b]; natural SG[b]
	North	**Subbase:** 152 mm modified SB[a] **Subgrade:** 305 mm 10% Portland cement stabilized SG[b]; natural SG[b]
12th	South	**Subbase:** 152 mm modified SB[a] **Subgrade:** 305 mm 10% fly ash stabilized SG[b]; natural SG[b]
	North	**Subbase:** 152 mm modified SB[a] **Subgrade:** 305 mm 15% fly ash stabilized SG[b]; natural SG[b]

Notes: [a]SB = subbase

        [b]SG = subgrade

Table 4.2. Summary statistics of FWD testing on each test section

		October 2012 Average Composite FWD Modulus, $E_{c(Oct)}$ (Mpa) [COV[a] (%)]	April 2013 Average Composite FWD Modulus, $E_{c(Apr)}$ (Mpa) [COV[a] (%)]	$E_{c(Apr)}$ / $E_{c(Oct)}$ [COV[a] (%)]
1st	South	163 [34]	22 [17]	0.15 [42]
	North	98 [39]	17 [11]	0.20 [57]
2nd	South	174 [24]	26 [16]	0.16 [25]
	North	128 [24]	26 [22]	0.21 [28]
3rd	South	44 [42]	16 [10]	0.42 [36]
	North	37 [19]	18 [12]	0.49 [21]
4th	South	74 [27]	25 [15]	0.36 [22]
	North	95 [28]	23 [58]	0.25 [60]
5th	South	103 [29]	20 [17]	0.20 [26]
	North	122 [28]	21 [12]	0.18 [26]
6th	South	246 [21]	116 [21]	0.48 [20]
	North	285 [17]	140 [35]	0.49 [34]
7th	South	176 [32]	91 [18]	0.54 [18]
	North	280 [16]	123 [16]	0.44 [20]
8th	South	63 [28]	13 [19]	0.22 [29]
	North	123 [66]	11 [19]	0.13 [59]
9th	South	195 [18]	44 [11]	0.23 [21]
	North	168 [29]	41 [23]	0.26 [27]
10th	South	43 [41]	14 [23]	0.39 [45]
	North	103 [27]	17 [23]	0.17 [35]
11th	South	324 [21]	54 [54]	0.16 [36]
	North	507 [28]	159 [23]	0.34 [39]
12th	South	237 [33]	29 [48]	0.12 [33]
	North	321 [15]	39 [29]	0.12 [23]

Notes: [a]COV = coefficient of variation

Table 4.3. Summary statistics of DCP testing on each test section

Test Section		October 2012 Testing		April 2013 Testing		May 2013 Testing	
		Average Subbase CBR, $CBR_{SB(Oct)}$ (%) [COV^a]	Average Subgrade CBR, $CBR_{SG(Oct)}$ (%) [COV^a]	Average Subbase CBR, $CBR_{SB(Apr)}$ (%) [COV^a]	Average Subgrade CBR, $CBR_{SG(Apr)}$ (%) [COV^a]	Average Subbase CBR, $CBR_{SB(May)}$ (%) [COV^a]	Average Subgrade CBR, $CBR_{SG(May)}$ (%) [COV^a]
1st	South	99 [20]	8 [57]	65 [16]	33 [50]	49 [14]	8 [19]
	North	73 [46]	5 [66]	96 [35]	40 [8]	35 [66]	4 [122]
2nd	South	77 [11]	13 [67]	60 [38]	35 [40]	23 [19]	9 [77]
	North	86 [48]	13 [30]	45 [53]	26 [49]	31 [8]	8 [5]
3rd	South	44 [38]	7 [92]	26 [50]	2 [29]	21 [36]	10 [63]
	North	38 [8]	10 [40]	24 [59]	9 [104]	22 [11]	5 [51]
4th	South	64 [93]	11 [47]	53 [20]	6 [53]	149 [22]	9 [18]
	North	88 [11]	8 [47]	47 [72]	3 [32]	58 [21]	6 [44]
5th	South	116 [33]	8 [61]	49 [12]	9 [57]	61 [21]	6 [90]
	North	138 [30]	10 [65]	49 [48]	2 [38]	72 [43]	9 [47]
6th	South	^{b}	^{b}	52 [^{c}]	4 [^{c}]	^{b}	^{b}
	North	164 [^{c}]	33 [^{c}]	77 [9]	5 [63]	189 [b]	12 [^{c}]
7th	South	^{b}	^{b}	44 [51]	6 [13]	268 [b]	10 [^{c}]
	North	^{b}	^{b}	52 [^{c}]	3 [^{c}]	101 [b]	26 [^{c}]
8th	South	57 [10]	8 [44]	43 [33]	3 [16]	54 [7]	10 [64]
	North	65 [12]	15 [59]	13 [38]	4 [35]	31 [24]	8 [34]
9th	South	^{b}	^{b}	49 [39]	4 [54]	64 [5]	7 [114]
	North	117 [15]	11 [64]	22 [30]	2 [13]	37 [8]	3 [19]
10th	South	32 [57]	2.6 [31]	26 [11]	2 [69]	45 [18]	3 [36]
	North	53 [13]	4 [9]	29 [14]	1 [35]	63 [31]	3 [68]
11th	South	86 [39]	44 [5]	25 [27]	14 [20]	29 [51]	48 [39]
	North	^{b}	^{b}	12 [16]	63 [39]	34 [17]	57 [21]
12th	South	144 [19]	21 [73]	39 [33]	10 [79]	33 [31]	32 [10]
	North	179 [13]	38 [32]	15 [43]	13 [57]	22 [36]	18 [18]

Notes: ^{a}COV = coefficient of variation
^{b}All DCP tests on test section reached refusal within subbase layer
^{c}Test section contained only one data point (i.e., indeterminate coefficient of variation)

Table 4.3. October 2012 testing and April/May 2013 testing multivariable models for FWD composite moduli as functions of subbase and subgrade PI values

Multivariable Analysis[a]	Term	Estimate	Standard Error (MPa)	t Ratio	Prob. > t[b]	r^2 Adj
Oct. 2012	b_o	3.261	1.339	25.7	**< 0.0001**	0.698
	b_1	-0.597	1.318	-5.0	**< 0.0001**	
	b_2	-0.731	1.282	-6.8	**< 0.0001**	
min[Apr. 2013, May 2013]	b_o	2.435	1.511	13.6	**< 0.0001**	0.662
	b_1	0.078	1.295	0.7	0.478	
	b_2	-0.799	1.210	-9.6	**< 0.0001**	

Notes: [a]$\log(E_c) = b_o + b_1 \log(PI_{SB}) + b_2 \log(PI_{SG})$
[b]Emboldened p values indicate statistical significance
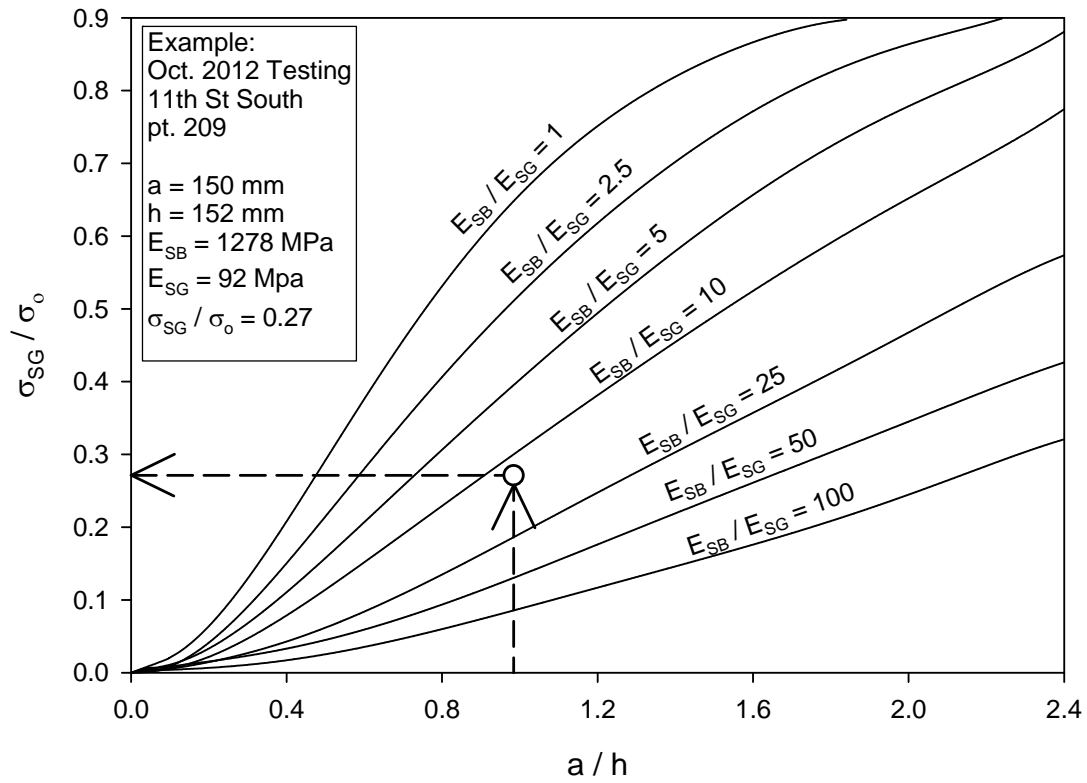
Figure 4.1. Vertical stress increase at interface of subbase and subgrade layers
(adapted from Huang, 2004)
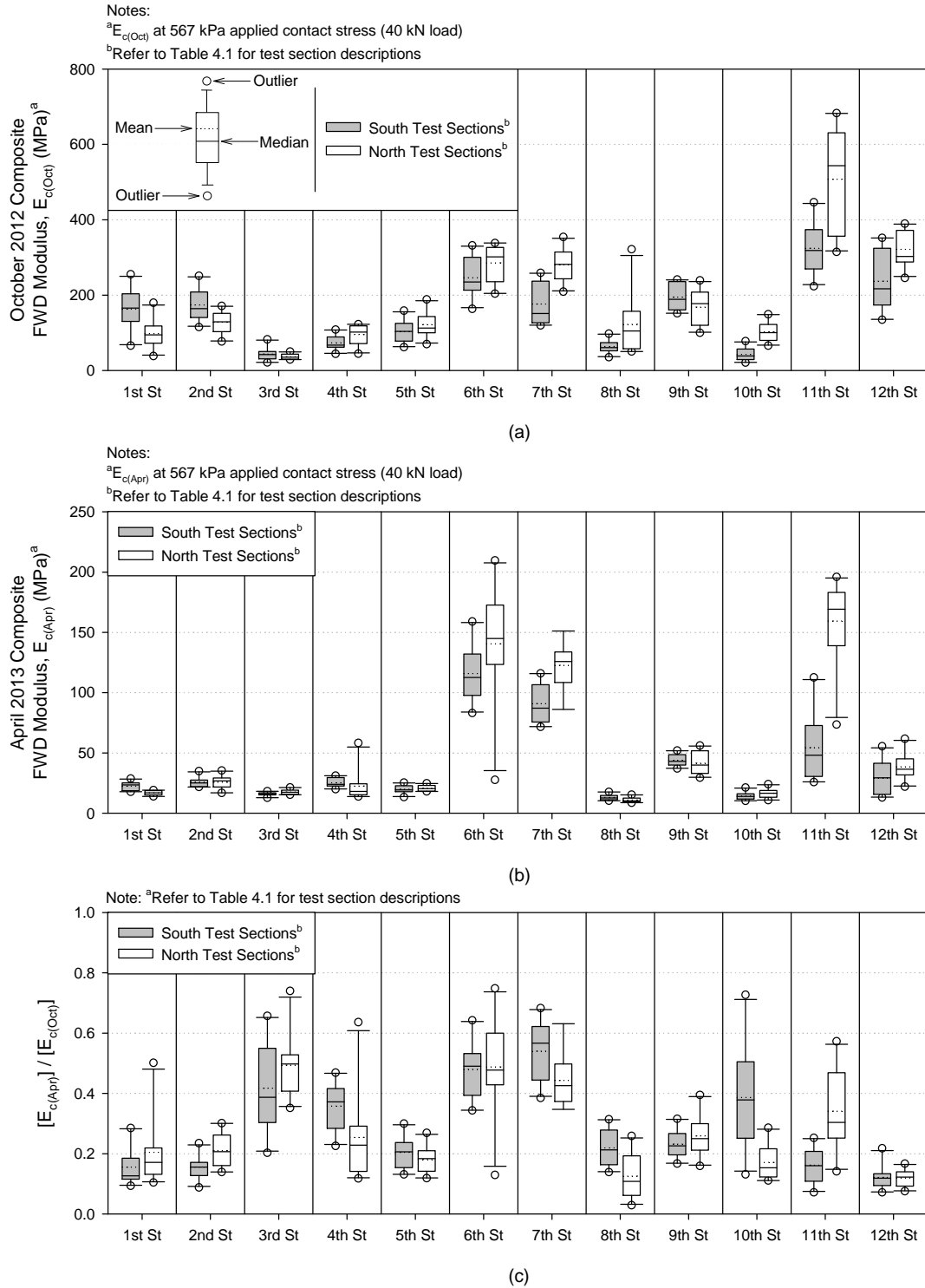
Figure 4.2. Average test section (a) composite moduli from October 2012 FWD testing, (b) composite modulit from April 2013 FWD testing, and (c) ratios of October 2012 to April 2013 FWD composite moduli

Notes:
[a]$E_{c(Oct)}$ and $E_{c(Apr)}$ at 567 kPa applied contact stress (40 kN load)
[b]PC = Portland cement
[c]Model comprised PC stabilized
 subbase and subgrade test points
[d]CI = confidence interval
[e]SE = standard error of estimate

△   No PC[b] stabilization
●   PC[b] stabilized subbase
○   PC[b] stabilized subgrade

[c]$E_{c(Apr)} = 13.5\ E_{c(Oct)}^{\ 0.398}$
$r^2 = 0.406$, n = 48, SE[e] = 28.2 MPa

95% CI[d]

95% CI[d]

$E_{c(Apr)} = 13.9\ \exp[0.0038\ E_{c(Oct)}]$
$r^2 = 0.525$, n = 191, SE[e] = 9.9 MPa

No seasonal change in E_c

April 2013 Composite FWD Modulus, $E_{c(Apr)}$ (MPa)[a]

October 2012 Composite FWD Modulus, $E_{c(Oct)}$ (MPa)[a]

Figure 4.3. Correlations between April 2013 composite FWD moduli and October 2012 composite FWD moduli

90

Figure 4.4. Average subbase layer California bearing ratio values from DCP testing during (a) October 2012, (b) April 2013, and (c) May 2013 for each test section

91

Notes:
[a]Refer to Table 1 for test section descriptions
[b]All tests on 6th St South, 7th St South, 7th St North, 9th St South, and 11th st North test sections reached refusal within subbase layer
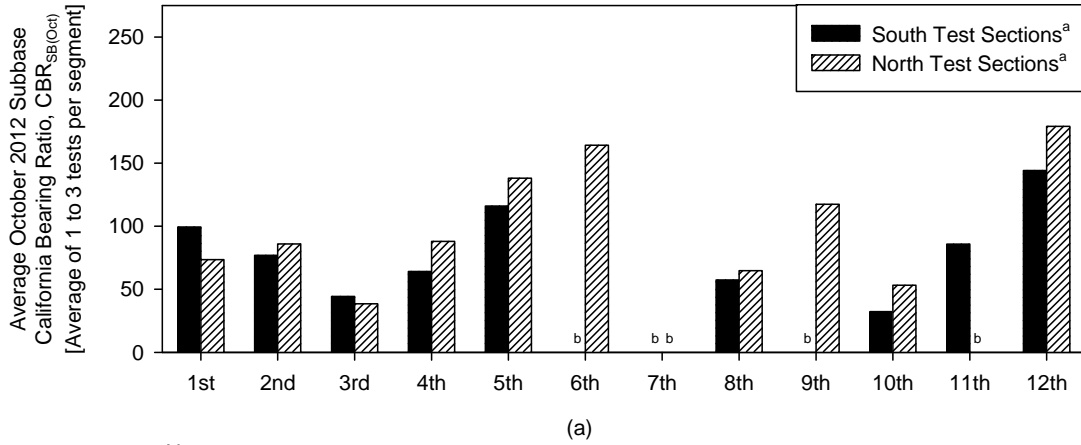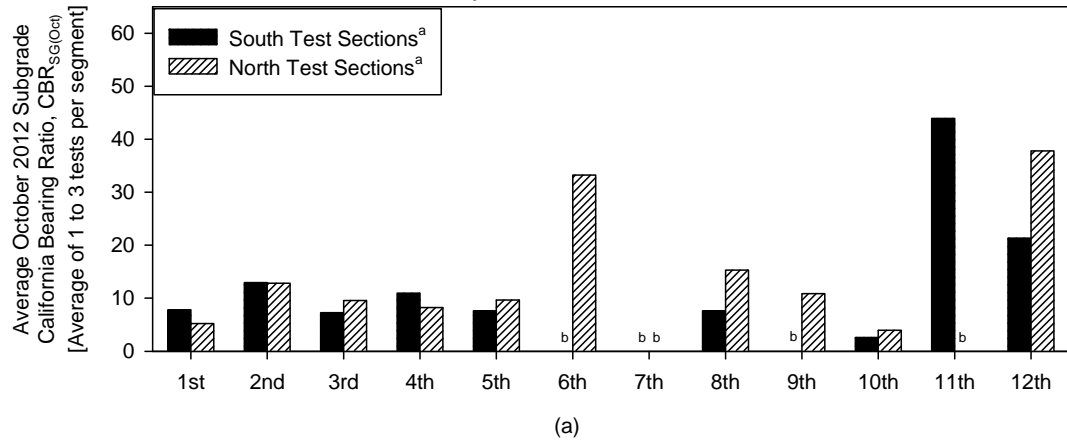
(a)

Notes:
[a]Refer to Table 1 for test section descriptions

(b)
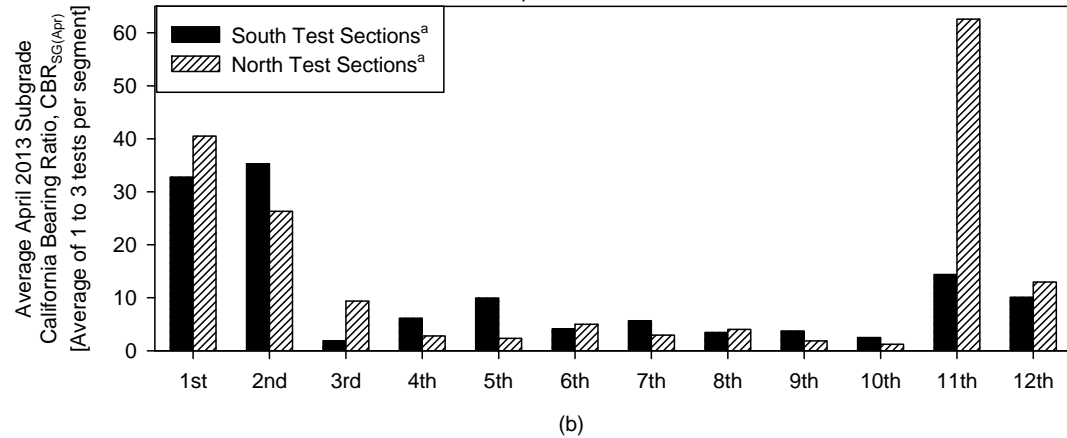
Notes:
[a]Refer to Table 1 for test section descriptions
[b]All tests on 6th St South test section reached refusal within subbase layer

(c)
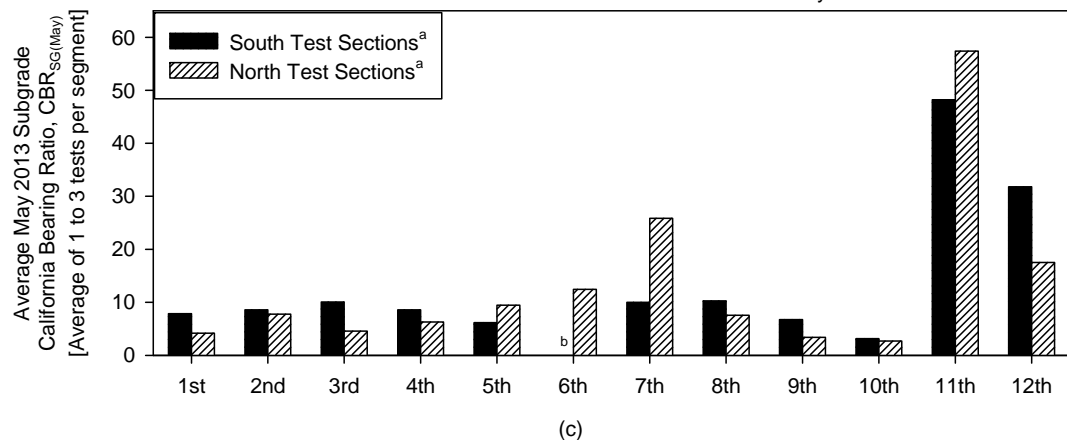
Figure 4.5. Average subgrade layer California bearing ratio values from DCP testing during (a) October 2012, (b) April 2013, and (c) May 2013 for each test section

Note: Test points with cement stabilization not shown due to DCP refusal in October 2012

No statistically significant correlation

$CBR_{SB(Apr)}$

$CBR_{SB(May)}$

No seasonal change in CBR

Minimum of April 2013 and May 2013 Subbase California Bearing Ratios, $min[CBR_{SB(Apr)}, CBR_{SB(May)}]$ (%)

October 2012 Subbase California Bearing Ratio, $CBR_{SB(Oct)}$ (%)
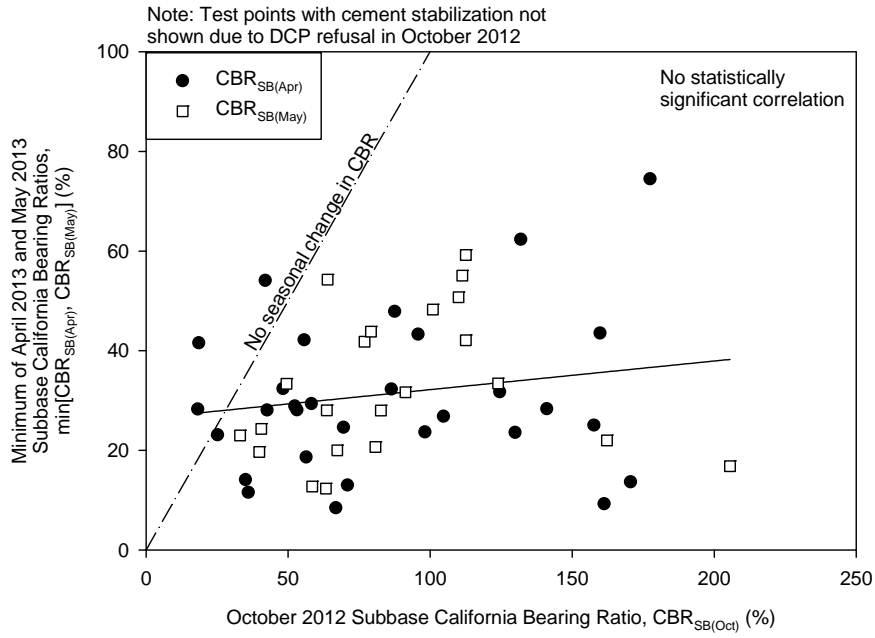
(a)

Notes:
[a]Test points with cement stabilization not shown due to DCP refusal in October 2012
[b]SE = standard error of estimate
[c]CI = confidence interval

$CBR_{SG(Apr)}$

$CBR_{SG(May)}$

$min[CBR_{SG(Apr)}, CBR_{SG(May)}] = 1.36 \, CBR_{SG(Oct)}^{0.57}$
$r^2 = 0.380$, $n = 52$, $SE^{b} = 3.7\%$

95% CI^{c}

No seasonal change in CBR

Minimum of April 2013 and May 2013 Subgrade California Bearing Ratios, $min[CBR_{SG(Apr)}, CBR_{SG(May)}]$ (%)

October 2012 Subgrade California Bearing Ratio, $CBR_{SG(Oct)}$ (%)
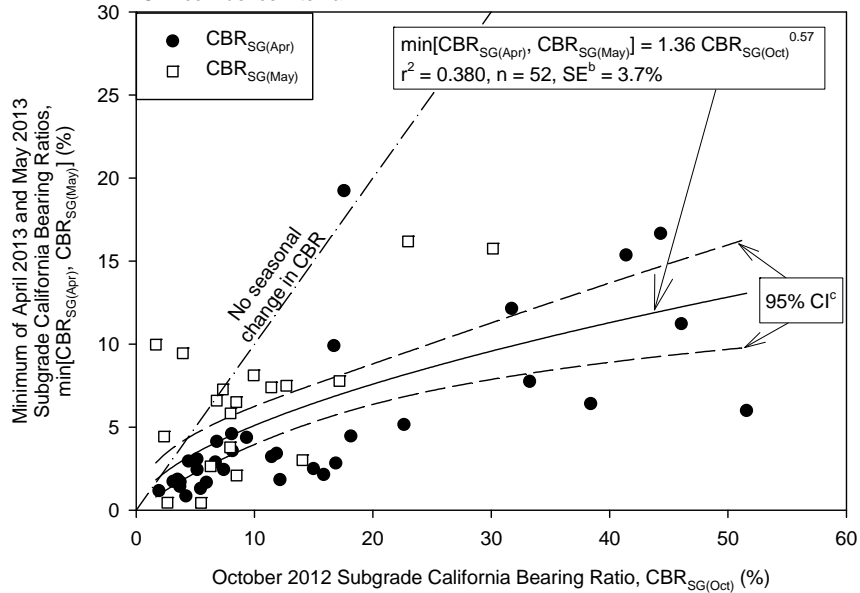
(b)

Figure 4.6. Correlations between (a) minimum of April 2013 and May 2013 subbase CBR values and October 2012 subbase CBR values and (b) minimum of April 2013 and May 2013 subgrade CBR values and October 2012 subgrade CBR values
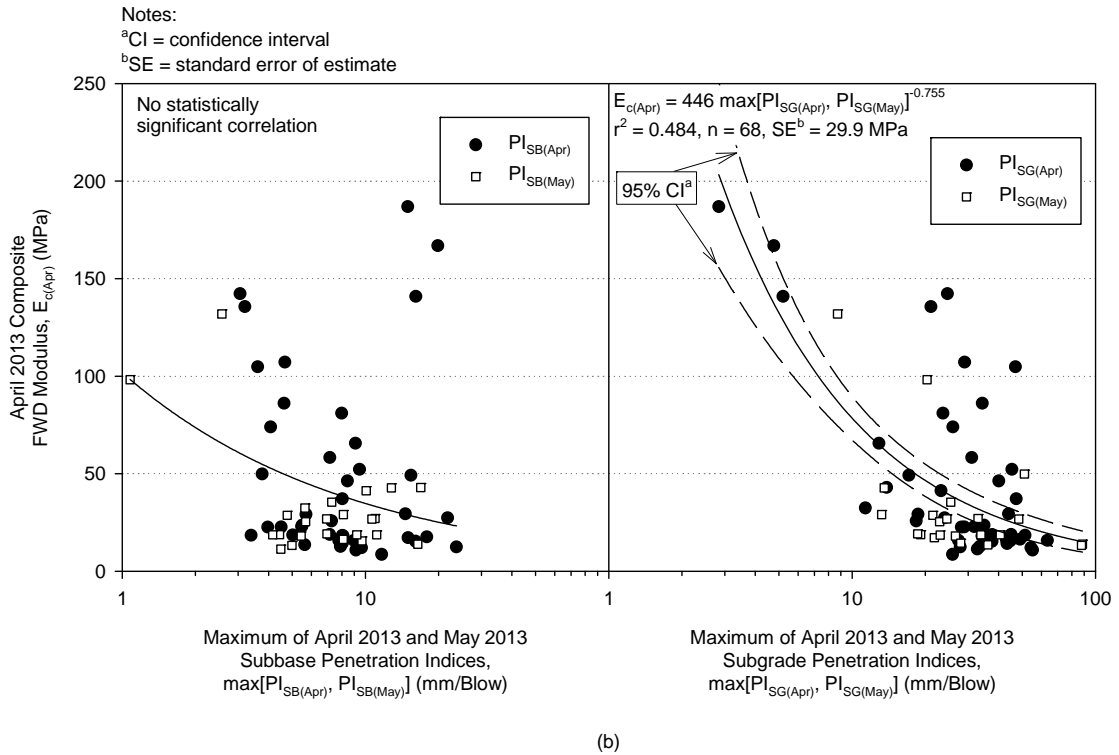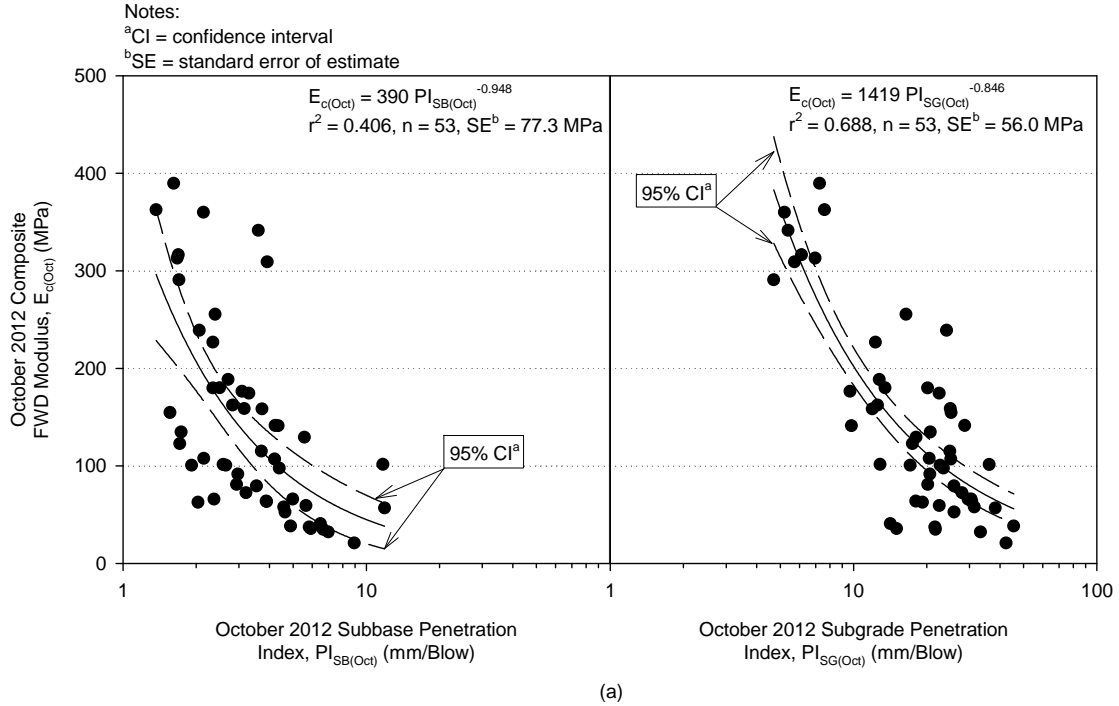
Figure 4.7. Correlations between (a) October 2012 FWD composite moduli and October 2012 subbase and subgrade CBR values and (b) April 2013 FWD composite moduli and minimum of April 2013 and May 2013 subbase and subgrade CBR values
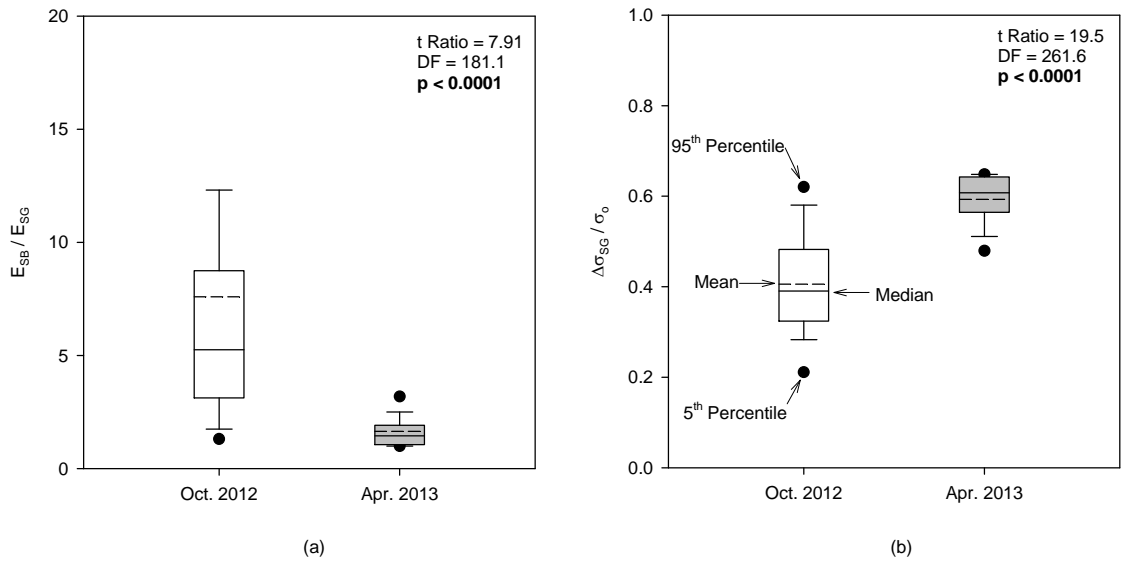
Figure 4.8. Comparisons between October 2012 and April 2013 (a) ratios of subbase to subgrade elastic moduli and (b) ratios of distributed stress on subgrade to applied surface stress

CHAPTER 5. INFLUENCE OF PAVEMENT FOUNDATION STIFFNESS ON ROLLER-INTEGRATED COMPACTION MONITORING FOR ASPHALT PAVEMENT CONSTRUCTION

Peter J. Becker, David J. White, and Pavana K.R. Vennapusa

A paper to be submitted to the International Journal of Pavement Engineering, Taylor & Francis Journals

5.1 Abstract

This paper presents results of an experimental investigation assessing the influence of pavement foundation condition on construction of asphalt pavements using roller-integrated compaction monitoring (RICM) technologies. Asphalt pavements overlying pavement foundations of variable stiffnesses were compacted using a Hamm HD+ 120 VV dual smooth-drum vibratory roller. The roller was equipped with an RICM system that yielded Hamm measurement value (HMV) and temperature measurements in real time. To compare influence of the pavement foundation, HMV measurements were taken on the subbase layer prior to paving then correlated to HMV measurements taken during paving. Comparisons were made between RICM measurements and quality control and quality assurance test methods such as relative compaction, falling weight deflectometer (FWD) modulus, and asphalt surface temperature. Recommendations are provided for improving asphalt pavement construction specifications that use RICM technologies.

5.2 Introduction

Recently, the Federal Highway Administration (FHWA) has sponsored demonstration projects across the United States (Chang, Xu, Rutledge, & Garber, 2014; Chang et al.,

2011; White & Vennapusa, 2008) to garner interest in implementing roller-integrated compaction monitoring (RICM) for asphalt pavement construction. Outcomes from the demonstration projects maintain that RICM is more suitable to traditional quality control (QC) and quality assurance (QA) methods because RICM provides continuous compaction control data that correlate well to performance-related properties (i.e., stiffness). As a result, FHWA produced a new guide specification [Federal Highway Administration (FHWA), 2014] to incorporate RICM into asphalt pavement construction applications. The guide specification recommends that, prior to paving, contractors 'pre-map' existing pavement foundations (subbase and subgrade) with a roller equipped with RICM, but solely to identify 'weak areas'.

Analysis of field data from Thurner and Sandström (1980) shows that RICM measurements taken on pavement subgrade and subbase layers both correlate to asphalt pavement layer RICM values (r^2 equalled 0.44 and 0.72, respectively), so pavement foundation quality likely influences the RICM values measured during asphalt pavement construction. White and Vennapusa (2008) reported a case study that support this finding in which subbase layer RICM measurements strongly correlated with asphalt pavement layer RICM measurements. Highway agencies will therefore need to revise their existing guide specifications to account for pavement foundation influence. This paper aims to confront this implementation obstacle by comparing RICM measurements taken on asphalt pavements that overlaid pavement foundations of varying stiffnesses and proposing recommendations for future research and for practice. The objectives of the study presented in this paper were to evaluate:

- comparisons of Hamm measurement values (HMV) measured on subbase, asphalt base course, and asphalt surface course layers;

- changes in HMV and relative compaction with increasing pass count;

- regression relationships between HMV, relative compaction, and FWD modulus by spatially pairing the data; and

- agreement between asphalt surface temperature measurements from roller-integrated temperature sensors and from a FLIR® thermal camera.

The results and analyses documented in this paper will help to develop improved specifications and guidelines for the construction of asphalt pavements.

5.3 RICM for Asphalt Pavement Construction

Compaction rollers that incorporate RICM technologies measure and analyse roller drum response to underlying pavement and subgrade layers. Drum response is quantified using RICM values calculated from accelerometer measurements, which are then georeferenced using built-in global positioning system (GPS) technologies. An in-cab computer uses the georeferenced measurements to display spatial maps of RICM values for roller operators in real time.

Commercially available RICM technologies generally report RICM values as either dimensionless indices (e.g., compaction control value) or as dynamic moduli (e.g., vibration modulus) (Kröber, Floss, & Wallrath, 2001). Index RICM values are calculated using selected frequency harmonics for set time intervals, and dynamic modulus RICM values are calculated from drum-ground interactions. The RICM value featured in this paper is of the dimensionless index type and is discussed further in the test methods section of the paper.

Several research studies (Chang et al., 2014; Chang et al., 2011; Gallivan, Chang, &

Horan, 2011; Scherocman, Rakowski, & Uchiyama, 2007; Vennapusa, White, & Schram,

2013; White & Vennapusa, 2008; Xu & Chang, 2013; Yoon, Hastak, & Lee, 2015) have

correlated RICM measurements with relative compaction and stiffness/modulus of

asphalt pavements. Correlations between RICM measurements and asphalt pavement

relative compaction are inconsistent. For example, Scherocman et al. (2007) reported two

field studies that correlated RICM measurements with relative compaction. For one of the

reported field studies, RICM measurements strongly correlated with relative compaction

($r^2 = 0.69$), while RICM measurements did not correlate with relative compaction for the

second field study. In general, RICM studies indicate that RICM measurements correlate

better with stiffness measurements [e.g., falling weight deflectometer (FWD) modulus]

than with relative compaction. This paper presents results comparing relative compaction

and FWD modulus measurements with RICM values from a project comprising

pavement foundations of varying stiffnesses and discusses the factors affecting the

correlations.

5.4 Project Conditions

The project site; which was located in Boone, Iowa, United States; comprised a grid

of gravel roadway sections that encompassed a combined length of 7.7 km. Subgrade soil

at the project site classified as clay of low plasticity or CL [AASHTO classification A-

6(5)], and the groundwater table was located at about 0.9 m to 1.5 m below grade.

Freeze-thaw processes caused excessive deterioration of the gravel roadways, so their

reconstruction was required (Becker, White, Vennapusa, & Dunn, 2014; Becker, White,

Vennapusa, White, & Zhang, 2015; White, Becker, Vennapusa, Dunn, & White, 2013;

Zhang, 2013). The roadways were reconstructed into 24–205 m long and 6 m wide test sections over the course of two phases—Phase I (pavement foundation construction) and Phase II (asphalt pavement placement). This paper, however, only discusses results from nine of the twenty-four test sections at the project site.

The Phase I contractor constructed the test section pavement foundations in summer 2012. In general, construction required removing 152 to 305 mm of gravel and subgrade from the pre-existing roadways, and then placing a nominal 152 mm thick layer of modified subbase [per Iowa Department of Transportation (DOT) (2016)] that classified as GP-GM (AASHTO classification A-1-a). Select test sections included an additional 152 mm thick layer of subbase that had been reclaimed from the pre-existing roadway gravel, which classified as SM (AASHTO classification A-1-a). The contractor incorporated different soil stabilisation technologies into the pavement foundations of seven test sections:

- woven geotextile fabric (TS-W);
- non-woven geotextile fabric (TS-NW);
- biaxial polymer geogrid (TS-BX);
- triaxial polymer geogrid (TS-TX);
- Portland cement (PC) stabilisation of reclaimed subbase layer (TS-PCSB);
- fly ash stabilisation of subgrade layer (TS-FASG); and
- PC stabilisation of subgrade layer (TS-PCSG).

Two control test sections did not include soil stabilisation technologies—compacted subgrade (TS-CSG) and natural subgrade (TS-NSG). Table 5.1 summarizes key features of the test section pavement foundations.

Phase II construction, which occurred in summer 2013, involved placing a 102 mm thick asphalt base course layer and a 51 mm thick asphalt surface course layer. Test section surface and base course layer asphalt mixes comprised different combinations of either warm mix or hot mix binder and either low or high absorption aggregate. Table 5.1 details the binder and aggregate types used in the test section asphalt pavement layers. All test section asphalt pavement layers were compacted using a Hamm HD+ 120 VV dual smooth-drum vibratory roller equipped with RICM technology that is discussed in the following section of the paper.

5.5 Test Methods

The following sections describe the test procedures used in this study—RICM, nuclear density gauge testing, asphalt cores, and FWD testing. In addition, a FLIR® thermal camera measured asphalt surface temperature (T_{FLIR}) for comparison with asphalt surface temperatures measured from roller-integrated temperature sensors (T_{Roller}). Both nuclear density gauge testing and RICM were conducted during asphalt pavement during the summer of 2013. RICM measurements were recorded on top of subbase layers before asphalt placement and during construction of asphalt base and surface course layers. FWD tests that were conducted on top of test section subbase layers were performed 3-months after subbase placement during October 2012, and FWD tests that were conducted on top of test section asphalt surface course layers were performed 2-months after asphalt pavement placement during September 2013.

5.5.1 RICM system

This study used a Hamm HD+ 120 VV dual smooth-drum vibratory roller (Figure 5.1a) to compact test section asphalt layers and collect RICM measurements. The roller

was equipped with Hamm's RICM system and real-time kinematic global positioning system using an on-site base station. Table 5.2 summarizes key features of the roller and the RICM system.

Hamm's RICM system uses the dimensionless index of Hamm measurement value (HMV) for compaction quality control. Sensors that are built into the drum measure vertical acceleration, and the on-board computer (Figure 1b) uses the measurements to calculate and then output HMV. According to Chang et al. (2014), HMV is identical to compaction meter value (CMV), so HMV is calculated using equation 5.1 (Sandström & Pettersson, 2004):

$$HMV = C \times \frac{A_{2\Omega}}{A_\Omega} \tag{5.1}$$

where HMV = Hamm measurement value, C = constant (equal to 300), $A_{2\Omega}$ = acceleration of the first harmonic component of the vibration, and A_Ω = acceleration of the fundamental component of the vibration.

5.5.2 Relative compaction

Nuclear density gauge testing per ASTM D 2950 was used to determine asphalt pavement relative compaction (RC_{NG}) in situ, and asphalt cores were used to determine asphalt pavement relative compaction (RC_{Core}) in laboratory. Both RC_{NG} and RC_{Core} were calculated using equation 5.2

$$RC(\%) = \frac{\gamma_t}{\gamma_w G_{mb}} \tag{5.2}$$

where RC = relative compaction; γ_t = total unit weight of asphalt mixture; γ_w = unit weight of water; and G_{mb} = bulk specific gravity (determined in laboratory per AASHTO T 166).

5.5.3 Falling weight deflectometer

A KUAB falling weight deflectometer (FWD) setup that was equipped with a 300 mm diameter loading plate assessed stiffnesses along the test sections. At each testing location, the FWD test setup applied one seating drop then four loading drops that ranged from 27 kN to 71 kN. A load cell within the FWD setup measured the actual applied loadings, and a seismometer measured vertical deflection at the centre of the loading plate. Composite elastic moduli (E_{FWD}) were calculated from FWD measurements using equation 5.3

$$E_{FWD} = \frac{\sigma_o r (1 - v^2) f}{\delta_o} \qquad (5.3)$$

where E_{FWD} = composite elastic modulus (MPa); σ_o = applied stress (kPa); r = loading plate radius (mm); v = Poisson's ratio (assumed as 0.4); f = stress distribution shape factor; and δ_o = deflection at loading plate centre. The FWD setup incorporated a four-part segmented plate that is assumed to provide uniform stress distribution, so the value for f was assumed as 2 [see Vennapusa & White (2009) for selection of shape factors depending on stress distribution]. E_{FWD} values in this study were calculated from δ_o values that had been normalized to loading drops equal to 40 kN [i.e., one-half equivalent single axle load (ESAL)] per American Association of State Highway and Transportation Officials (AASHTO) (1993). For FWD tests conducted on test section surface course layers, pavement temperatures were measured and δ_o values were normalized to 20 °C per AASHTO (1993).

Using FWD tests conducted on subbase layers and FWD tests conducted on surface course layers, equations 5.4 and 5.5 were used to calculate elastic moduli for asphalt pavement layers (i.e., combined base and surface course layers)

$$\delta_{o(SC)} = 2\sigma_o r \left\{ \left[\frac{(1 - v_{SB}{}^2)}{E_{FWD(SB)}} \right] \left[1 - \frac{1}{\sqrt{1 + \left(\frac{nh}{r}\right)^2}} \right] + \frac{(1 - v_{AP}{}^2)}{E_{AP}\sqrt{1 + \left(\frac{h_e}{r}\right)^2}} \right\} \quad (5.4)$$

$$h_e = nh \sqrt[3]{\frac{E_{AP}}{E_{FWD(SB)}} \frac{(1 - v_{SB}{}^2)}{(1 - v_{AP}{}^2)}} \quad (5.5)$$

where $\delta_{o(SC)}$ = deflection measured on surface course layer and normalized to 20 °C; σ_o = applied stress; r = loading plate radius; v_{SB} = Poisson's ratio for subbase and subgrade layers (assumed as 0.4); $E_{FWD(SB)} = E_{FWD}$ from FWD tests conducted on subbase layer; n = empirical coefficient (equal to 0.9); h = nominal thickness of asphalt pavement layer; v_{AP} = Poisson's ratio for asphalt pavement layers; E_{AP} = elastic modulus for asphalt pavement layer, and h_e = equivalent thickness of asphalt pavement layer. Equations 5.4 and 5.5 are based off of the equivalent thickness theory from Odemark (1949), which uses the concept of flexural rigidity to approximate the layered stress distribution solution from Burmister (1945). Values for v_{AP} equalled 0.25 per the level 3 design input for asphalt Poisson's ratio from the mechanistic-empirical pavement design guide (MEPDG) (National Cooperative Highway Research Program (NCHRP), 2008).

5.6 Statistical Methods

Statistical methods used in this paper include the first-order, variance-based sensitivity analyses of multivariable models and the comparison of measurement method agreement. Statistical significance in this study was based on an alpha value of 0.05 (i.e., 95% confidence).

5.6.1 First-order, variance-cased sensitivity analysis

The authors of this paper developed multivariable models to empirically predict HMV measurements from subbase FWD composite moduli $[E_{FWD(SB)}]$ and asphalt pavement moduli (E_{AP}). First-order, variance-based sensitivity analyses of the multivariable models assessed the sensitivity of HMV measurements to changes $E_{FWD(SB)}$ and E_{AP}. Per Sobol' (1990), the influences of $E_{FWD(SB)}$ and E_{AP} on HMV measurements were quantified using sensitivity indices (S) that are calculated from equations 5.6 and 5.7

$$S_i = \frac{V_i}{V_Y} \tag{5.6}$$

$$V_Y = \sum_{i=1}^{N} V_i \tag{5.7}$$

where S_i = sensitivity index of ith independent variable; V_i = partial variance of ith independent variable; V_Y = total unconditional variance; and N = number of independent variables. The summation of all sensitivity indices for a given model must equal unity (Sobol', 1990); therefore the authors interpreted sensitivity index for each independent variable as the percent influence of the independent variable on the predicted dependent variable.

5.6.2 Agreement between different measurement methods

Comparisons between two indirect methods of measurement are oftentimes misleading because both methods are expected to generate measurement error, so Bland & Altman (1999) recommend comparing measurement agreement instead of correlating measurements with one another. Bland Altman plots graphically represent measurement

agreement by plotting difference in measurements versus average of measurements, and measurement agreement limits quantify measurement agreement. If the difference in measurements distributes uniformly, then the measurement agreement limits are calculated from equation 5.8

$$AL = \bar{d} \pm sZ_{\alpha/2} \qquad (5.8)$$

where AL = agreement limits; $\bar{d}$ = mean of difference in measurements; s = standard deviation of difference in measurements; and $Z_{\alpha/2}$ = two-tailed standard score for a given alpha value. Bland & Altman (1999) detail a regression-based approach for calculating agreement limits when the difference in measurements distributes nonuniformly.

5.7 Results and Analysis

5.7.1 underlying layer influence on HMV

Figure 5.2 presents boxplot comparisons of HMV_{SB} and final pass HMV_{BC} and HMV_{SC} for each test section along the centreline, and Table 5.3 summarizes the average and coefficient of variation values for the HMV_{SB} and final pass HMV_{BC} and HMV_{SC} measurements by test section. On average, HMV_{SB} ranges from 7 to 67, HMV_{BC} ranges from 8 to 24, and HMV_{SC} ranges from 21 to 48.

Test section pavement foundations ranged from soft to very stiff, as evidenced by average FWD moduli measured on top of subbase layers [$E_{FWD(SB)}$] (Table 5.3). Average $E_{FWD(SB)}$ values on stiff pavement foundation test sections (TS-PCSB, TS-FASG, and TS-PCSG) ranged from 280 to 507 MPa, and average $E_{FWD(SB)}$ values on soft pavement

106

foundation test sections (TS-W, TS-NW, TS-BX, TS-TX, TS-CSG, and TS-NSG) ranged from 43 MPa to 122 MPa.

In general, stiff pavement foundation test sections differed from soft pavement foundation test sections in that the stiff pavement foundation test sections yielded significantly higher HMV_{SB}, HMV_{BC}, and HMV_{SC} measurements. On stiff pavement foundation test sections, average HMV_{SB} ranged from 33 to 67, average HMV_{BC} ranged from 17 to 24, and HMV_{SC} ranged from 38 to 48; and, on soft pavement foundation test sections, average HMV_{SB} ranged from 7 to 10, average HMV_{BC} ranged from 8 to 10, and HMV_{SC} ranged from 21 to 26. Therefore, HMV measured during asphalt pavement construction reflects the stiffness of underlying pavement foundation.

Table 5.4 summarizes statistical comparisons between HMV_{SB}, HMV_{BC}, and HMV_{SC} by test section. In general, HMV measurements on soft pavement foundation test sections increase with each additional layer (i.e., $HMV_{SC} > HMV_{BC} > HMV_{SB}$). However, stiff pavement foundation layer HMV decreases from subbase to base course (i.e., $HMV_{SB} > HMV_{BC}$) and then increases from base course to surface course (i.e., $HMV_{SC} > HMV_{BC}$). TS-PCSG [average $E_{FWD(SB)}$ equalled 507 MPa] was an exception in that HMV_{SB} significantly exceeded both HMV_{BC} and HMV_{SC}.

Differences in HMV_{SB}, HMV_{BC}, and HMV_{SC} were all statistically significant across the test sections, except the comparison of HMV_{SB} and HMV_{BC} on TS-BX (p = 0.49). Additional t testing showed that HMV_{SB} on TS-BX was significantly greater than HMV$_{SB}$ on all other soft pavement foundation test sections (all p values were less than 0.0001), even though $E_{FWD(SB)}$ on TS-BX (equalled 103 MPa) was not substantially greater than all other soft pavement foundation E$_{FWD(SB)}$ values. Therefore, the biaxial polymer

geogrid underlying the TS-BX subbase may have influenced HMV measurements on that test section.

Figure 5.3 presents a scatterplot matrix for associations between spatially paired HMV_{SB}, final pass HMV_{BC}, and final pass HMV_{SC} measurements across the test sections. In general, HMV_{SB}, HMV_{BC}, and HMV_{SC} all positively correlated with one another. Because HMV_{SB} did not distribute normally (skewed right), nonlinear equations best fit the associations between HMV_{SB} and HMV_{BC} ($r^2 = 0.55$) and between HMV_{SB} and HMV_{SC} ($r^2 = 0.58$). The distributions for both HMV_{BC} and HMV_{SC} were approximately normal, so a linear equation best fit the association between HMV_{BC} and HMV_{SC} ($r^2 = 0.52$). Results from the regression analyses are consistent with findings from White and Vennapusa (2008) and further demonstrate how underlying layers influence HMV measured during asphalt pavement construction.

5.7.2 Comparisons between RICM and QC spot test methods

During asphalt base course layer construction, RC_{NG} and T_{FLIR} in situ spot measurements with increasing roller pass number were obtained at a single location within each test section. The in situ testing process was repeated for asphalt surface course layer construction, although tests were conducted at separate locations within the test sections. GPS coordinates were obtained for each in situ spot test location to spatially pair RC_{NG} and T_{FLIR} measurements with RICM data.

5.7.2.1 Comparison of HMV with nuclear density gauge relative compaction

Figure 5.4 presents asphalt base and surface course RC_{NG} and HMV measurements with increasing roller pass number for all of the test sections combined. For both base course and surface course asphalt layers, RC_{NG} increased with increasing roller pass

number. Hyperbolic models best fit the associations between base course RC_{NG} [$RC_{NG(BC)}$] and roller pass number ($r^2 = 0.83$) and between surface course RC_{NG} [$RC_{NG(SC)}$] and roller pass number ($r^2 = 0.90$).

Although asphalt layers quite evidently densify with additional compactive effort, there is little to no change in HMV with increasing roller pass numbers. No statistically significant correlation exists between HMV_{BC} and number of roller passes, and a slight correlation exists between HMV_{SC} and number of roller passes ($r^2 = 0.16$). Interpretation of Figure 5.4 suggests that HMV measurements do not strongly associate with RC_{NG}, so the authors used data from all test sections to conduct regression analyses (Table 5.5) between HMV$_{BC}$ and RC$_{NG(BC)}$ and between HMV_{SC} and $RC_{NG(SC)}$, and, as suspected, neither regression analysis yielded a statistically significant correlation.

However, Vennapusa and White (2013) noted that relative compaction and RICM measurements do not correlate well with one another when data sets comprise heterogeneous underlying layer conditions (e.g., data combined from multiple test locations). Therefore, regression analyses between $RC_{NG(BC)}$ and HMV_{BC} and between $RC_{NG(SC)}$ and HMV_{SC} by test section are summarized in Table 5.5. On the sole basis of r^2 value, the majority of regression analyses did not yield statistically significant correlations; however, r^2 values for certain test sections were considerably large (e.g., r^2 equalled 0.89 for TS-PCSB base course). Despite the occasional large r^2 value, F-tests indicated that only one of the correlations (TS-PCSG) was statistically significant because, in general, the test section regression analyses had insufficient amounts of degrees of freedom. So, neither base course nor surface course HMV adequately predicts

its respective RC_{NG}, even after data sets representing the entire project site were separated and grouped together by test section.

5.7.2.2 Agreement between roller-integrated temperature sensor and FLIR® thermal camera asphalt surface temperature measurements

According to West, Watson, Turner, and Casola (2010); mix temperature is one of the primary factors affecting asphalt pavement compactibility. Asphalt mix temperature must be high enough for the binder to act as a lubricant, thereby facilitating the movement of aggregates in a dense configuration. In addition, asphalt mixes become stiffer and more resistant to compaction with decreasing mix temperature (Roberts, Kandal, Brown, Lee, & Kennedy, 1996). Therefore, control of asphalt mix temperature is critical to the construction of quality pavements.

Figure 5.5a presents the Bland Altman plot comparing asphalt surface temperatures measured from the roller-integrated temperature sensors (T_{Roller}) and from the FLIR® thermal camera (T_{FLIR}). There was an apparent relationship between temperature measurement difference and average temperature measurement, so the authors logarithmically transformed the temperature measurement data as recommended by Bland and Altman (1999). Despite the logarithmic transformation, the relationship remained ($r^2 = 0.38$) so the authors used the regression-based approach detailed by Bland & Altman (1999) to develop the agreement interval. In general, T_{Roller} measurements tended to be lower than T_{FLIR} measurements with the measurement discrepancy increasing in magnitude with decreasing temperature.

Figure 5.5b presents the results of the agreement comparison as a plot of T_{Roller} versus T_{FLIR}. Consistent with the Bland Altman plot, T_{Roller} and T_{FLIR} values seem to be

approximately equal to one another at warm FLIR® temperatures (T_{FLIR} equals about 90 to 110 °C), but T_{FLIR} tended to be increasingly greater than T_{Roller} with decreasing FLIR® temperature. The upper agreement limit intersects the line of equality (i.e., $T_{Roller} = T_{FLIR}$) at T_{FLIR} equal to 87.4 °C, so T_{Roller} and T_{FLIR} values are in agreement with another when FLIR® temperature exceeds 87.4 °C (zone of agreement). T_{Roller} and T_{FLIR} values are not in agreement when FLIR® temperature is less than 87.4 °C (zone of disagreement). Average T_{Roller} to T_{FLIR} ratios ranged from 0.8 to 1.0 within the zone of agreement and from 0.7 to 0.8 within the zone of disagreement. Therefore, the roller-integrate temperatures sensors in this study adequately measured asphalt surface temperature at high temperatures (greater than 87.4 °C), but underestimated asphalt surface temperature at low temperatures (less than 87.4 °C).

5.7.3 Regression analyses between HMV and QA properties

The overseeing transportation agency used relative compaction determined from core samples as acceptance criteria. Immediately after asphalt pavement placement, transportation agency technicians extracted core samples from both base course and surface course layers. For both base and surface course layers, technicians extracted one or two core samples from each of the test sections. Authors of the study conducted 10 FWD tests on each test section subbase layer before and after asphalt pavement placement. GPS coordinates were obtained for the locations of each core sample and FWD test to spatially pair with RICM data.

5.7.3.1 Comparison of HMV with asphalt core relative compaction

Figure 5.6a presents comparisons between base course core relative compaction [$RC_{Core(BC)}$] and HMV_{SB}, HMV_{BC}, and HMV_{SC} measurements, and Figure 5.6b presents

comparisons between surface course core relative compaction [$RC_{Core(SC)}$)] and HMV_{SB},

HMV_{BC}, and HMV_{SC} measurements. Neither $RC_{Core(BC)}$ nor $RC_{Core(SC)}$ correlated with

statistical significance to any HMV measurement. Because only 1 or 2 core samples were

extracted from each test section, the authors did not perform regression analyses between

RC_{Core} and HMV measurement by test section. Despite the lack of regression analyses by

test section, the comparisons between RC_{Core} and HMV measurements are consistent

with comparisons between RC_{NG} and HMV measurements that the authors discussed

earlier in this paper. Therefore, results from this study suggest that asphalt pavement

relative compaction does not correlate with RICM measurements.

5.7.3.2 Comparison of HMV with FWD measurements

Figure 5.7a presents regression analyses between FWD modulus measured on test

section subbase layers [$E_{FWD(SB)}$)] and HMV_{SB}, HMV_{BC}, and HMV_{SC} measurements, and

Figure 5.7b presents regression analyses between FWD modulus measured on test section

surface course layers [$E_{FWD(SC)}$] and HMV_{SB}, HMV_{BC}, and HMV_{SC}. $E_{FWD(SB)}$ correlated

with statistical significance to all HMV measurements—HMV_{SB} ($r^2 = 0.79$), HMV_{BC} ($r^2 =$

0.39), and HMV_{SC} ($r^2 = 0.50$). In addition, $E_{FWD(SC)}$ correlated with statistical

significance to all HMV measurements—HMV_{SB} ($r^2 = 0.55$), HMV_{BC} ($r^2 = 0.62$), and

HMV_{SC} ($r^2 = 0.60$).

The strong correlations between HMV measurements and FWD moduli are consistent

with previous studies that report RICM measurements typically correlating well with

stiffness measurements. Simple linear models best fit all associations between FWD

moduli and HMV measurements, except for the association between $E_{FWD(SC)}$ and

HMV_{SB}, which followed a nonlinear model. The nonlinear relationship between $E_{FWD(SC)}$

and HMV_{SB}, which is similar to the relationships between HMV_{BC} and HMV_{SB} and between HMV_{SC} and HMV_{SB} that were reported earlier in this paper, may be the result of load spreading in layered systems (Burmister, 1945). This hypothesis, however, is a mere conjecture that requires additional research to validate or reject.

Figure 5.7c presents regression analyses between asphalt pavement (i.e., combined base and surface courses) modulus (E_{AP}) and HMV_{SB}, HMV_{BC}, and HMV_{SC}. Although this study has already shown that HMV measurements correlate quite well with stiffness measurements, none of the HMV measurements correlated with E_{AP} (r^2 values ranged from 0.01 to 0.07). However, an F-test indicated that the association between E_{AP} and HMV_{SB} was statistically significant (p value equalled 0.01). This unexpected statistically significant association may be due to the fact that $E_{FWD(SB)}$, which strongly correlates with HMV_{SB}, was used to calculate E_{AP}.

5.8 Implications for RICM in Practice

Results from this paper have indicated with statistical significance that HMV does not correlate with asphalt pavement relative compaction, which is consistent with previous RICM studies. The lack of correlations between RICM measurements and relative compaction poses an obstacle for implementing RICM for QC and QA because many asphalt pavement contractors in the United States currently use relative compaction measurements for QC. However, the presence of this obstacle attests more so to the necessity of a paradigm shift end-result to performance-related construction specifications than to the limitations of RICM.

According to Epps et al. (2002), asphalt pavement performance is governed by the prevalence of fatigue cracking and rutting in pavement wheel paths, which are both

related to in situ strains and therefore asphalt pavement modulus. In this study, FWD tests showed that average test section asphalt pavement moduli (E_{AP}) ranged from 385 to 7,140 MPa, even though RC_{Core} values ranged from 90% to 95% and 89% to 95%, respectively. Due to this observed discrepancy between RC_{Core} and E_{AP}, the authors contend that relative compaction is not a good indicator of asphalt pavement modulus and therefore not a good indicator of pavement performance.

As discussed earlier in this paper, HMV values strongly correlate with performance-related QA measurements (i.e., FWD modulus), so the QC applicability for RICM technologies in asphalt pavement construction is quite promising. However, there is a caveat to the relationship between RICM measurements and stiffness because of the degree to which underlying layer stiffness affects RICM measurements during asphalt pavement construction. This study compared asphalt base and surface course HMV with asphalt pavement layer elastic modulus, but found no statistically significant correlations. However, when these correlations are expanded to account for pavement foundation elastic modulus [i.e., $E_{FWD(SB)}$] in addition to asphalt pavement modulus, then asphalt pavement elastic modulus becomes a statistically significant predictor of HMV.

Table 5.6 presents results from multivariable analyses relating E_{AP} and $E_{FWD(SB)}$ together with HMV_{BC} and HMV_{SC} measurements. In both multivariable models, E_{AP} and $E_{FWD(SB)}$ are statistically significant predictors of HMV. For the multivariable model predicting HMV_{BC} (r^2 adj = 0.46), E_{AP} sensitivity index equaled 0.036 and $E_{FWD(SB)}$ sensitivity index equaled 0.964, so E_{AP} accounts for 3.6% of HMV_{BC} and $E_{FWD(SB)}$ accounts for 96.4% of HMV_{BC}. For the multivariable model predicting HMV_{SC} (r^2 adj = 0.58), E$_{AP}$ sensitivity index equaled 0.019 and $E_{FWD(SB)}$ sensitivity index equaled 0.981,

so E_{AP} accounts for 1.9% of HMV_{SC} and $E_{FWD(SB)}$ accounts for 98.1% of HMV_{SC}.

Therefore, RICM systems can potentially be used as QC for asphalt pavement layer modulus, provided that the composite modulus of the pavement foundation is known.

5.9 Summary and Key Conclusions

This reports an experimental investigation into the influence of pavement foundation condition (i.e., stiffness) on RICM measurements [Hamm measurement value (HMV)] taken during asphalt pavement construction and before asphalt pavement construction (i.e., on pavement foundation). Asphalt pavements comprising warm mix and hot mix asphalt were placed on test sections of varying pavement foundation stiffnesses. Correlations are made between HMV measurements and quality control and quality assurance test measurements. The key findings presented in this paper are as follows:

- In general, HMV values during asphalt pavement construction are higher when placing asphalt over stiff pavement foundations. All HMV measurements correlated with statistical significance to one another.

- For asphalt construction over soft pavement foundations, HMV increased with each additional pavement layer. For asphalt construction over stiff foundations in general, pavement foundation HMV was greater than base course HMV, and base course HMV was less than surface course HMV.

- Asphalt pavement surface temperature measurements from the RICM temperature sensors were in agreement with FLIR® thermal camera temperatures at higher temperatures (greater than 87.4 °C), but tended to underestimate pavement surface temperatures at lower temperatures (less than 87.4 °C).

- Asphalt pavement relative compaction from neither nuclear density gauge tests nor pavements cores correlated with HMV measurements. However, falling weight deflectometer (FWD) measurements strongly correlate with HMV measurements.

- Based on multivariable analyses, RICM systems can potentially be used as QC for asphalt pavement layer modulus, provided that the composite modulus of the pavement foundation is known.

5.10 Acknowledgments

5.11 References

American Association of State Highway and Transportation Officials (AASHTO). (1993). *AASHTO guide for design of pavement structures*. Washington, D.C.: American Association of State Highway and Transportation Officials.

Becker, P.J., White, D.J., Vennapusa, P.K.R., & Dunn, M.J. (2014, January). Freeze-thaw performance assessment of stabilized pavement foundations. *Paper presented at the 93rd Annual Meeting of the Transportation Research Board*, Washington, D.C.

Becker, P.J., White, D.J., Vennapusa, P.K.R., White, C.I., & Zhang, Y. (2015). Performance comparison of recycled pavement foundation layers. *Transportation Research Record*: Journal of the Transportation Research Board, 2509, 29–39. doi: 10.3141/2509-04

Brandl, H., & Adam, D. (1997, September). Sophisticated continuous compaction control of soils and granular materials. *Paper presented at the 14th International Conference on Soil Mechanics and Foundation Engineering*, Hamburg, Germany.

Burmister, D.M. (1945). The general theory of sresses and displacements in layered systems: I. *Journal of Applied Physics*, 16(89), 89–94. doi: 10.1063/1.1707562

Chang, G., Xu, Q., Rutledge, J., Garber, S. (2014). *A study on intelligent compaction and in-place asphalt density* (FHWA-HIF-14-017). Washington, D.C.: Federal Highway Administration.

Chang, G., Xu, Q., Rutledge, J., Horan, B., Michael, L., White, D., and Vennapusa, P. (2011). *Accelerated implementation of intelligent compaction technology for embankment subgrade soils, aggregate base, and asphalt pavement materials* (FHWA-IF-12-002). Washington, D.C.: Federal Highway Administration.

Epps, J.A., Hand, A., Seeds, S., Schulz, T., Alavi, S., Ashmore, C., Monismith, C.L., Deacon, J.A., Harvey, J.T., & Leahy, R. (2002). *Recommended performance-related specification for hot-mix asphalt construction: Results of the Westrack project* (NCHRP 455). Washington, D.C.: National Cooperative Highway Research Program.

Federal Highway Administration (FHWA). (2014). *Intelligent compaction technology for asphalt applications–generic IC specifications for asphalt materials*. Washington, D.C.: Federal Highway Administration.

Floss, R., Gruber, N., & Obermayer, J. (1983, May). A dynamical test method for continuous compaction control. *Paper presented at the 8th European Conference on Soil Mechanics and Foundation Engineering*, Helsinki.

Gallivan, V.L., Chang, G.K., & Horan, R.D. (2011, March). Practical implementation of intelligent compaction technology in hot mix asphalt pavements. *Paper presented at the 86th Association of Asphalt Paving Technologists Annual Meeting*, Tampa, Florida.

Iowa Department of Transportation (DOT). (2016). *Standard specifications with GS-15002: Section 2115. Modified subbase*. Ames, Iowa: Iowa Department of Transportation.

Kröber, W., Floss, E., & Wallrath, W. (2001, January). Dynamic soil stiffness as quality criterion for soil compaction, *Paper presented at Geotechnics for Roads, Rail Tracks and Earth Structures*, Lisse, Netherlands.

National Cooperative Highway Research Program (NCHRP). (2004). *Guide for mechanistic-empirical design of new and rehabilitated pavement structures* (NCHRP 1-37A). Washington, D.C.: National Cooperative Highway Research Program.

Roberts, F.L., Kandal, P.S., Brown, E.R., Lee, D., & Kennedy, T.W. (1996). *Hot mix asphalt materials, mixture design, and construction* (2nd Ed.). Auburn, Alabama: National Center for Asphalt Technology.

Sandström, Å., & Pettersson, C.B. (2004, January). Intelligent systems for QA/QC in soil compaction. *Paper presented at the 83rd Annual Meeting of the Transportation Research Board*, Washington, D.C.

Scherocman, J., Rakowski, S., & Uchiyama, K. (2007, November). Intelligent compaction, does it exist?. *Paper presented at the 52nd Annual Conference of the Canadian Technical Asphalt Association*, Niagara Falls, Canada.

Sobol', I.M. (1990). On sensitivity estimation for nonlinear mathematical models. *Matematicheskoe modelirovanie*, 2(1), 112–118.

Thurner, H., & Sandström, Å. (1980, April). A new device for instant compaction control, *Paper presented at the International Conference on Compaction*, Paris, France.

Vennapusa, P., White, D.J. (2009). Comparison of light weight deflectometer measurements for pavement foundation materials. *Geotechnical Testing Journal*, 32(3), 239–251.

doi: 10.1520/GTJ101704

Vennapusa, P.K.R., White, D.J., & Schram, S. (2013). Roller-integrated compaction monitoring for hot-mix asphalt overlay construction. *Journal of Transportation Engineering*, 139(12), 1164–1173. doi: 10.1061/(ASCE)TE.1943-5436.0000602

West, R.C., Watson, D.E., Turner, P.A., & Casola, J.R. (2010). *Mixing and compaction temperatures of asphalt binders in hot-mix asphalt* (NCHRP 648). Washington, D.C.: National Cooperative Highway Research Program.

White, D.J., Becker, P., Vennapusa, P.K.R., Dunn, M.J., & White, C.I. (2013). Assessing Soil Stiffness of Stabilized Pavement Foundations. *Transportation Research Record*, 2335, 99–109. doi: 10.3141/2335-11

White, D.J., & Vennapusa, P. (2008). *Accelerated implementation of intelligent compaction monitoring technology for embankment subgrade soils, aggregate base, and asphalt pavement materials* (TPF-5(128)). Washington, D.C.: Federal Highway Administration.

Xu, Q., & Chang, G.K. (2014). Experimental and numerical study of asphalt material

geospatial heterogeneity with intelligent compaction technology on roads.

Construction and Building Materials, 72, 189–198. doi:

10.1016/j.conbuildmat.2014.09.003

Yoon, S., Hastak, M., & Lee, J. (2015). *Intelligent compaction of asphalt pavement*

implementation (FHWA/IN/JTRP‐2015/05). Indianapolis, Indiana: Indiana

Department of Transportation.

Zhang, Y. (2013). *Frost-Heave and Thaw-Weakening of Pavement Foundation Materials*

(Master's thesis). Available from ProQuest Dissertations and Theses database.

(UMI No. 1531431)

Table 5.1. Descriptions of Test Section Pavement Cross Sections

Pavement Layers by Test Section		Layer Description
TS-W	Asphalt Surface Course	51 mm warm mix asphalt binder with low absorption aggregate
	Asphalt Base Course	102 mm warm mix asphalt binder with low absorption aggregate
	Subbase Layer	152 mm modified subbase[a] underlain by woven geotextile fabric
	Subgrade Layer	Natural subgrade[b]
TS-NW	Asphalt Surface Course	51 mm warm mix asphalt binder with low absorption aggregate
	Asphalt Base Course	102 mm warm mix asphalt binder with low absorption aggregate
	Subbase Layer	152 mm modified subbase[a] underlain by non-woven geotextile fabric
	Subgrade Layer	Natural subgrade[b]
TS-BX	Asphalt Surface Course	51 mm warm mix asphalt binder with low absorption aggregate
	Asphalt Base Course	102 mm warm mix asphalt binder with low absorption aggregate
	Subbase Layer	152 mm modified subbase[a] underlain by biaxial polymer geogrid
	Subgrade Layer	Natural subgrade[b]
TS-TX	Asphalt Surface Course	51 mm warm mix asphalt binder with low absorption aggregate
	Asphalt Base Course	102 mm warm mix asphalt binder with low absorption aggregate
	Subbase Layer	152 mm modified subbase[a] underlain by triaxial polymer geogrid
	Subgrade Layer	Natural subgrade[b]
TS-PCSB	Asphalt Surface Course	51 mm hot mix asphalt binder with high absorption aggregate
	Asphalt Base Course	102 mm hot mix asphalt binder with low absorption aggregate
	Subbase Layer	152 mm modified subbase[a] underlain by 152 mm reclaimed subbase[c] stabilized with 5% Portland cement
	Subgrade Layer	Natural subgrade[b]

Notes: [a]Modified subbase classifies as GP-GM (A-1-a)
[b]Compacted/natural subgrade classifies as CL [A-6(5)]
[c]Reclaimed subbase classifieds as SM (A-1-a)
[d]Synthetic subsurface drainage layer included in northernmost 175 m portion of 205 m long test section

Table 5.1. Descriptions of Test Section Pavement Cross Sections (continued)

Pavement Layers by Test Section		Layer Description
TS-NSG	Asphalt Surface Course	51 mm warm mix asphalt binder with high absorption aggregate
	Asphalt Base Course	102 mm hot mix asphalt binder with low absorption aggregate
	Subbase Layer	152 mm modified subbase[a]
	Subgrade Layer	Natural subgrade[b]
TS-CSG	Asphalt Surface Course	51 mm warm mix asphalt binder with high absorption aggregate
	Asphalt Base Course	102 mm hot mix asphalt binder with low absorption aggregate
	Subbase Layer	152 mm modified subbase[a]
	Subgrade Layer	305 mm compacted subgrade[b] underlain by natural subgrade[b]
TS-FASG	Asphalt Surface Course	51 mm warm mix asphalt binder with high absorption aggregate
	Asphalt Base Course	102 mm warm mix asphalt binder with low absorption aggregate
	Subbase Layer	152 mm modified subbase[a]
	Subgrade Layer	305 mm compacted subgrade[b] stabilized with 20% fly ash underlain by natural subgrade[b]
TS-PCSG	Asphalt Surface Course	51 mm warm mix asphalt binder with high absorption aggregate
	Asphalt Base Course	102 mm warm mix asphalt binder with low absorption aggregate
	Subbase Layer	Synthetic subsurface drainage layer[d] underlain by 152 mm modified subbase[a]
	Subgrade Layer	305 mm compacted subgrade[b] stabilized with 10% Portland cement underlain by natural subgrade[b]

Notes: [a]Modified subbase classifies as GP-GM (A-1-a)
              [b]Compacted/natural subgrade classifies as CL [A-6(5)]
              [c]Reclaimed subbase classifieds as SM (A-1-a)
              [d]Synthetic subsurface drainage layer included in northernmost 175 m portion of 205 m long test section

Table 5.2. Key Features of RICM Roller Used on Project

Feature	Description
Manufacturer	Hamm AG
Model	HD+ 120 VV
Roller type	Dual smooth drum vibratory roller
Compaction measurement	HAMM measurement value (HMV)
Output documentation	Date/time, location (latitude/longitude/elevation), HMV, surface temperature, roller pass number, amplitude, frequency, direction (forward/reverse), vibration (on/off),
Axle loading	6565 kg (front drum) and 6285 kg (rear drum)
Drum width	1980 mm (front and rear drums)
Drum diameter	1400 mm (front and rear drums)
Vibration frequency	40/50 Hz (front and rear drums)
Amplitude	0.49/0.88 mm (front and rear drums)

Table 5.3. Summary Statistics of RICM and FWD Measurements on Each Test Section

Test Section	Average HMV on Subbase, HMV_{SB} [COV (%)]	Average HMV on Base Course, HMV_{BC} [COV (%)]	Average HMV on Surface Course, HMV_{SC} [COV (%)]	Average E_{FWD} on Subbase, $E_{FWD(SB)}$ (MPa) [COV (%)]	Average E_{FWD} on Surface Course, $E_{FWD(SC)}$ (MPa) [COV (%)]	Average Asphalt Pavement Modulus, E_{AP} (MPa) [COV (%)]
TS-W	8 [43]	9 [36]	26 [22]	74 [27]	277 [19]	7077 [76]
TS-NW	7 [23]	9 [69]	22 [21]	95 [28]	268 [33]	3755 [80]
TS-BX	10 [48]	10 [95]	21 [26]	103 [29]	219 [16]	1537 [64]
TS-TX	7 [37]	8 [64]	22 [25]	122 [28]	215 [16]	994 [64]
TS-PCSB	36 [38]	24 [26]	43 [21]	280 [16]	594 [14]	3429 [33]
TS-NSG	9 [36]	9 [58]	22 [35]	43 [41]	181 [19]	7140 [109]
TS-CSG	8 [48]	9 [26]	22 [29]	103 [27]	248 [18]	2773 [98]
TS-FASG	33 [42]	17 [33]	38 [27]	324 [21]	478 [21]	1252 [39]
TS-PCSG	67 [23]	20 [22]	48 [13]	507 [28]	415 [17]	385 [32]

Table 5.4. Statistical comparisons of HMV$_{SB}$, HMV$_{BC}$, and HMV$_{SC}$ on each test Section

Test Section	HMV value Comparison	Mean Difference	Standard Error Difference	Mean Difference 95% Confidence Limits		p Value[a]
				Lower Bound	Upper Bound	
TS-W	HMV$_{SC}$ – HMV$_{SB}$	17.79	0.14	17.46	18.12	**< 0.0001**
	HMV$_{SC}$ – HMV$_{BC}$	16.71	0.17	16.31	17.11	**< 0.0001**
	HMV$_{BC}$ – HMV$_{SB}$	1.08	0.16	0.70	1.46	**< 0.0001**
TS-NW	HMV$_{SC}$ – HMV$_{SB}$	14.71	0.15	14.35	15.07	**< 0.0001**
	HMV$_{SC}$ – HMV$_{BC}$	13.39	0.18	12.99	13.81	**< 0.0001**
	HMV$_{BC}$ – HMV$_{SB}$	1.31	0.16	0.94	1.68	**< 0.0001**
TS-BX	HMV$_{SC}$ – HMV$_{SB}$	11.13	0.22	10.62	11.64	**< 0.0001**
	HMV$_{SC}$ – HMV$_{BC}$	11.401	0.26	10.81	12.01	**< 0.0001**
	HMV$_{BC}$ – HMV$_{SB}$	-0.28	0.24	-0.85	0.29	0.492
TS-TX	HMV$_{SC}$ – HMV$_{SB}$	15.21	0.14	14.88	15.55	**< 0.0001**
	HMV$_{SC}$ – HMV$_{BC}$	13.64	0.18	13.22	14.06	**< 0.0001**
	HMV$_{BC}$ – HMV$_{SB}$	1.57	0.16	1.19	1.95	**< 0.0001**
TS-PCSB	HMV$_{SC}$ – HMV$_{SB}$	7.08	0.37	10.84	12.97	**< 0.0001**
	HMV$_{SC}$ – HMV$_{BC}$	18.99	0.49	17.84	20.13	**< 0.0001**
	HMV$_{BC}$ – HMV$_{SB}$	-11.91	0.45	-12.97	-10.84	**< 0.0001**
TS-NSG	HMV$_{SC}$ – HMV$_{SB}$	12.22	0.21	11.72	12.72	**< 0.0001**
	HMV$_{SC}$ – HMV$_{BC}$	12.78	0.23	12.25	13.30	**< 0.0001**
	HMV$_{BC}$ – HMV$_{SB}$	-0.55	0.22	-1.06	-0.04	**0.032**
TS-CSG	HMV$_{SC}$ – HMV$_{SB}$	14.56	0.15	14.21	14.92	**< 0.0001**
	HMV$_{SC}$ – HMV$_{BC}$	13.59	0.18	13.16	14.01	**< 0.0001**
	HMV$_{BC}$ – HMV$_{SB}$	0.98	0.16	0.601	1.34	**< 0.0001**
TS-FASG	HMV$_{SC}$ – HMV$_{SB}$	4.45	0.38	3.60	5.39	**< 0.0001**
	HMV$_{SC}$ – HMV$_{BC}$	21.15	0.41	20.20	22.11	**< 0.0001**
	HMV$_{BC}$ – HMV$_{SB}$	-4.45	0.38	-5.39	-3.60	**< 0.0001**
TS-PCSG	HMV$_{SC}$ – HMV$_{SB}$	-19.30	0.47	-20.41	-18.19	**< 0.0001**
	HMV$_{SC}$ – HMV$_{BC}$	27.55	0.57	26.21	28.88	**< 0.0001**
	HMV$_{BC}$ – HMV$_{SB}$	-46.85	0.48	-47.97	-45.73	**< 0.0001**

Note: [a]Emboldened p values indicate statistical significance

Table 5.5. Correlations of $RC_{NG(BC)}$ with HMV_{BC} and $RC_{NG(SC)}$ with HMV_{SC} for each test section and combined test sections

Asphalt Layer	Test Section	Estimated Parameters		n	r^2	F Ratio	p value[b]
		a	b				
Base Course[a]	All test sections	1.952	0.015	54	0.054	2.98	0.090
	TS-W	2.096	-0.148	4	0.850	11.35	0.078
	TS-NW	1.958	0.003	7	0.007	0.03	0.861
	TS-BX	1.934	0.034	6	0.099	0.44	0.544
	TS-TX	1.973	-0.014	5	0.006	0.02	0.904
	TS-PCSB	1.445	0.409	3	0.886	7.75	0.220
	TS-NSG	1.992	-0.023	5	0.050	0.16	0.717
	TS-CSG	1.933	0.043	9	0.115	0.91	0.372
	TS-FASG	1.976	-0.006	7	0.001	0.01	0.945
	TS-PCSG[c]	1.839	0.114	8	0.368	3.49	0.111
Surface Course[d]	All test sections	1.948	0.013	60	0.049	3.01	0.088
	TS-W	1.830	0.093	4	0.697	4.61	0.165
	TS-NW	1.956	0.010	5	0.011	0.03	0.868
	TS-BX	1.982	-0.017	4	0.607	3.09	0.221
	TS-TX	1.526	0.309	4	0.427	1.49	0.346
	TS-PCSB	1.931	0.025	11	0.054	0.52	0.490
	TS-NSG	1.992	-0.023	5	0.050	0.16	0.717
	TS-CSG	1.967	0.052	9	0.000	0.00	0.958
	TS-FASG	1.979	-0.007	8	0.002	0.01	0.912
	TS-PCSG[c]	1.887	0.051	8	0.775	20.67	**0.004**

Notes: [a]$\log[RC_{NG(BC)}] = a + b \log(HMV_{BC})$
[b]Emboldened p values indicate statistical significance
[c]Testing conducted on portion of test section with synthetic subsurface drainage layer
[d]$\log[RC_{NG(SC)}] = a + b \log(HMV_{SC})$

Table 5.6. Multivariable models for HMV_{BC} and HMV_{SC} as functions of $E_{FWD(SB)}$ and E_{AP}

Multivariable Analysis	Term	Estimate	Standard Error	t Ratio	p Value	r^2 Adj
HMV_{BC}[a]	b_o	-1.079	1.94	-3.76	**0.0003**	0.462
	b_1	0.616	1.17	8.85	**< 0.0001**	
	b_2	0.269	1.13	5.13	**< 0.0001**	
HMV_{SC}[b]	b_o	-0.173	1.53	-0.94	0.352	0.579
	b_1	0.489	1.11	10.93	**< 0.0001**	
	b_2	0.171	1.08	5.07	**< 0.0001**	

Notes: [a]$\log(HMV_{BC}) = b_o + b_1 \log(E_{FWD(SB)}) + b_2 \log(E_{AP})$
[b]$\log(HMV_{BC}) = b_o + b_1 \log(E_{FWD(SB)}) + b_2 \log(E_{AP})$
[c]Emboldened p values indicate statistical significance
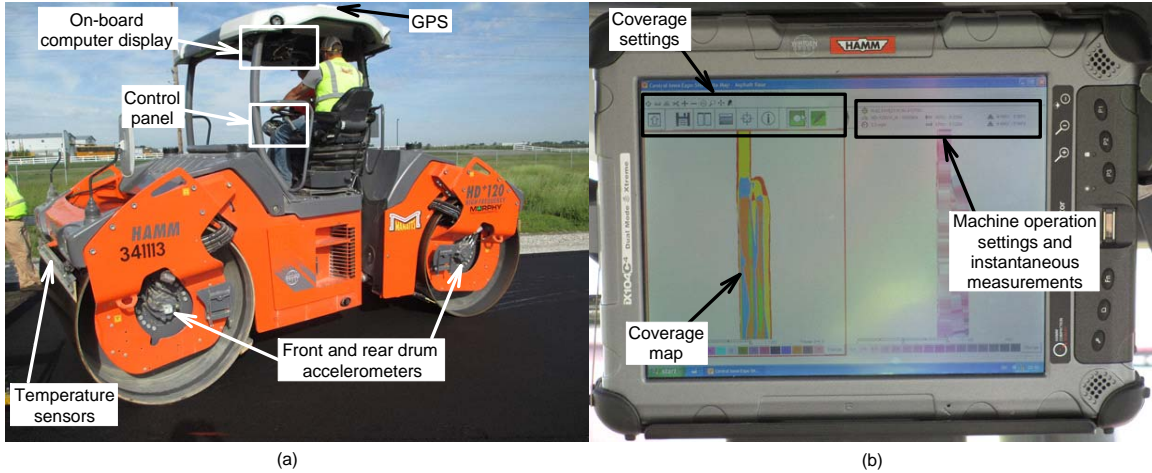
Figure 5.1. (a) Hamm HD+ 120 VV dual smooth-drum vibratory roller used to compact test section asphalt base course and surface course layers; (b) on-board computer that recorded RICM measurements, which the operator viewed in real time
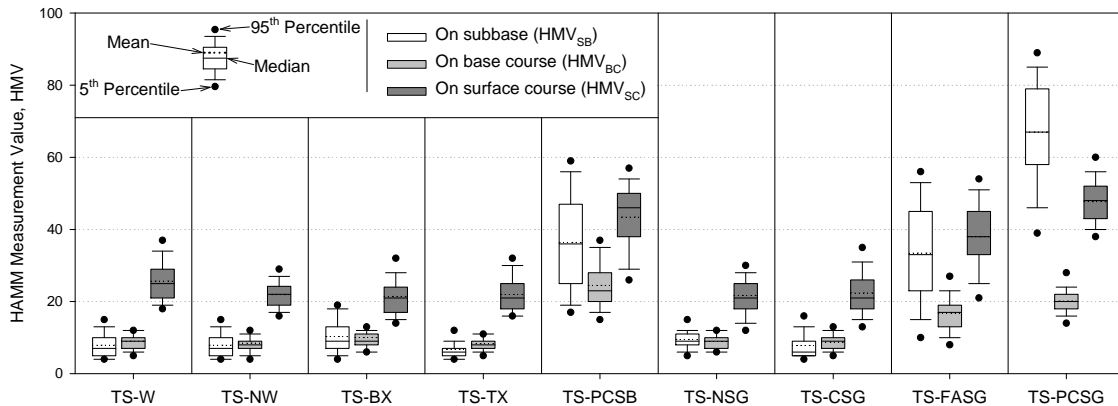
Figure 5.2. Comparisons of pre-construction HMV measured on subbase, final pass HMV measured on base course, and final pass HMV measured on surface course along centreline each test section
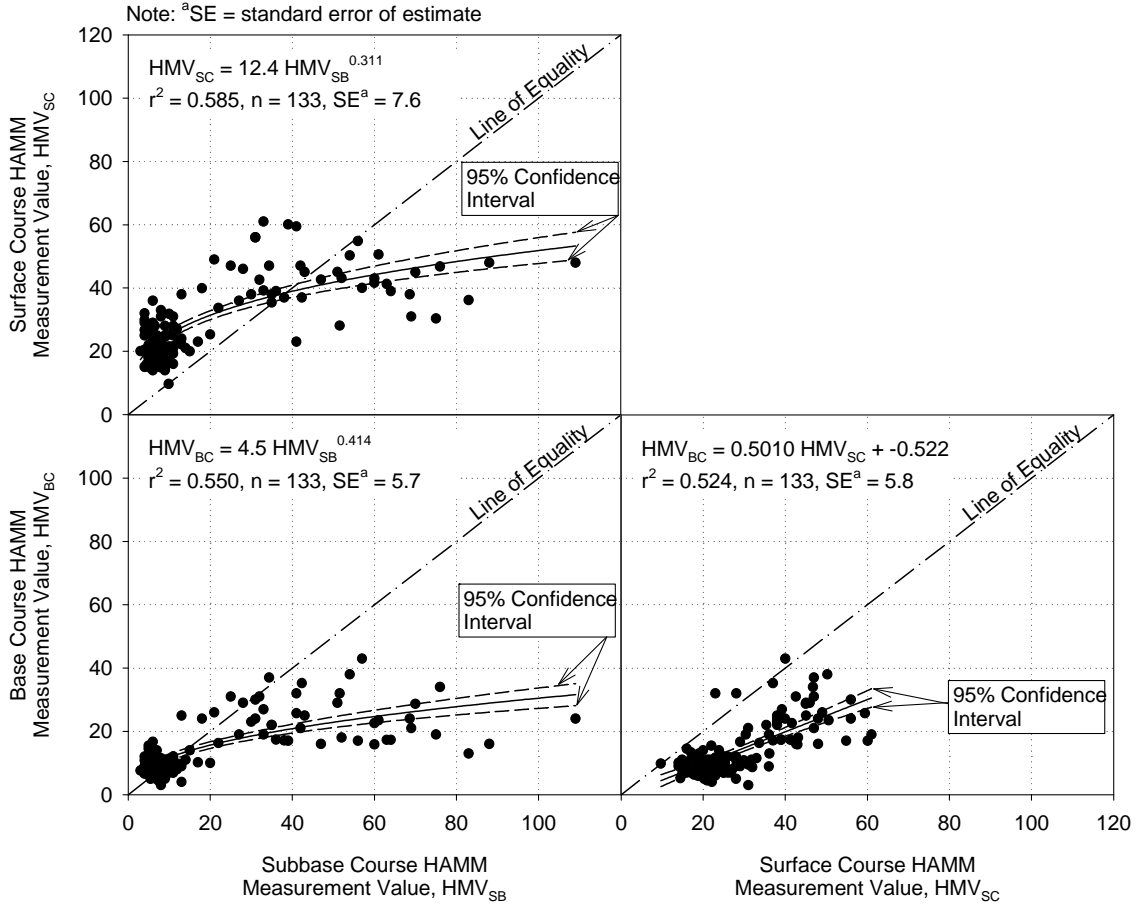
Figure 5.3. Scatter plot matrix for correlations between subbase HMV, asphalt base course HMV, and surface course HMV

129
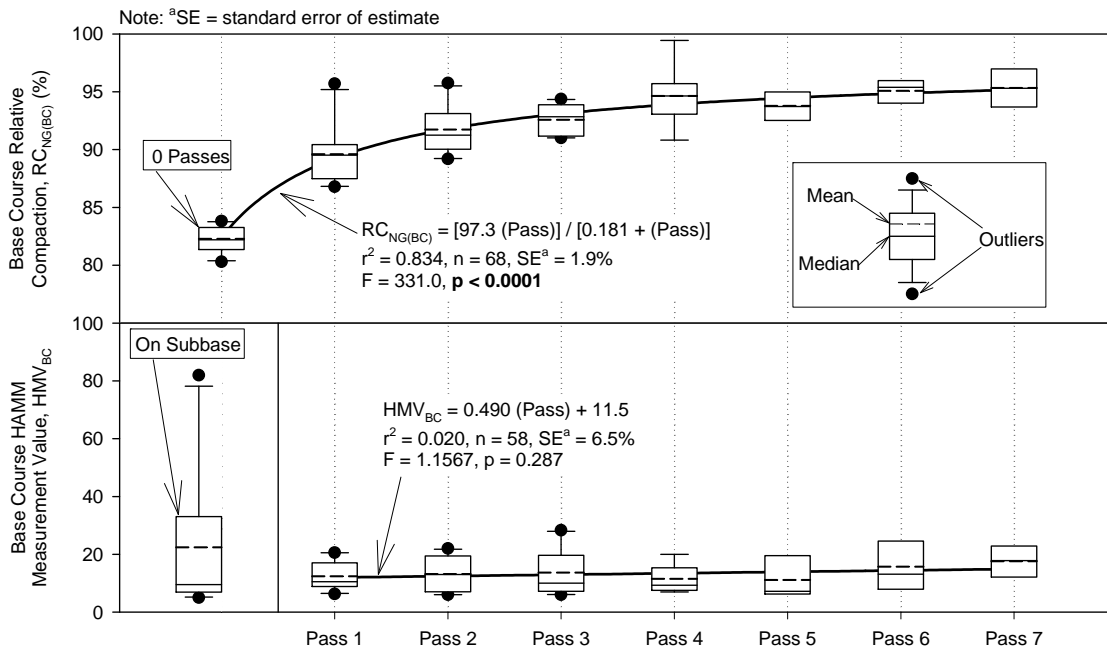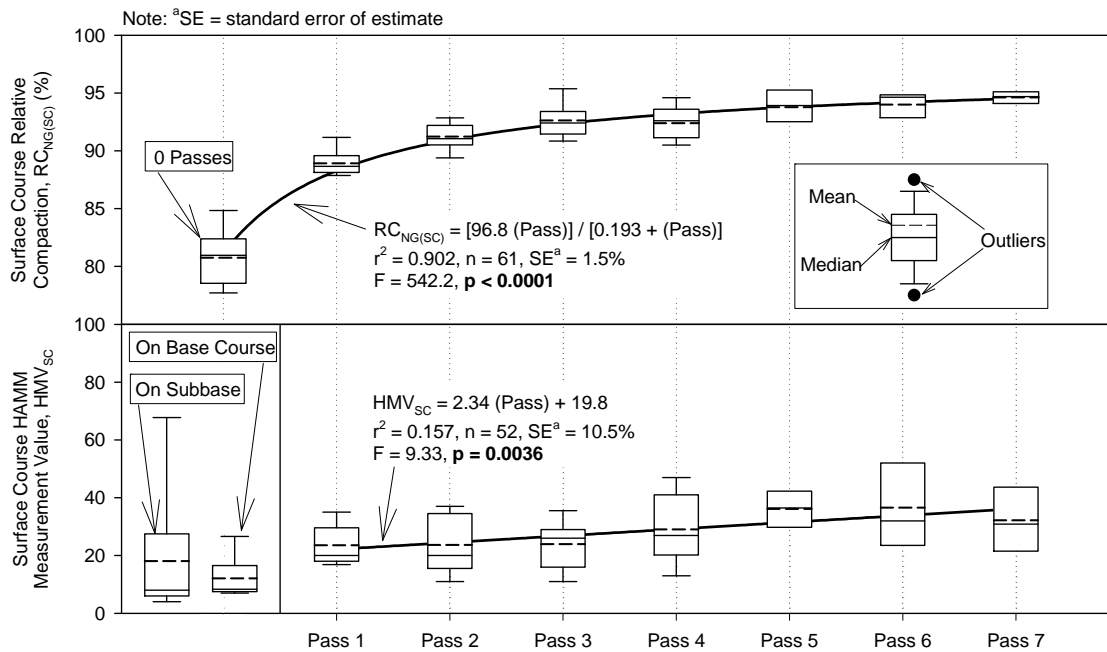
Figure 5.4 Comparison of relative compaction with HMV with increasing roller pass number for (a) asphalt base course layer and (b) asphalt surface course layer
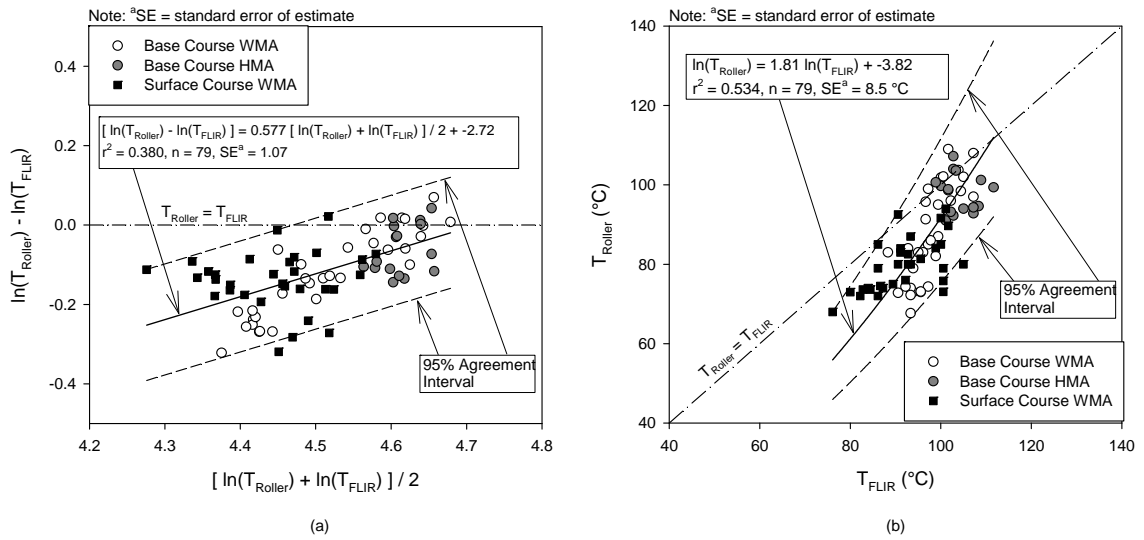
Figure 5.5. Comparison of agreement between roller-integrated temperature sensor and FLIR thermal camera for measuring asphalt mix temperature during compaction; (a) logarithmically transformed Bland-Altman plot, (b) correlation between roller-integrated temperature sensor and FLIR thermal camera measurements
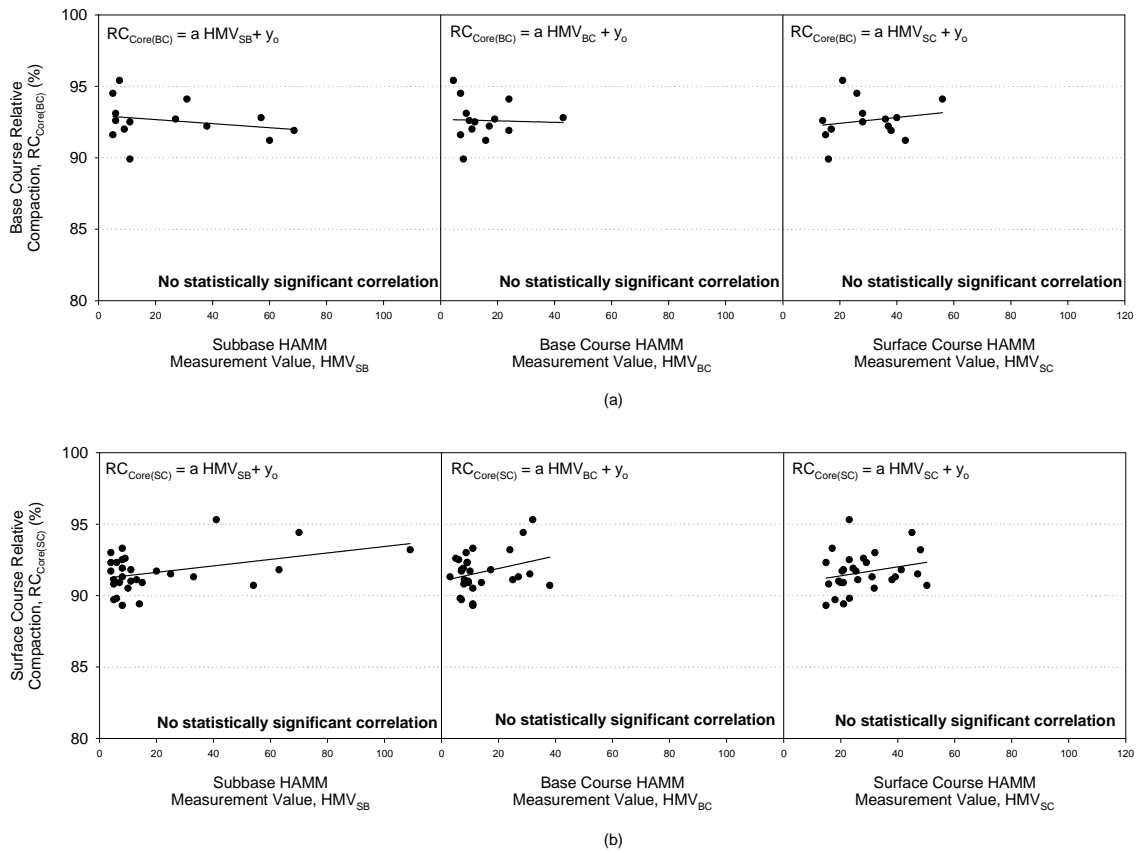
Figure 5.6. Correlations of subbase HMV, asphalt base course HMV, and asphalt surface course HMV with relative compaction values for (a) asphalt base course and (b) asphalt surface course
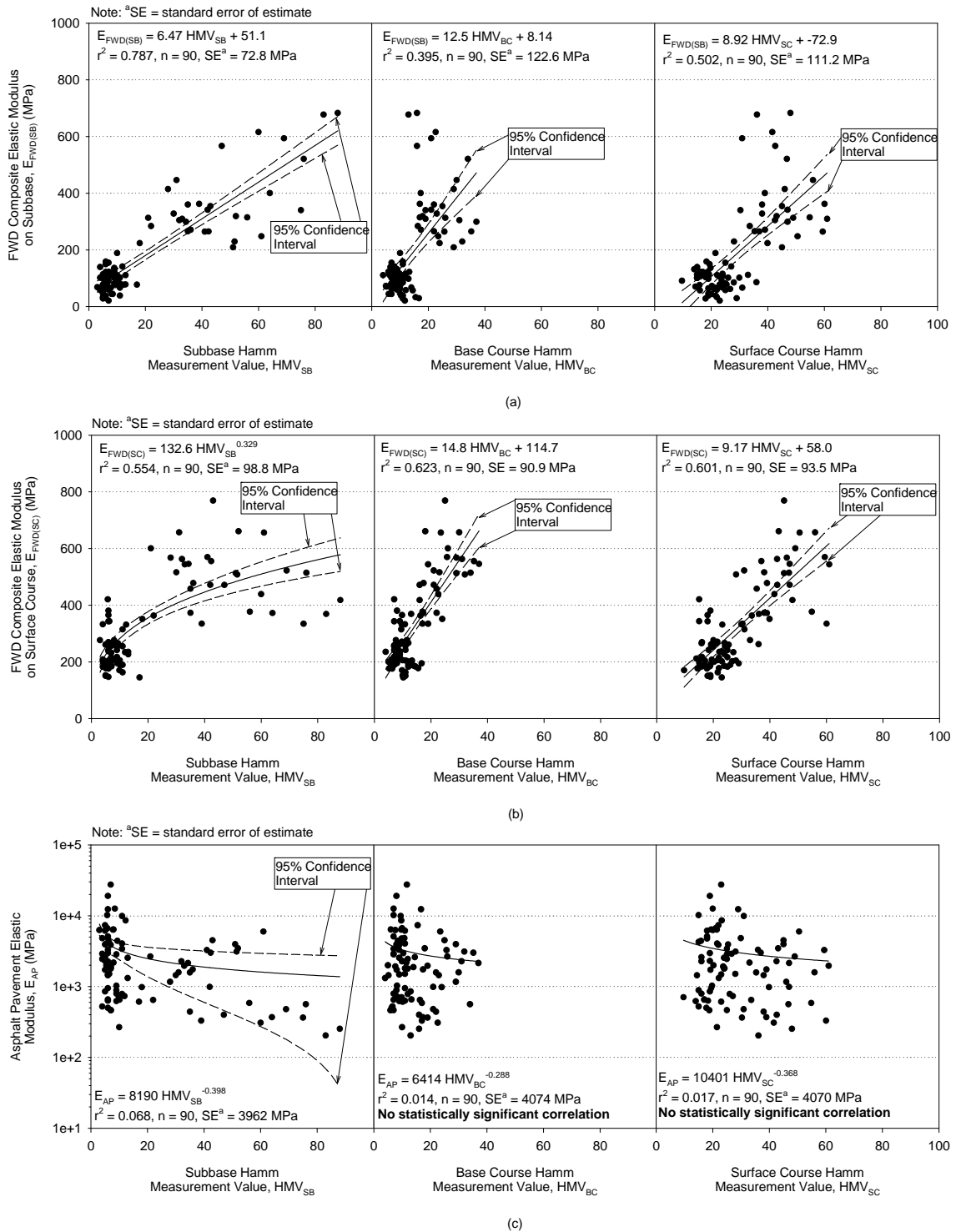
Figure 5.7. Correlations of subbase HMV, asphalt base course HMV, and asphalt surface course HMV with (a) E_{FWD} on subbase, (b) E_{FWD} on asphalt surface course, and (c) asphalt pavement elastic modulus

CHAPTER 6. PERFORMANCE COMPARISON OF RECYCLED PAVEMENT FOUNDATION LAYERS

Peter J. Becker, David J. White, Pavana K.R. Vennapusa, Christianna I. White, and Yang Zhang

6.1 Abstract

This paper describes results from a study comparing the performance of side-by-side test sections of pavement foundation layers constructed with on-site recycled materials and surfaced with hot mix asphalt. Test sections included recycled materials blended with subgrade to create a mechanically stabilized subgrade layer and recycled materials placed in an over excavated subgrade layer. In situ falling weight deflectometer (FWD) and dynamic cone penetration (DCP) tests, and laboratory freeze-thaw tests were used to assess the performance of the test sections, in comparison with a control section where recycled materials were not used. Field testing was conducted at seasonal intervals over two years after construction and the results were statistically analyzed using two-tailed Welch's t tests to account for unequal variances. Findings indicate that test sections with on-site recycled materials provided improved support conditions for the pavements during both before and after freeze-thaw conditions, when compared to the control section. FWD and DCP test results indicated that recycled material blended with subgrade showed more thaw-weakening compared to recycled material alone. Laboratory freeze-thaw test results corroborated with the comparisons observed in the field test

results. Correlations between FWD test measurements on the foundation layer and on the pavement yielded a statistically significant regression relationship, which indicates the importance of support conditions on the surface layer performance. Analysis of bid prices to construct the test sections indicated no statistical evidence to suggest that the unit costs for the test sections are different from one another.

6.2. Introduction

Sustainable engineering and construction practices in the transportation infrastructure decision making process have become increasingly important in recent years (Mansfield & Hartell, 2012; Maurer, Mansfield, Lane, & Hunkins, 2013). Pavement rehabilitation is one type of transportation infrastructure construction that is now benefitting from sustainable practices. Past methods of pavement reconstruction required the complete removal of existing pavement layers and replacement with virgin materials. Recent experience with on-site recycling of pavement materials has been documented as a sustainable (Cross, Kearney, Justus, & Chesner, 2010; Lee, Mueller, & Singh, 2014) and cost effective (Bemanian, Polish, & Maurer, 2006; Diefenderfer, Apeagyei, Gallo, Dougald, & Weaver, 2012; Mallick, Bonner, Bradbury, Andrews, Kandhal, & Kearney, 2002; Miller, Kestler, Amatrudo, Eaton, & Hall, 2011; Stroup-Gardiner, 2012) solution for pavement rehabilitation. Several cases have demonstrated successful use of on-site pavement recycling rehabilitation techniques by transportation agencies (Bemanian et al., 2006; Diefenderfer et al., 2012; Lewis, Jared, Torres, & Mathews, 2006; Mallick et al., 2002; Maurer, Bemanian, & Polish, 2007; Miller et al., 2011; Romanoschi, Hossain, Gisi, & Heitzman, 2004; Wen, Tharaniyil, Ramme, & Krebs, 2004).

On-site recycling of pavement materials has proven to be successful for pavement structure rehabilitation, but questions remain on whether or not on-site recycled pavement materials can increase pavement foundation performance. Unsuitable pavement foundations (e.g., use of frost susceptible materials) have detrimental effects on pavement performance (Christopher, Schwartz, & Boudreau, 2006; Saad, 2014). Case histories of pavement rehabilitation with on-site recycled materials indicated that the pavements had deteriorated because the pavement foundations consisted of unsuitable subgrade (Becker, White, Vennapusa, & Dunn, 2014; Miller et al., 2011; Diefenderfer et al., 2012; White, Becker, Vennapusa, Dunn, & White, 2013).

The purpose of this paper is to compare the in situ performance and relative costs of pavement foundation test sections constructed with on-site recycled materials. Two methods of using on-site recycled pavement materials to improve pavement foundation and rehabilitate pavements were compared: (1) overexcavation and replacement with on-site recycled pavement materials and (2) mechanical stabilization of fine-grained subgrade with on-site granular recycled pavement materials. Falling weight deflectometer (FWD) and dynamic cone penetrometer (DCP) tests were conducted on one control section and four test sections constructed with on-site recycled pavement materials. Laboratory testing of the pavement foundation materials provided index properties and frost susceptibility ratings.

6.3 Project Conditions

The project test site is located in Boone, Iowa, where monthly average temperatures range from –13°C to 28°C (The Weather Channel, 2016). The project site comprised a grid of 24-205 m long, 6 m wide roadway sections that were constructed in 2007.

Subgrade soil classified as CL or A-6(5), and the groundwater table was located about 0.9 to 1.5 m below grade. At the project location, annual freeze-thaw cycles contributed to the deterioration so reconstruction was required (Becker et al., 2014; White et al., 2013; Zhang, 2013).

Pavement reconstruction took place in two phases. The Phase I contractor, who submitted the lowest of six bids, constructed the pavement foundations in summer 2012. The original roadway sections in this study consisted of a 152 mm thick layer of gravel base that was topped with an asphalt chip seal coat layer (Figure 6.1a). Phase I construction began with recycling of the asphalt chip seal coat and gravel base layers by rubblizing, removing, mixing, and stockpiling the recycled material. The recycled material, which was classified as SM or A-1-a, was used to construct pavement foundations of the four 205 m test sections (TS-OE and TS-MS). Phase II involved placing a 102 mm hot mix asphalt (HMA) base course and a 51 mm HMA surface course in summer 2013.

The 205 m control section (TS-C) consisted of a nominal 152 mm crushed limestone subbase over the existing natural subgrade (Figure 6.1b). Following the on-site recycling process, two test sections (TS-OE) were overexcavated 152 mm below grade and backfilled with a nominal 152 mm layer of the on-site recycled material (Figure 6.1c). The contractor also constructed two test sections (TS-MS) by placing a nominal 152 mm layer of the on-site recycled material over the natural subgrade and using a soil reclaimer to mix the recycled and subgrade materials that resulted in a nominal 305 mm mechanically stabilized subgrade layer. The subgrade was then compacted with a smooth drum vibratory roller and covered with a nominal 152 mm layer of crushed limestone

subbase (Figure 6.1d). Table 6.1 summarizes the soil index properties and engineering parameters for the pavement foundation geomaterials.

6.4 Test Methods

The following sections describe the two in situ test procedures, falling weight deflectometer (FWD) and dynamic cone penetrometer (DCP) tests, and the laboratory freeze-thaw test procedure. FWD tests were conducted on top of the crushed limestone subbase layers before HMA placement in July 2012, October 2012, and April 2013 (spring thaw period), and on top of the HMA layers after placement in September 2013 and April 2014 (spring thaw period). DCP tests were conducted before HMA placement in October 2013, April 2013, and May 2013 (spring thaw period), and after HMA placement in April 2014 (spring thaw period).

6.4.1 Falling weight deflectometer (FWD)

FWD tests were conducted with a Kuab FWD setup that was equipped with an 300 mm diameter loading plate. At each testing location, one seating drop was applied then three to four loading drops that ranged from 27 kN to 71 kN were applied. A load cell measured the actual applied loadings, and seismometers mounted on the FWD measured peak deflections under the plate in accordance with ASTM 4694-09. Peak deflections for loads normalized to 27 kN, 40 kN, and 62 kN loads were calculated in this study. Elastic modulus values were determined using Equation 6.1:

$$E_{FWD} = \frac{\sigma_o r (1 - \nu^2)}{\delta_o} \times f \qquad (6.1)$$

where E_{FWD} = FWD elastic modulus (MPa); δ_o = measured vertical deflection under center of loading plate (mm); ν = Poisson's ratio (assumed as 0.4); σ_o = applied stress

(kPa); r = loading plate radius (mm); and f = shape factor depending on stress distribution. The loading plate used in this study was a segmented plate and leads to a uniform stress distribution so the shape factor f equaled 2. For FWD tests conducted on HMA layers, pavement temperatures were measured and δ_o values were normalized to 20 ℃ per American Association of State Highway and Transportation Officials (AASHTO) (1993) for E$_{FWD}$ calculations.

6.4.2 Dynamic cone penetrometer (DCP)

DCP tests were conducted according to ASTM D6951 to determine layer penetration index (mm per blow) values. Tests were terminated at either refusal per ASTM D6951 (i.e., advancement of 2 mm or less after 5 blows) or upon reaching the maximum penetration depth that was about 0.85 m. For tests performed after paving, a 305 mm diameter core was obtained to expose the crushed limestone subbase layer and the DCP tests were conducted directly on the foundation layers. California bearing ratio (CBR) values for crushed limestone subbase, recycled, and mechanically stabilized materials were determined in accordance with ASTM D6951 using Equation 6.2, where CBR = California bearing ratio and PI = penetration index.

$$CBR = \frac{292}{PI^{1.12}} \tag{6.2}$$

Because subgrade classified as CL, CBR values for subgrade soils were determined from equation 6.3, where CBR = California bearing ratio and PI = penetration index.

$$CBR = \begin{cases} \dfrac{1}{(0.017019PI)^2}, & CBR < 10 \\ \dfrac{292}{PI^{1.12}}, & CBR > 10 \end{cases} \tag{6.3}$$

6.4.3 Laboratory freeze-thaw testing

Freeze-thaw tests were conducted according to ASTM D5918. Detailed description of the test equipment is provided in Johnson (2012) and Zhang (2013). Two specimens were prepared for each material at their respective optimum moisture contents and compacted with standard Proctor effort (i.e., 600 kN-m/m^3). A CBR test was conducted on one specimen prior to freeze-thaw testing and the other specimen was subjected to freeze-thaw testing and the tested for CBR. CBR tests were conducted according to ASTM D1883 with CBR calculated from the penetration stress recorded at 5 mm depth.

6.5 Statistical Data Analysis

To provide an unbiased assessment of the test sections, two-tailed Welch's t tests (i.e., unequal variances) were conducted to compare the mean CBR and E$_{FWD}$ values and anticipated construction costs for TS-OE, TS-MS, and TS-C (Welch, 1947). Welch's t test is conducted using the t-distribution and equations 6.4 and 6.5, where t = test statistic; df = degrees of freedom; $\bar{X}_i$ = ith data set sample mean; s_i = ith data set sample standard deviation; and n = ith data set sample size.

$$t = \frac{\bar{X}_1 - \bar{X}_2}{\sqrt{\frac{s_1{}^2}{n_1} + \frac{s_2{}^2}{n_2}}} \tag{6.4}$$

$$df \approx \frac{\left(\frac{s_1{}^2}{n_1} + \frac{s_2{}^2}{n_2}\right)^2}{\frac{s_1{}^4}{n_1{}^2(n_1-1)} + \frac{s_2{}^4}{n_2{}^2(n_2-1)}} \tag{6.5}$$

T distributions using t values and df values yielded p-values (p) for data set comparisons. Statistical significance in this study corresponded to 95% confidence level so p-values that were less than 0.025 indicated statistical significance. If p-values were

statistically significant, then it was concluded that there was sufficient evidence that the means of two different data sets are different (with one being either higher or lower than the other).

T test analysis results in this study are reported as Tukey box plots. Solid lines on box plots represent data set lower quartiles, medians, and upper quartiles and dotted lines on box plots represent data set sample means. In this paper, $p < 0.025$ are reported in bold on the data plots to emphasize statistical significance of a comparison.

6.6 Results and Discussion

Results from field FWD testing from different testing times on the three test sections are presented in Figure 6.2. Statistical mean and coefficient of variation (COV) values of these measurements obtained from each testing time are summarized in Table 6.2. Results indicate that the E_{FWD} values increased in October 2012, when compared to testing performed shortly after construction in July 2012. This change is attributed to trafficking on the crushed limestone subbase layer after construction and potential moisture regime changes in the foundation layers. FWD tests in April 2013 during freeze-thaw showed the lowest E_{FWD} values of all testing times, in all test sections. FWD tests conducted on HMA pavement showed higher E_{FWD} values in April 2014 compared to tests conducted in September 2013. This increase in E_{FWD} values is attributed to asphalt binder curing (note that tests in September 2013 were within 15 to 20 days after paving).

Results in Figure 6.3 further indicate that variations observed between test points on the crushed limestone subbase layer in October 2012 prior to paving track well with variations after paving in September 2013 after paving. Regression and F test analyses between measurements obtained from these two times in all three test sections yielded a

statistically significant relationship ($p < 0.0001$) with an R^2 value equal to 0.4657. This finding emphasizes the influence of support conditions on the measurements obtained on the surface layer.

Representative DCP-CBR profiles from each test section are presented in Figure 6.4. Mean and COV values of CBR measurements obtained from each testing time are summarized in Table 6.3. The seasonal variations in CBR profiles corroborate with changes observed seasonally in the E_{FWD} values.

6.6.1 Comparison of measurements on foundation layers

E_{FWD} test results obtained from each test section on the crushed limestone subbase layer (i.e., pavement foundation) from July 2012, October 2012, and April 2013 for three loading drops are presented as box plots in Figure 6.5. Statistical p-values determined by comparing the means of two data sets are included in these plots, while values shown in bold represent statistically significant values.

The t tests indicated statistically significant differences in E_{FWD} measurements between TS-MS and TS-C sections, and between TS-OE and TS-C sections, at all testing times with lower values in the TS-C section. Comparisons between TS-MS and TS-OE did not show statistically significant differences in July and October 2012 testing (with the exception of 62 kN loading in October 2012), but did indicate statistically significant differences in April 2013 testing. The TS-OE sections showed higher E_{FWD} values than the TS-MS section, which indicates the potential to thaw-weakening of the mechanically stabilized subgrade layer (verified using laboratory testing as described below).

The t test results for CBR values presented in Figure 6.4 also corroborate with the findings from FWD test results. CBR values were lower in all layers during thawing in

May 2013 and April 2014 than in October 2012. The CBR of the mechanically stabilized subgrade layer reduced from an average of about 16% in October 2012 to about 7% in May 2013, while the CBR of the recycled material reduced from an average of about 115% to 51%.

Table 6.4 presents the results of freeze-thaw laboratory test data of the pavement foundation materials. According to the ASTM D5918 frost-heave criteria, all of the materials showed *high* frost-heave susceptibility. However, based on the ASTM D5918 thaw-weakening criteria, the subgrade and the mechanically stabilized subgrade materials showed *very high* susceptibility while recycled material showed *medium* susceptibility. Before freeze-thaw, the CBR values of mechanically stabilized subgrade and recycled material were similar (about 9%), but the CBR of the mechanically stabilized subgrade material reduced to 1.8% and the recycled material reduced to 4.6% after freeze-thaw. These reductions are also observed in the field test results described above. The support capacity of mechanically stabilized layers is influenced by the degree of saturation and the percentage of clay particles in the mixture (Hopkins, Beckham, & Hunsucker; 1995). Because the recycled material is non-plastic (i.e., has no clay particles), its reduction in support capacity after freeze-thaw (i.e., when saturated) is not as substantial as with the presence of fine-grained particles mechanically stabilized subgrade material.

6.6.2 Comparison of measurements on HMA pavement

E_{FWD} test results obtained from each test section on the HMA layer from September 2013 and April 2014 are shown in Figure 6.6. The t test results indicated statistically significant differences in the measurements from all three test sections in September 2013, with TS-C being the lowest and TS-OE being the highest of all three. During April

2014 testing, TS-C showed the lowest values, but there were no statistically significant differences between TS-OE and TS-MS. The DCP tests conducted in April 2014, however, showed statistically significant differences between the TS-OE and TS-MS sections with low CBR values in the mechanically stabilized subgrade layer than in the recycled layer. Additional seasonal performance testing is underway to further evaluate the differences between the performance of the TS-OE and TS-MS sections.

6.6.3 Construction costs

Pavement foundation construction unit costs (per km) calculated for each test section based on bid proposals received from six contractors are shown in Figure 6.7. The foundation construction costs were calculated based on individual bid items as applicable for each test section and are summarized in Figure 6.7. The t-test analysis indicated that no statistically significant differences exist between the mean construction costs of the three sections.

6.7 Summary and Key Conclusions

This paper compares the performance of overexcavation and replacement (OE) and mechanical stabilization (MS) of subgrade that used on-place recycled pavement materials to stabilize pavement foundation layers. FWD and DCP tests were conducted on a control test section (TS-C) and four test sections (TS-OE and TS-MS) to assess in situ pavement foundation performance. Laboratory freeze-thaw tests were conducted on samples of the pavement foundation materials to determine frost susceptibility of the materials. Cost data for the on-site recycling technologies were used to gauge the relative cost effectiveness of the two stabilization methods using on-site recycled materials. The following key findings can be determined from this study:

- As-constructed, the TS-MS and TS-OE pavement foundations were stiffer than the TS-C pavement foundation. There was no statistical evidence to suggest that the TS-OE pavement foundation performed better than the TS-MS pavement foundation, or vice versa.

- During optimum environmental conditions three-months after Phase I construction the TS-MS and TS-OE pavement foundations were stiffer than the TS-C pavement foundation. Stress stiffening effects caused the TS-OE pavement foundation to perform better than the TS-MS pavement foundation at high loading levels.

- After the first spring thaw period, the TS-MS and TS-OE pavement foundations were stiffer than the TS-C pavement foundation. The TS-OE pavement foundation was stiffer than the TS-MS pavement foundation.

- Laboratory freeze-thaw testing showed that the mechanically stabilized subgrade used in this study exhibits strength and stiffness behavior similar to the on-site recycled material at optimum environmental conditions. During thaw-weakening conditions, the mechanically stabilized subgrade exhibits strength and stiffness behavior similar to the subgrade.

- After HMA placement and during optimum environmental conditions, the TS-MS and TS-OE pavement structures performed better than the TS-C pavement structure. The TS-OE pavement structure performed better than the TS-MS pavement structure. Pavement foundation performance therefore affects pavement structure performance.

- After the second spring thaw period, the TS-MS and TS-OE pavement structures were stiffer than the TS-C pavement structure. There was no statistical evidence to suggest that the TS-OE pavement foundation performed better than the TS-MS pavement foundation, or vice versa.

- Correlations between overall pavement system stiffness and pavement foundation stiffness during optimum environmental conditions and during thaw-weakened conditions indicated with statistical significance that pavement foundation stiffness impacts overall pavement system stiffness.

- A comparison of the unit costs of the two methods of pavement foundation stabilization with on-site recycled materials did not show measureable differences.

6.8 Acknowledgments

6.9 References

American Association of State Highway and Transportation Officials (AASHTO). (1993). *AASHTO guide for design of pavement structures*. Washington, D.C.: American Association of State Highway and Transportation Officials.

Becker, P.J., White, D.J., Vennapusa, P.K.R., & Dunn, M.J. (2014, January). Freeze-thaw performance assessment of stabilized pavement foundations. *Paper presented at the 93rd Annual Meeting of the Transportation Research Board*, Washington, D.C.

Bemanian, S., Polish, P., & Maurer, G. (2006). Cold in-place recycling and full-depth reclamation projects by Nevada Department of Transportation: State of the practice. *Transportation Research Record*, 1949, 2006, 54-71. doi: 10.3141/1949-06

Christopher, B.R., Schwartz, C., & Boudreau, R. (2006). *Geotechnical aspects of pavement*s (FHWA NHI-05-037). Washington, D.C.: National Highway Institute.

Cross, S.A., Kearney, E.R., Justus, H.G., & Chesner, W.H. (2010). *Cold-in-place recycling in New York State* (C-06-21). Long Beach, New York: Chesner Engineering P.C.

Diefenderfer, B.K., Apeagyei, A.K., Gallo, A.A., Dougald, L.E. & Weaver, C.B. (2012). In-place pavement recycling on I-81 in Virginia. *Transportation Research Record*, 2306, 21-27. doi: 10.3141/2306-03

Hopkins, T.C., Beckham, T.L., & Hunsucker, D.Q. (1995). *Modification of highway soil subgrades* (KTC-94-11). Lexington, Kentucky: Kentucky Transportation Center.

Johnson, A. (2012). *Freeze-thaw performance of pavement foundation materials* (Master's thesis). Available from ProQuest Dissertations and Theses database. (UMI No. 1531431)

Lee, K.W.W., Mueller, M. & Singh, A. (2014). Cold in-place recycling as a sustainable pavement practice. *Journal of Civil Engineering and Architecture*, 8(6), 680-692.

Lewis, D.E., Jared, D.M., Torres, H., & Mathews, M. (2006). Georgia's use of cement-stabilized reclaimed base in full-depth reclamation. *Transportation Research Record*, 1952, 125-133. doi: 10.3141/1952-14

Mallick, R.B., Bonner, D.S., Bradbury, R.L., Andrews, J.O., Kandhal, P.S., & Kearney, E.J. (2002). Evaluation of performance of full-depth reclamation mixes. *Transportation Research Record*, 1809, 199-208. doi: 10.3141/1809-22

Mansfield, T.J., & Hartell, A.M. (2012). Institutionalizing sustainability at the level of state departments of transportation: Quantitative assessment of transportation sustainability plan quality. *Transportation Research Record*. 2271, 9-18. doi: 10.3141/2271-02

Maurer, G., Bemanian, S., & Polish, P. (2007). Alternative strategies for rehabilitation of low-volume roads in Nevada. *Transportation Research Record*, 1989, 309-320. doi: 10.3141/1989-78

Maurer, L.K., Mansfield, T.J., Lane, L.B., & Hunkins, J. (2013). Blueprint for sustainability: One department of transportation's pursuit of performance-based accountability. *Transportation Research Record*, 2357, 12-23. doi: 10.3141/2357-02

Miller, H.J., Kestler, M.A., Amatrudo, M., Eaton, R., & Hall, A. (2011). Comparison of test sections of low-volume roadways reconstructed with conventional techniques and full-depth reclamation. *Transportation Research Record*, 2204, 206-214. doi: 10.3141/2204-26

Romanoschi, S.A., Hossain, M., Gisi, A., & Heitzman, M. (2004). Accelerated pavement testing evaluation of the structural contribution of full-depth reclamation material stabilized with foamed asphalt. *Transportation Research Record*, 1896, 199-207. doi: 10.3141/1896-20

Saad, B. (2014). Analysis of excess water impact on the structural performance of flexible pavements. *International Journal of Pavement Engineering*, 15(5), 409-426. doi: 10.1080/10298436.2013.790546

Stroup-Gardiner, M. (2012). Selection guidelines for in-place recycling projects. *Transportation Research Record*, 2306. 3-10. doi: 10.3141/2306-01

Weather Channel, The (2016). [Average monthly temperatures for Boone, Iowa] *Weather History for KBNW*. Retrieved from http://www.wunderground.com/history/airport/KBNW/2016/01/25/DailyHistory.html?req_city=Boone&req_state=IA&reqdb.zip=50036&reqdb.magic=1&reqdb.wmo=99999.

Welch, B. L. (1947). The generalization of `student's' problem when several different population variances are involved. *Biometrika*, 34(1/2), 28-35. doi: 10.2307/2332510

Wen, H., Tharaniyil, M.P., Ramme, B., & Krebs, S. (2004). Field performance evaluation of class C fly ash in full-depth reclamation: Case history study. *Transportation Research Record*, 1869, 41-46. doi: 10.3141/1869-05

White, D.J., Becker, P., Vennapusa, P.K.R., Dunn, M.J., & White, C.I. (2013). Assessing Soil Stiffness of Stabilized Pavement Foundations. *Transportation Research Record*, 2335, 99–109. doi: 10.3141/2335-11

Zhang, Y. (2013). *Frost-Heave and Thaw-Weakening of Pavement Foundation Materials* (Master's thesis). Available from ProQuest Dissertations and Theses database. (UMI No. 1531431)

Table 6.1. Geomaterial Index Properties and Engineering Parameters

Parameter	Subgrade	On-site Recycled	Mechanically Stabilized Subgrade with On-site Recycled	Crushed Limestone Subbase
Gravel Content (%)	5.3	37.2	18.4	65.2
Sand Content (%)	39.7	48.4	48.3	27.7
Fines Content (%)	55.0	14.4	33.3	7.1
Effective Size (mm)	NA	0.025	0.001	0.300
Coefficient of Uniformity	NA	160	744	34
Coefficient of Curvature	NA	2	4	4
Liquid Limit	33	NP	32	NP
Plasticity Index	15	NP	13	NP
Specific Gravity	2.6	2.6	2.6	2.7
USCS Classification	CL	SM	SC	GP-GM
AASHTO Classification	A-6(5)	A-1-a	A-2-6(1)	A-1-a
Maximum Dry Unit Weight (kN/m^3)	18.14	19.62	19.24	21.32
Optimum Moisture Content (%)	13.5	7.9	9.5	8.8

Notes: [a]NP = non-plastic
[b]Specific gravity assumed

Table 6.2. Means and Coefficients of Variation for Test Section E$_{FWD}$

	TS-MS	TS-OE	TS-C
	Mean E$_{FWD}$	Mean E$_{FWD}$	Mean E$_{FWD}$
	(MPa)	(MPa)	(MPa)
Testing Condition	[COV(%)]	[COV(%)]	[COV(%)]
On CLSB: July 2012; 6 kip Loading	79 [32]	86 [30]	25 [27]
July 2012; 9 kip Loading Drop	68 [32]	75 [29]	22 [23]
July 2012; 14 kip Loading Drop	58 [33]	65 [29]	18 [21]
Oct. 2012; 6 kip Loading Drop	179 [27]	207 [24]	54 [42]
Oct. 2012; 9 kip Loading Drop	150 [28]	181 [24]	43 [40]
Oct. 2012; 14 kip Loading Drop	119 [29]	157 [23]	32 [48]
Apr. 2013; 6 kip Loading Drop	28 [19]	46 [18]	16 [26]
Apr. 2013; 9 kip Loading Drop	26 [18]	43 [18]	14 [23]
Apr. 2013; 14 kip Loading Drop	25 [20]	40 [18]	14 [13]
On HMA: Sept. 2013; 6 kip Loading Drop	306 [23]	360 [16]	181 [19]
Sept. 2013; 9 kip Loading Drop	278 [22]	327 [15]	164 [16]
Sept. 2013; 14 kip Loading Drop	263 [22]	304 [12]	154 [15]
Apr. 2014; 6 kip Loading Drop	362 [11]	385 [9]	283 [4]
Apr. 2014; 9 kip Loading Drop	347 [10]	365 [8]	273 [5]
Apr. 2014; 14 kip Loading Drop	329 [9]	341 [8]	231 [6]

Table 6.3. Means and Coefficients of Variation for Test Section Layer CBR from DCP Testing

Testing Condition	TS-MS Mean Layer CBR (%) [[a]COV%]	TS-OE Mean Layer CBR (%) [[a]COV%]	TS-C Mean Layer CBR (%) [[a]COV%]
October 2012; [b]CLSB	98 [34]	229 [41]	122 [26]
October 2012; [c]MSSG/[d]OSR/[e]NS	16 [40]	115 [43]	11 [41]
May 2013; [b]CLSB	26 [24]	60 [62]	46 [27]
May 2013; [c]MSSG/[d]OSR/[e]NS	7 [87]	51 [41]	4 [34]
April 2014; [b]CLSB	35 [17]	82 [4]	56 [19]
April 2014; [c]MSSG/[d]OSR/[e]NS	6 [38]	57 [4]	5 [48]

Notes: [a]COV = Coefficient of variation

[b]CLSB= Crushed limestone subbase

[c]MSSG = Mechanically stabilized subgrade

[d]OSR = On-site recycled

[e]NS = Natural subgrade

Table 6.4. Freeze-thaw test results on select geomaterials

Test Result	Subgrade	On-site Recycled	Mechanically Stabilized Subgrade with In-place Recycled
First freeze-thaw Cycle Frost-heave rate (mm/day)	9.5	9.6	7.0
Second freeze-thaw Cycle Frost-heave rate (mm/day)	11.4	15.6	10.2
Frost Susceptibility Based on Frost-heave Rate	High	High	High
CBR without Freeze-thaw cycles (%)	2.8	8.8	9.1
CBR after Two Freeze-thaw cycles (%)	1.4	4.6	1.8
Thaw-Weakening Susceptibility Based on CBR	Very High	Medium	Very High
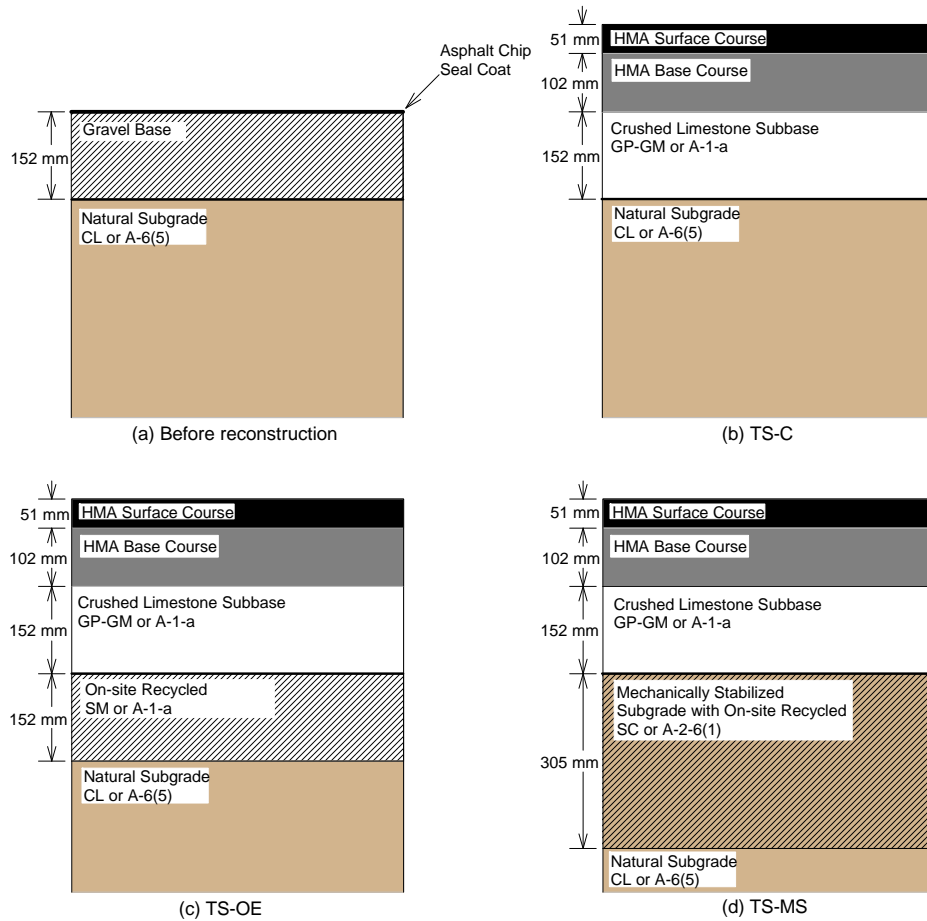
Figure 6.1. Pavement cross sections showing (a) pavement conditions before reconstruction; (b) TS-C; (c) TS-OE; and (d) TS-MS.

Figure 6.2. FWD Test Results from Different Testing Times on (a) TS-MS, (b) TS-OE, and (c) TS-C.

Notes:
$^{a}E_{FWD}$ calculated from 40 kN loading drop
^{b}CLSB = crushed limestone subbase
^{c}RMSE = root mean squared error

Figure 6.3 Correlations Between E_{FWD} Measured in September 2013 on HMA and E_{FWD} Measured in October 2012 on Crushed Limestone Subbase.

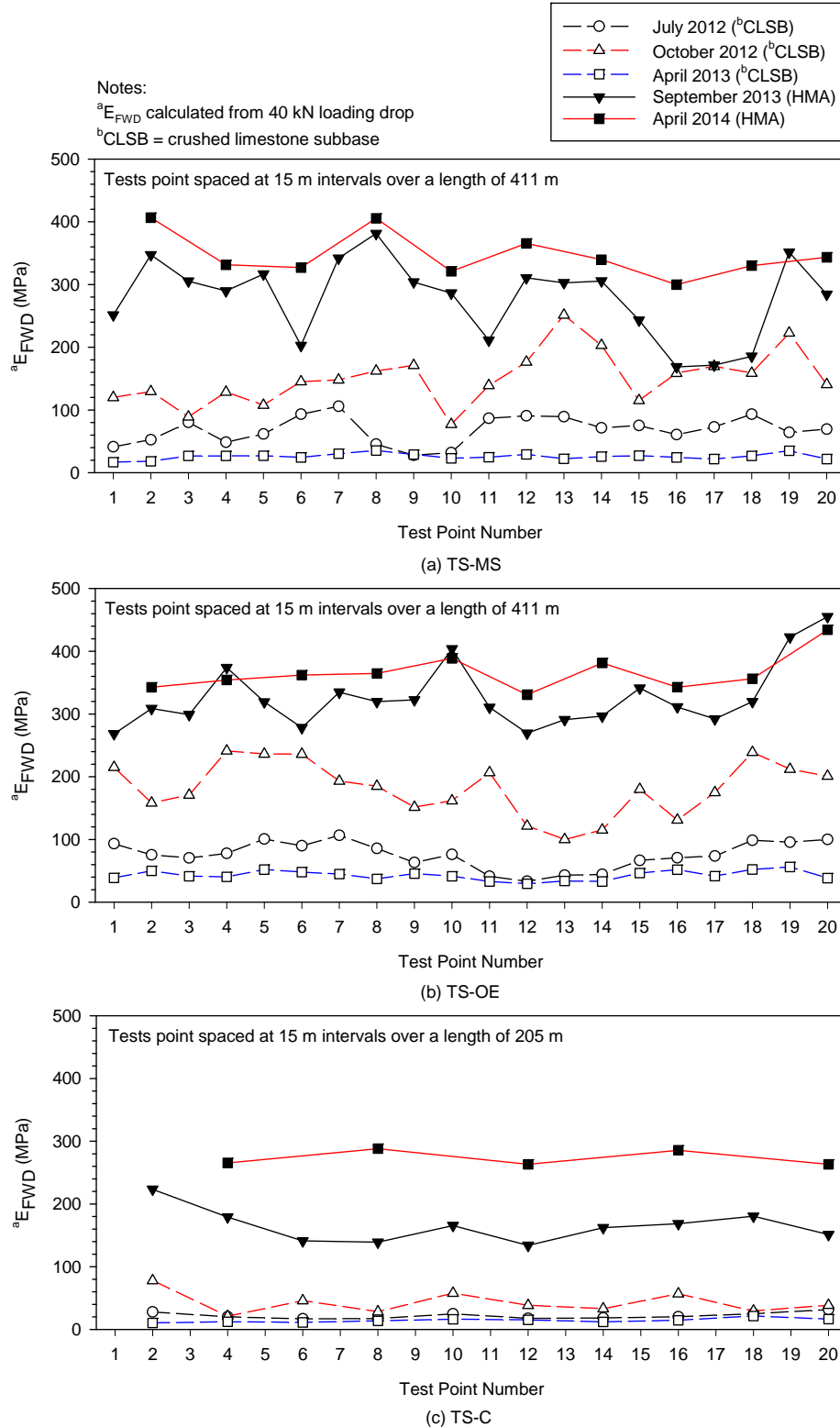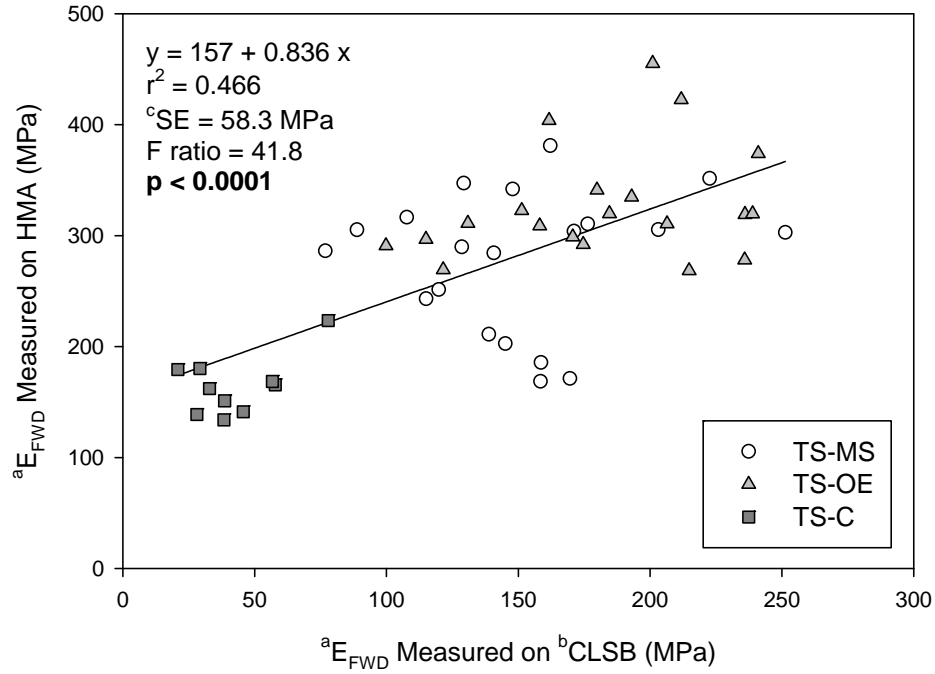Notes:
[a]CLSB = Crushed limestone subbase
[b]MSSG = Mechanically stabilized subgrade with on-site recycled
[c]OSR = On-site recycled
[d]NS = Natural subgrade
[e]Average CBR represents top 305 mm of natural subgrade

Average CBR in
[a]CLSB Layer:
TS-MS vs. TS-OE (p = 0.127)
TS-MS vs. TS-OE (p = 0.342)
TS-OE vs. TS-C (p = 0.176)

Average CBR in
[b]MSSG / [c]OSR / [d,e]NS Layer:
TS-MS vs. TS-OE (p = 0.216)
TS-MS vs. TS-OE (p = 0.267)
TS-OE vs. TS-C (p = 0.207)

(a) October 2012

Average CBR in
[a]CLSB Layer:
TS-MS vs. TS-OE (p = 0.108)
TS-MS vs. TS-OE (p = 0.096)
TS-OE vs. TS-C (p = 0.450)

Average CBR in
[b]MSSG / [c]OSR / [d,e]NS Layer:
TS-MS vs. TS-OE (**p = 0.008**)
TS-MS vs. TS-OE (p = 0.269)
TS-OE vs. TS-C (**p = 0.007**)

(b) May 2013

Average CBR in
[a]CLSB Layer:
TS-MS vs. TS-OE (**p = 0.001**)
TS-MS vs. TS-OE (p = 0.184)
TS-OE vs. TS-C (p = 0.155)

Average CBR in
[b]MSSG / [c]OSR / [d,e]NS Layer:
TS-MS vs. TS-OE (**p = 0.002**)
TS-MS vs. TS-OE (p = 0.775)
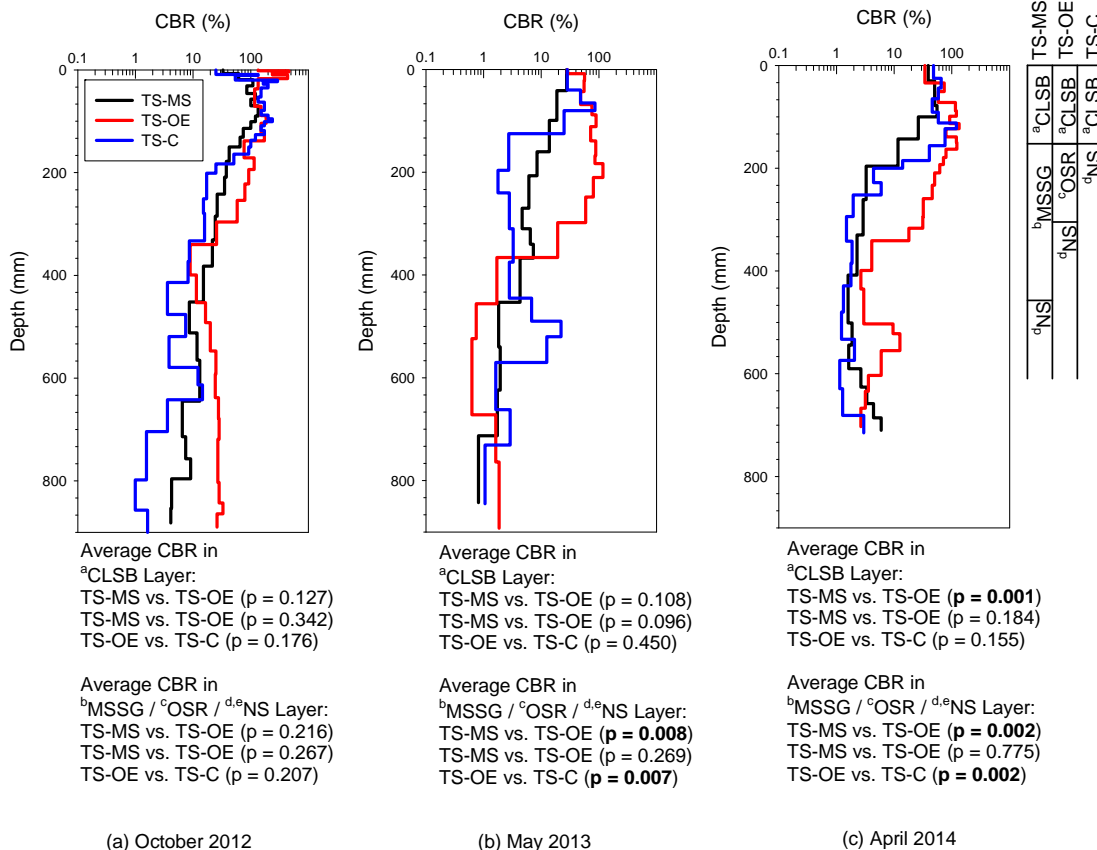TS-OE vs. TS-C (**p = 0.002**)

(c) April 2014

Figure 6.4 DCP Test CBR Profiles in (a) October 2012, (b) May 2013, (c) April 2014.
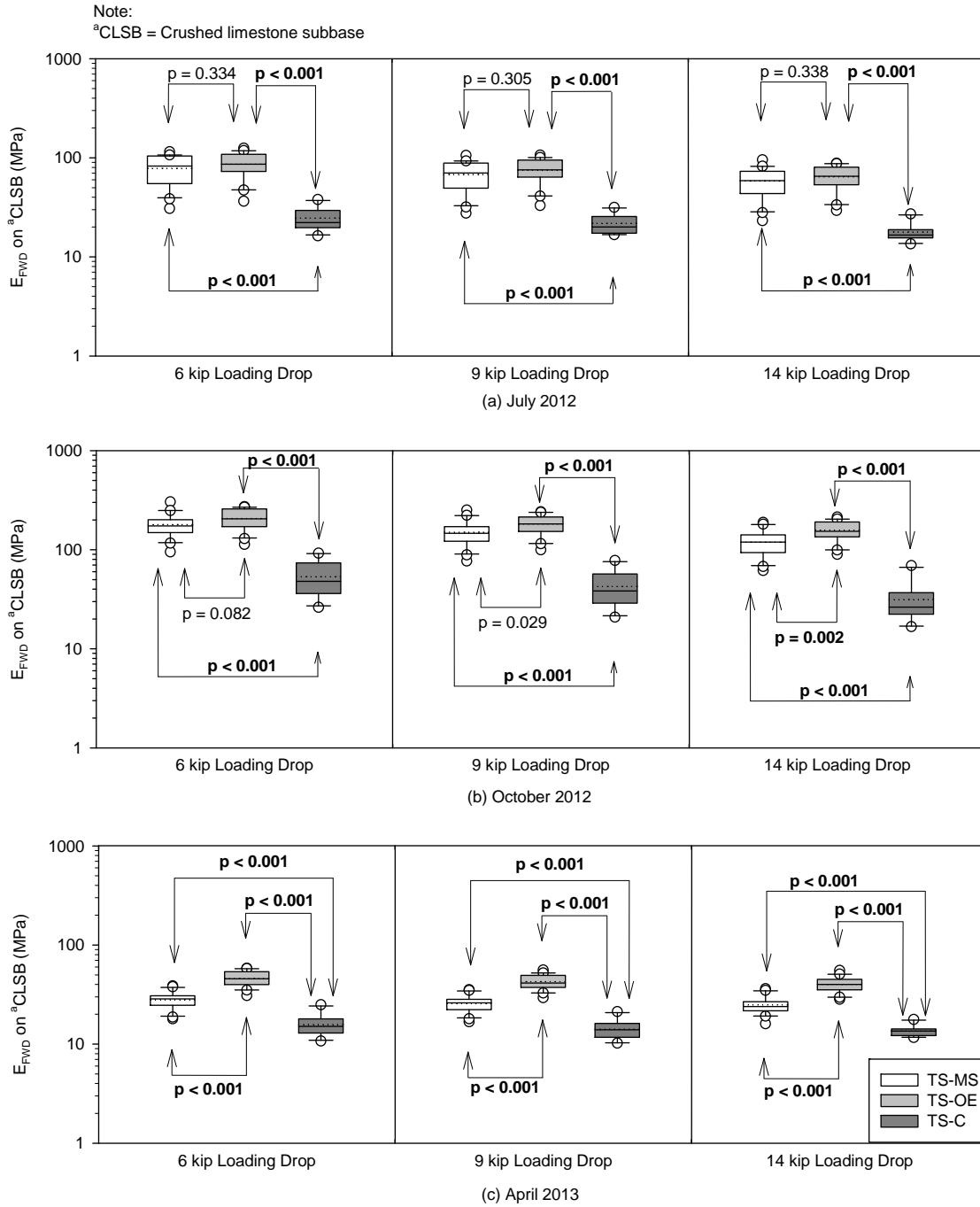
157

Figure 6.5 FWD Test Results on Test Section Pavement Foundations in (a) July 2012, (b) October 2012, and (c) April 2013.
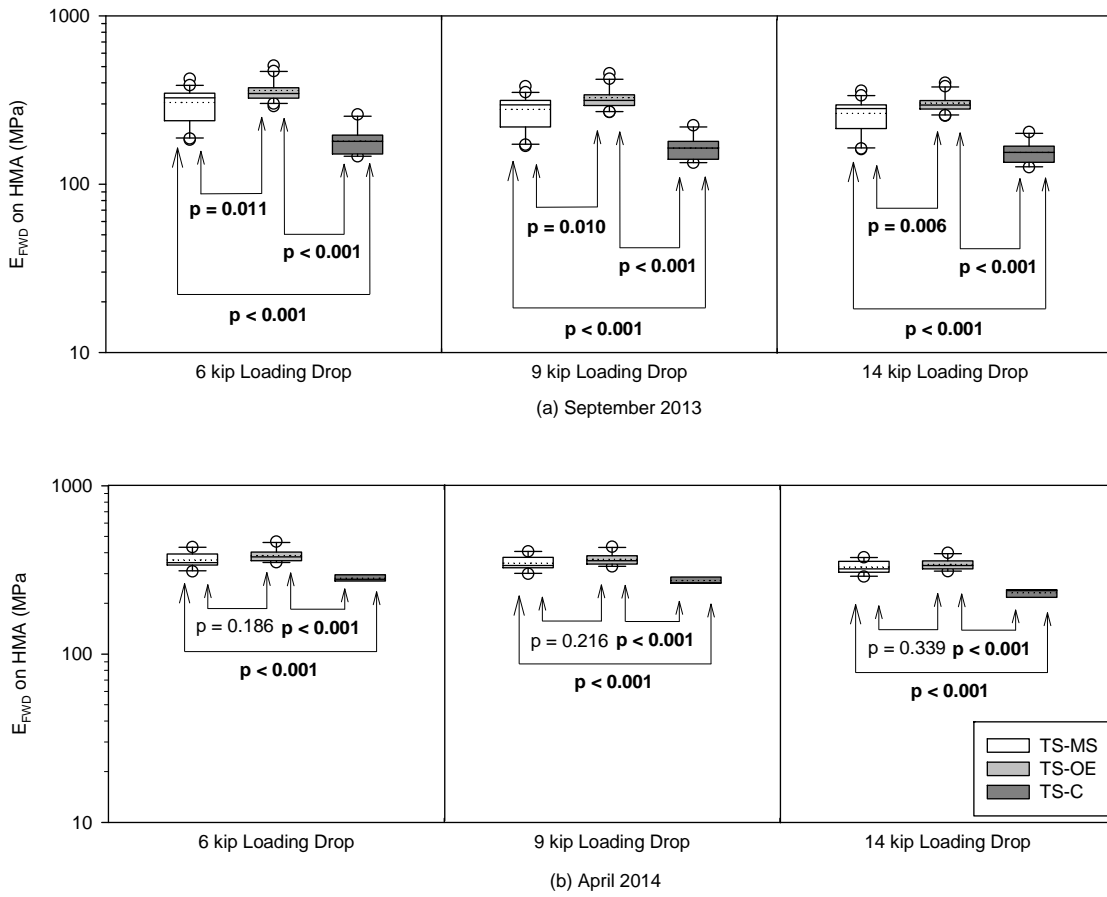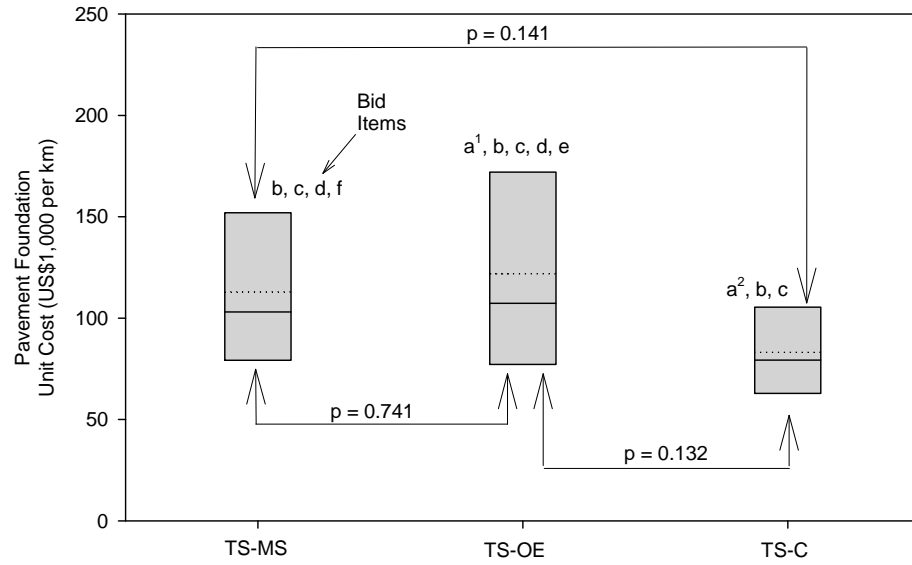
158

Figure 6.6. FWD Test Results on Test Section HMA Pavements in (a) September 2013 and (b) April 2014.

Item	Description	Cost Range
a	Excavation (waste) [1]subgrade [2]gravel base + chip seal	US\$7.36 to US\$12.08 per m^3
b	Crushed limestone subbase material	US\$43.53 to US\$58.48 per m^3
c	Construction of crushed limestone subbbase (152 mm)	US\$4.89 to US\$55.65 per m^3
d	Rubblizing, removing, mixing, and stockpiling recycled	US\$7.18 to US\$31.39 per m^3
e	Construction of on-site recycled subbase (152 mm)	US\$4.89 to US\$55.65 per m^3
f	Construction of mechanically stabilized subgrade (305 mm)	US\$6.82 to US\$17.04 per m^3

Figure 6.7. Comparisons of test section unit costs.

CHAPTER 7. CONCLUSIONS AND RECOMMENDATIONS FOR FUTURE WORK

7.1 Summary

This dissertation discusses the influence of pavement foundation condition on the design, construction, and performance of flexible pavements at a project site comprising pavement foundations of varying stiffnesses. In situ tests including falling weight deflectometer (FWD), dynamic cone penetrometer (DCP), light weight deflectometer (LWD), and roller-integrated compaction monitoring (RICM) assessed pavement foundation stiffness and its influence on the overall flexible pavement structure. Laboratory testing corroborated the in situ test results.

The preceding chapters presented an overview of pavement foundation design and construction and four scholarly journal articles that to fulfill the following objectives:

- to assess the applicability of strength- and stiffness-based spot testing and RICM continuous compaction control (CCC) for pavement foundation construction;

- to study in situ the effects of freeze-thaw weakening on stabilized pavement foundation mechanical properties (i.e., stiffness);

- to study the influence of pavement foundation condition on RICM measurements taken during asphalt pavement construction; and

- to compare the in situ performance and relative costs of pavement foundation test sections constructed with on-site recycled materials.

Specific conclusions related to each objective are provided in the chapters above. General conclusions from this study and recommendations for future research are provided below.

7.2 Conclusions

7.2.1 Strength- and stiffness-based pavement foundation construction control

- Regression analysis demonstrated that the LWD is correlated to the FWD, but does not reflect stiff underlying layers as measured from the FWD. The measurement influence depth is greater for the FWD compared to the LWD. Ground stresses were higher for the FWD.

- The roller-integrated compaction values (CMV and MDP*) provided near-continuous electronic records of ground stiffness and showed variations between the test sections and locations of lower stiffness materials within sections.

- The CMV values correlated better to the LWD and FWD values than MDP* values. CMV values correlated better to FWD values than LWD values.

- The QC/QA nuclear density testing showed that this approach to quality assessment can lead to shortcomings (including lack of reproducibility and infrequent testing) and does not capture the wide range in stiffness values measured from the other devices.

7.2.2 Stabilized pavement foundation freeze-thaw weakened performance

- For the freeze-thaw weakened state, test sections with PC stabilized subgrade or PC stabilized reclaimed gravel subbase produced the highest stiffness values. Test sections with fly ash stabilized subgrade or untreated reclaimed gravel subbase produced relatively high stiffness values as well.

- Correlations between thaw-weakened and never-frozen stiffness values suggest that PC stabilized pavement foundations are less susceptible to thaw-weakening than untreated pavement foundations or fly ash stabilized pavement foundations.

Because of a lack of data, DCP results could neither support nor oppose this claim.

- There is no correlation between thaw-weakened and never-frozen subbase CBR values, so thaw-weakened subbase CBR is likely independent of never-frozen subbase CBR. However, there is a statistically significant correlation between thaw-weakened and never-frozen subgrade CBR values, so so never-frozen subgrade CBR is likely an indicator of thaw-weakened subgrade CBR.

- Multivariable analyses that related pavement foundation composite stiffness to subbase and subgrade layer stiffnesses showed with statistical significance that both subgrade and subbase layer stiffnesses account for overall pavement foundation stiffness during the never-frozen condition (83.5% and 16.5%, respectively), while only subgrade layer stiffness account for overall pavement foundation stiffness during the thaw-weakened condition.

- Loss in subbase layer load-spreading effectiveness during thaw-weakening may explain why subbase layer stiffness does not contribute to overall pavement foundation stiffness during thaw-weakening. Application of Burmister stress distribution with backcalculated layer elastic moduli showed that the average distributed stress on the subgrade layer increased by about 1.5 times on average as conditions transitioned from never-frozen to thaw-weakened.

7.2.3 Influence of pavement foundation condition on asphalt pavement RICM

measurements

- In general, HMV values during asphalt pavement construction are higher when
  placing asphalt over stiff pavement foundations. All HMV measurements
  correlated with statistical significance to one another.

- For asphalt construction over soft pavement foundations, HMV increased with
  each additional pavement layer. For asphalt construction over stiff foundations in
  general, pavement foundation HMV was greater than base course HMV, and base
  course HMV was less than surface course HMV.

- Asphalt pavement surface temperature measurements from the RICM temperature
  sensors were in agreement with FLIR® thermal camera temperatures at higher
  temperatures (greater than 87.4 °C), but tended to underestimate pavement surface
  temperatures at lower temperatures (less than 87.4 °C).

- Asphalt pavement relative compaction from neither nuclear density gauge tests
  nor pavements cores correlated with HMV measurements. However, falling
  weight deflectometer (FWD) measurements strongly correlate with HMV
  measurements.

- Based on multivariable analyses, RICM systems can potentially be used as QC for
  asphalt pavement layer modulus, provided that the composite modulus of the
  pavement foundation is known.

7.2.4 Recycled pavement foundation performance and construction cost

- In general, the mechanically stabilized test section (TS-MS) and overexcavation test section (TS-OE) pavement foundations were stiffer than the excavation to grade test section (TS-C) pavement foundation

- Laboratory freeze-thaw testing showed that the mechanically stabilized subgrade used in this study exhibits strength and stiffness behavior similar to the on-site recycled material at optimum environmental conditions. During thaw-weakening conditions, the mechanically stabilized subgrade exhibits strength and stiffness behavior similar to the subgrade.

- Correlations between overall pavement system stiffness and pavement foundation stiffness during optimum environmental conditions and during thaw-weakened conditions indicated with statistical significance that pavement foundation stiffness impacts overall pavement system stiffness.

- A comparison of the unit costs of the two methods of pavement foundation stabilization with on-site recycled materials did not show measureable differences.

7.3 Recommendations for Future Research

The following future work is recommended to build upon the findings from this research:

- Continue documenting the field performance of stabilized pavement foundations.

- Predict in situ strains that relate to pavement performance using in situ stiffness data. Flexible pavement rutting, for example, is related to vertical strain on the top

of the subgrade, so determination of in situ strains will provide better ideas of pavement performance.

- Validate FWD backcalculation models for determining layer moduli.

- Test the hypothesis that Portland cement stabilization yields better performing pavement foundations during freeze-thaw weakening than all other stabilization techniques.

- Use intrusive in situ testing techniques (e.g., dynamic cone penetrometer) to validate and expand upon the concept of measurement influence depth.

- Develop better correlations for predicting stiffness from dynamic cone penetrometer measurements.

- Perform meta-analyses of individual RICM studies. There are several studies that report correlations of RICM measurements with density, but only because pavement foundation conditions are relatively homogenous. A global comparison of RICM measurements as they relate to density will contribute tom ending this misconception.

- Develop a model for predicting layer stiffness from RICM measurements of underlying layers.

- Analyze savings in reduced maintenance costs for pavements with stabilized pavement foundations.

- Analyze reduction in carbon footprint of pavements using recycled pavement foundations.

ACKNOWLEDGMENTS

I would like to thank my committee members Dr. David White, Dr. Douglas Gransberg, Dr. Pavana Vennapusa, Dr. Halil Ceylan, and Dr. Huaiqing Wu for serving on my committee and providing constructive comments on my work.

This research was made possible by the support of several agencies, research centers, and private companies. The Iowa Department of Transportation (IADOT) sponsored the Central Iowa Expo pavement foundation stabilization and paving project to provide a proper home for the biennial Farm Progress Show. The Center for Earthworks Engineering Research (CEER) at Iowa State University, of which I belong, conducted research both before and after project construction. Engineers from FOTH were the engineers of record for the project; JB Holland Construction, Inc. constructed the pavement foundations; and Manatts, Inc. constructed the asphalt and concrete pavements.

Several graduate and undergraduate research assistants from CEER and IADOT supported this research by performing laboratory and field testing and collecting samples: Dustin Wheatley, Jesus Rodriguez, Stephen Quist, Lance Keltner, Kyle Gross, and Nick Buse. Christianna White provided writing support that allowed me develop as a writer in addition to an engineer/researcher. Pavana Vennapusa was always available to lend me support, regardless of whether that support was some quick career advice or working with me past midnight to submit a journal article before its deadline passed.

Outside of conducting research, I worked for many semesters as a teaching assistant at Iowa State University, so I would like to thank Dr. David White, Dr. Vernon Schaefer, Dr. Beth Hartman, and Dr. Mat Rouse for allowing me to assist in their classes.

I have nothing but praise for Dr. David White. With the patience of a saint, he advised my research and guided me toward my goal of earning my PhD. There were multiple times when I questioned myself to the point that I wanted to abandon my doctoral research, but Dr. White always believed in me and redirected me back toward my goal. Although eventually triumphant, I absolutely struggled with the emotional aspects of doctoral research, and, in hindsight, I relied greatly on the kindness and understanding of Dr. White. In my master's thesis, I proclaimed that Dr. White was my mentor because of his "infinite knowledge and wisdom," but I have come to understand that Dr. White is my mentor because of his remarkable affinity for providing his students with trust, acceptance, compassion, encouragement, and kindness.

Finally, I must thank my wife, Rita, my son, Monty, and my daughter, Evie, because without them this dissertation would have never come to fruition. They had to endure a herculean amount of stress because of my ambitions, and never once did their love and support for me relent. I am very fortunate to have them.